
Electronic Thesis and Dissertation Repository

5-12-2014 12:00 AM


Nasopharyngeal method for selective brain cooling and development of a time-resolved near-infrared technique to monitor brain temperature and oxidation status during hypothermia

Mohammad Fazel Bakhsheshi
The University of Western Ontario

Supervisor
Dr. Ting-Yim Lee
The University of Western Ontario

Graduate Program in Medical Biophysics
A thesis submitted in partial fulfillment of the requirements for the degree in Doctor of Philosophy
© Mohammad Fazel Bakhsheshi 2014

Follow this and additional works at: <https://ir.lib.uwo.ca/etd>

 Part of the [Bioimaging and Biomedical Optics Commons](#), and the [Biomedical Devices and Instrumentation Commons](#)

Recommended Citation

Fazel Bakhsheshi, Mohammad, "Nasopharyngeal method for selective brain cooling and development of a time-resolved near-infrared technique to monitor brain temperature and oxidation status during hypothermia" (2014). *Electronic Thesis and Dissertation Repository*. 2066.
<https://ir.lib.uwo.ca/etd/2066>

This Dissertation/Thesis is brought to you for free and open access by Scholarship@Western. It has been accepted for inclusion in Electronic Thesis and Dissertation Repository by an authorized administrator of Scholarship@Western. For more information, please contact wlsadmin@uwo.ca.

Nasopharyngeal method for selective brain cooling and
development of a time-resolved near-infrared technique to monitor
brain temperature and oxidation status during hypothermia

(Thesis format: Integrated-Article)

by

Mohammad Fazel Bakhsheshi

Graduate Program

in

Medical Biophysics

A thesis submitted in partial fulfilment of the requirements for the degree of

Doctor of Philosophy

The School of Graduate and Postdoctoral Studies

The University of Western Ontario

London, Ontario, Canada

© **Mohammad Fazel Bakhsheshi 2014**

Abstract

Mild hypothermia at 32-35°C (HT) has been shown to be neuroprotective for neurological emergencies following severe head trauma, cardiac arrest and neonatal asphyxia. However, HT has not been widely deployed in clinical settings because: firstly, cooling the whole body below 33-34°C can induce severe complications; therefore, applying HT selectively to the brain could minimize adverse effects by maintaining core body temperature at normal level. Secondly, development of an effective and easy to implement selective brain cooling (SBC) technique, which can quickly induce brain hypothermia while avoiding complications from whole body cooling, remains a challenge. In this thesis, we studied the feasibility and efficiency of selective brain cooling (SBC) through nasopharyngeal cooling. To control the cooling and rewarming rate and because core body temperature is different from brain temperature, we also developed a non-invasive technique based on time-resolved near infrared spectroscopy (TR-NIRS) to measure local brain temperature. In normal brain, cerebral blood flow (CBF) and energy metabolism as reflected by the cerebral metabolic rate of oxygen (CMRO₂) is tightly coupled leading to an oxygen extraction efficiency (OEF) of around ~33%. A decoupling of the two as in ischemia signifies oxidative stress and would lead to an increase in OEF beyond the normal value of ~33%. The final goal of this thesis is to evaluate TR-NIRS methods for measurements of CBF and CMRO₂ to monitor for oxidative metabolism in the brain with and without HT treatment.

Chapter 2 presents investigations on the feasibility and efficiency of the nasopharyngeal SBC by blowing room temperature or humidified cooled air into the nostrils. Effective brain cooling at a median cooling rate of 5.6 ± 1.1 °C/hour compared to whole body cooling rate of 3.2 ± 0.7 was demonstrated with the nasopharyngeal cooling method.

Chapter 3 describes TR-NIRS experiments performed to measure brain temperature non-invasively based on the temperature-dependence of the water absorption peaks at ~740 and 840nm. The TR-NIRS method was able to measure brain temperature

with a mean difference of $0.5 \pm 1.6^{\circ}\text{C}$ ($R^2 = 0.66$) between the TR-NIRS and thermometer measurements.

Chapter 4 describes the TR-NIR technique developed to measure CBF and CMRO_2 in a normoxia animal model under different anesthetics at different brain temperatures achieved by whole-body cooling. Both CBF and CMRO_2 decreased with decreasing brain temperature but the ratio $\text{CMRO}_2:\text{CBF}$ (OEF) remained unchanged around the normal value of $\sim 33\%$. These results demonstrate that TR-NIR can be used to monitor the oxidative status of the brain in neurological emergencies and its response to HT treatment.

In summary, this thesis has established a convenient method for selective brain cooling without decreasing whole body temperature to levels when adverse effects could be triggered. TR-NIRS methods are also developed for monitoring local brain temperature to guide SBC treatment and for monitoring the oxidation status of the brain as treatment progresses.

Keywords

Temperature, Hypothermia, Nasopharyngeal cooling, Respiratory cooling, Time-Resolved Near-infrared Spectroscopy, Cerebral blood flow, Cerebral metabolic rate of oxygen, oxygen extraction efficiency, Oxidative Status, Piglets

Co-Authorship Statement

With the exception of Chapters 1 and 5, all chapters in this thesis are adapted from published conference/journal articles, or manuscripts to be submitted in the near future. While the author of this thesis was the primary author in each of these publications, they have emerged from collaborative research involving a number of different scientists, technicians and clinicians.

Chapter 2 has been adapted from the paper entitled “Feasibility of Selective Brain Cooling Using a Nasopharyngeal Method in Piglets”, submitted to the *Journal of Critical Care Medicine* by: Mohammad Fazel Bakhsheshi, Errol E. Stewart, Joo Ho Tai, Lynn Keenlside and Ting-Yim Lee. Ting-Yim Lee and Errol E. Stewart assisted with the design of this study, provided supervision throughout the project; additionally, they reviewed the manuscript. Joo Ho Tai was responsible for carrying out all tissue staining protocols and all histochemical analysis. Lynn Keenlside assisted with technical support in assembling the cooling device. Laura B. Morrison and Jennifer Hadway assisted in the animal care and surgical procedures. I was responsible for designing this study, performing the experiments, collecting and analyzing the data, and writing the manuscript.

Chapter 3 has been adapted from the paper entitled “Monitoring Brain Temperature by Time-Resolved Near-Infrared Spectroscopy: A Pilot Study”, submitted to the *Journal of Biomedical Optics* by: Mohammad Fazel Bakhsheshi, Mamadou Diop, Keith St. Lawrence and Ting-Yim Lee. Ting-Yim Lee provided supervision and grant support, assisted with the design of the experiment, and reviewed the manuscript. Mamadou Diop designed and engineered the time-resolved instrument, and assisted with the editing of the manuscript. Keith St. Lawrence consulted on the analysis of the data, and assisted with the editing of the manuscript. Lise Desjardins and Jennifer Hadway provided support with the animal experimentation. I was responsible for designing this study, performing the experiments, collecting and analyzing the data, and writing the manuscript.

Chapter 4 have been adapted from the paper entitled “Coupling of Cerebral Blood Flow and Oxygen Consumption During Hypothermia Under Different Anesthetics in Newborn Piglets Measured with a Time-Resolved Near-Infrared Technique”, submitted to the *Biomedical Optics Express* by: Mohammad Fazel Bakhsheshi, Mamadou Diop, Keith St. Lawrence and Ting-Yim Lee. Ting-Yim Lee provided supervision and grant support, intellectual input and assistance with the design of the experiment, consulted on the analysis of the data, and reviewed the manuscript. Mamadou Diop provided key intellectual contributions during discussions, and assisted with the editing of the manuscript. Keith St. Lawrence provided support and input regarding the data analysis, and assisted with the editing of the manuscript. Laura B. Morrison and Lise Desjardins conducted the surgical procedures and animal preparations, and assisted with the computed tomography (CT) acquisition. I was responsible for designing this study, performing the experiments, collecting and analyzing the CT perfusion and near-infrared data, and writing the manuscript.

Appendix A has been adapted from the paper entitled “Brain Cooling With Ventilation of Cold Air Over Respiratory Tract: an Experimental and Numerical study”, submitted to the *International Communications in Heat and Mass Transfer* by: Mohammad Fazel Bakhsheshi, Errol E. Stewart, Hadi Vafadar, Lynn Keenlside and Ting-Yim Lee. Ting-Yim Lee and Errol E. Stewart assisted with the design of this study, provided intellectual input, supervision throughout the project and reviewed the manuscript. Hadi Vafadar assisted with numerical simulations. Lynn Keenlside assisted with technical support in designing of the cooling device. Laura B. Morrison and Lise Desjardins assisted in the animal care and surgical procedures. I was responsible for designing and conducting the animal experiments and programmed the simulations, collecting and analyzing the data, and writing the manuscript.

Dedication

To my parents for their endless love, support and encouragement.

Acknowledgements

The work contained within this thesis was accomplished with the help of a number of individuals. First and foremost, I would like to thank my supervisor, Dr. Ting-Yim Lee, for his guidance and support throughout my PhD course. You have no doubt had a major impact on my scientific development, and for that I am extremely grateful. Thank you for bringing me along on this journey and giving me this fabulous opportunity. I also would like to express my grateful thanks and appreciation to my co-supervisor, Dr. Mamadou Diop. Without his insight guidance, patience, encouragement and support, accomplishment of this research would have not been possible.

I am also thankful to my advisory committee members, Dr. Keith St. Lawrence for providing me with support and guidance these last few years and Dr. David Lee, who have generously taken his time and providing me a guidance to the direction of my research with regards to it clinical significance. Also, a warm thanks to Lynn Keenlside who help me with design and manufacturing of our cooling devices and kept me excited about research. My gratitude to the wonderful team of animal technicians led by Jennifer Hadway cannot be overstated. Jennifer, along with Laura Morrison and Lise Desjardins, provided continuous support with submitting protocols, running the CT scanner, and of course, conducting the animal experiments. Also, very special thanks to Professor John Dingley who designed and constructed the Xenon delivery system.

I thank all of the faculty and the staff at the Department of Medical Bio-Physics in the University of Western Ontario for their assistance during my study in UWO. My utmost gratitude goes out to Anne Leaist, her tireless work-ethic and meticulous devotion to the group has truly been appreciated. Thanks to my great friend Dr. Mohamadreza Najiminaini for his special support. Finally, I would like to thank all my friends, family and the students and post-doctoral fellows of Ting's labs who provided academic advice, support and friendship.

Table of Contents

Abstract.....	ii
Dedication.....	vi
Acknowledgements.....	vii
Table of Contents.....	viii
List of Figures.....	xiii
List Of Tables.....	xvi
List of Acronyms and Abbreviations.....	xvii
CHAPTER 1.....	1
INTRODUCTION.....	1
1.1 Overview.....	1
1.2 Neonatal Hypoxia-Ischemia.....	2
1.3 Pathophysiology of HI.....	3
1.4 Clinical Management of HI.....	4
1.4.1 Therapeutic Hypothermia.....	6
a) Neuroprotective Mechanism.....	7
b) Current Methods of Hypothermia Induction.....	12
(i) Whole Body Cooling.....	12
(ii) Potential Side Effects of Whole-Body Cooling.....	13
(iii) Selective Brain Cooling.....	13
c) Rewarming.....	15
1.5 Current Methods of Brain Temperature Measurement.....	15
1.5.1 Tympanic Membrane Thermometry.....	16

1.5.2 Zero-Heat-Flow Method	17
1.5.3 Magnetic Resonance Thermometry	18
1.5.4 Microwave Radiometry	19
1.5.5 Ultrasound Thermometry	19
1.6 Near-Infrared Spectroscopy	20
1.6.1 Optical Characteristics of Tissue.....	21
1.6.2 Light Scattering in Tissue	22
1.6.3 Light Absorption in Tissue.....	23
a) Water	24
b) Hemoglobin	24
c) Lipids and Other Absorbing Compounds	25
1.6.4 <i>in-vivo</i> spectroscopy.....	26
1.6.5 Temperature Monitoring by Near-Infrared Spectroscopy	28
1.7 Cerebral Blood Flow and Cerebral Metabolic Rate of Oxygen	30
1.7.1 Current Techniques	30
1.7.2 Cerebral Blood Flow Measurement by NIRS	33
1.7.3 Cerebral Metabolic Rate of Oxygen Measurement by NIRS.....	35
1.8 Thesis objectives	36
1.9 References	37
CHAPTER 2.....	48
FEASIBILITY OF SELECTIVE BRAIN COOLING USING A NASOPHARYNGEAL METHOD IN PIGLETS.....	48
2. Introduction	48
2.1 Materials and Methods	50

2.1.1	Animals preparation and experimental procedure.....	50
2.1.2	Method of nasopharyngeal brain cooling.....	51
2.1.3	H&E histopathological examination.....	52
2.1.4	Statistical analysis.....	53
2.2	Results.....	53
2.3	Discussion.....	61
2.4	References.....	66
CHAPTER 3.....		71
MONITORING BRAIN TEMPERATURE BY TIME-RESOLVED NEAR-INFRARED SPECTROSCOPY: A PILOT STUDY.....		71
3.	Introduction.....	71
3.1	Materials and Methods.....	73
3.1.1	Instrumentation.....	73
3.1.2	Optical Properties Measurement.....	74
3.1.3	Tissue mimicking Phantom Experiments.....	75
3.1.4	Animal Preparation and Experimental Procedure.....	75
3.2	Data Analysis.....	77
3.2.1	Temperature Fitting Algorithm.....	77
3.3	Statistical Analysis.....	79
3.4	Results.....	80
3.5	Discussion.....	84
3.6	References.....	87
CHAPTER 4.....		92
COUPLING OF CEREBRAL BLOOD FLOW AND OXYGEN CONSUMPTION DURING HYPOTHERMIA UNDER DIFFERENT ANESTHETICS IN NEWBORN PIGLETS MEASURED BY TR-NIRS.....		92

4.	Introduction	92
4.1	Materials and Methods	94
4.1.1	Instrumentation	94
4.1.2	Determination of Cerebral Blood Flow.....	95
4.1.3	Determination of cerebral metabolic rate of Oxygen.....	96
4.1.4	Animal Preparation and Experimental Procedure and Groups	98
4.1.5	Computed Tomography Measurement.....	99
4.1.6	Statistical Analysis	100
4.2	Results	101
4.3	Discussion	108
4.4	References	111
	CHAPTER 5.....	115
	CONCLUSIONS AND FUTURE WORK.....	115
5.	Summary of Stated Objectives	115
5.1	Whole-Body and Selective Brain Cooling Approach	116
(i)	Selective Brain Cooling Using Nasopharyngeal Method.....	116
(ii)	Whole-Body Cooling with Mechanical Ventilation of Cold Air via the Respiratory Tract 117	
5.2	Monitoring of Brain Temperature by TR-NIRS Technique.....	117
5.3	Coupling of Cerebral Blood Flow and Oxygen Consumption During HT Under Different Anaesthetics Measured with a TR-NIRS Technique	118
5.4	Future Work	119
(i)	Advances in the Selective Brain Cooling Approach.....	119
(ii)	Improvement in Temperature Prediction	120
(iii)	Investigate the Effects of HT/Xe Administration on Flow-Metabolism Coupling in a Hypoxic-Ischemic Model Using TR-NIR.....	121

5.5 Conclusion.....	121
APPENDIX A.....	123
BRAIN COOLING WITH VENTILATION OF COLD AIR OVER RESPIRATORY TRACT: EXPERIMENTAL AND NUMERICAL STUDY	123
A. Introduction	123
A.1 Materials and Methods	124
A.1.1 Theoretical Model.....	124
A.1.2 Animals Preparation and Experimental Procedure	127
A.1.3 Pulmonary Cooling Approach	128
A.1.4 Statistical Analysis.....	129
A.2 Results	129
A.3 Discussions.....	133
A.4 References	136
APPENDIX B.....	139
COMPARISON OF SELECTIVE BRAIN COOLING IN JUVENILE AND NEWBORN PIGLETS USING A NASOPHARYNGEAL METHOD	139
B.1 Materials and Methods	139
B.2 Results	140
B.3 Conclusions	143

List of Figures

Figure 1.1: Neuroprotective therapies and their optimal moment of administration, according to their mechanisms of action.....	5
Figure 1.2: Schematic illustrating the effects of hypothermia on ischemia/reperfusion injury.	8
Figure 1.3: Tympanic thermometer.	16
Figure 1.4: Principle of the zero-heat-flux (ZHF) method.....	17
Figure 1.5: Specific absorption spectra of H ₂ O, Hb, and HbO ₂ in the NIR range. Values for H ₂ O is adjusted by a factor of 10, for illustrative purposes. Extinction coefficients of pure water and oxy- and deoxy-hemoglobin were taken from literature.....	21
Figure 1.6: Schematic illustration of the three main types of NIRS instrumentation.	26
Figure 1.7: NIR absorption spectra of pure water at various temperatures. Extinction coefficients of pure water as function of temperature were taken from literature.....	29
Figure 2.1. (a) Cerebral blood and brain are chilled by heat exchange between internal carotid arteries and cavernous sinuses and; (b) cerebrospinal fluid also cools the whole brain through the circulation.....	49
Figure 2.2. Schematic representation of the cooling circuit used for nasal cooling. The 7 Litre container was filled with a cryogenic cooling liquid (Ethylene glycol).	52
Figure 2.3. (a) Mean brain cooling rate with different nasopharyngeal cooling methods; (b) Changes in brain temperature over time for each method in Figure 2.3(a). * signifies a statistically significant ($P<0.05$) difference between high flow rate versus low flow rate at both cold and room temperature; # signifies a statistically significant ($P<0.05$) difference between cold temp versus room temp at low flow rate (3-4 L.min ⁻¹).....	55
Figure 2.4. Brain and rectal temperature over time for nasopharyngeal cooling method with (a) room temperature and (b) $-1 \pm 2^{\circ}\text{C}$ air at a flow rate of 3-4 L.min ⁻¹	57
Figure 2.5. Brain and rectal temperature over time for nasopharyngeal cooling method with (a) room temperature and (b) $-8 \pm 2^{\circ}\text{C}$ air at a flow rate of 14-15 L.min ⁻¹ . * signifies a statistically significant ($P<0.05$) difference between brain and rectal temperature.	59
Figure 2.6. Changes in the brain-rectal temperature over time for intra-nasal cooling method with setting the air flow rate to 14-15 L.min ⁻¹ at (a) room temperature and (b) cold temperature. * a statistically significant ($P<0.05$) difference compared to the baseline.	60

Figure 2.7. Representative H&E histology shows (a) normal brain cells in grey and white matter of the frontal lobe and (b) & (c) intact pseudostratified cilia and conchae (turbinates) cells in the nasal cavity after the nasal cooling process.61

Figure 3.1: (a) Correlation plot comparing temperature in the tissue-mimicking phantom calculated using data acquired by TR-NIRS against temperature measured with a thermometer (labeled Predicted Temperature and Measured Temperature, respectively). Each symbol type represents data from one of seven experiments with the tissue-mimicking phantom. The solid line represents the average of all individual linear regression lines and the dotted line indicates the line of identity (slope =1). (b) Bland-Altman plot comparing Predicted and Measured temperature. The dotted line shows the mean difference and dash-dotted lines show the limits of agreement (mean±2 SD) between the two temperature measurements.81

Figure 3.2: (a) Correlation plot comparing temperature in the piglet brain calculated using data acquired by TR-NIRS against temperature measured with a thermometer (labeled Predicted Temperature and Measured Temperature, respectively). Each symbol type represents data from one of eight piglets. The solid line represents the average of all individual linear regression lines and the dotted line indicates the line of identity (slope =1). (b) Bland-Altman plot comparing Predicted and Measured temperature. The dotted line shows the mean difference and dash-dotted lines show the limits of agreement (mean±2 SD) between the two temperature measurements.....83

Figure 4.1. (a) Coronal CT image showing the location of the TR-NIR probes and the ROIs enclosing an ellipse-shaped trajectory that light travel from the source to the detector. (b-e) Corresponding CBF maps at 38° (normothermia), 36°, 34° and 32°C. The region of interest used to measure CBF from the CBF map in each case is also shown.102

Figure 4.2. TR-NIR and CT CBF measurements in piglets (N=7) plotted as a function of brain temperature (N=7).103

Figure 4.3. (a) Correlation plot comparing CT and the TR-NIR CBF. The solid line represents the average of all individual linear regression (slope = 1.3 and intercept = -19 ml.min⁻¹.100g⁻¹). (b) Bland-Altman plot of CT and TR-NIR CBF. The dotted line shows the mean difference and dash-dotted lines show the limits of agreement (mean ± 2 SD).104

Figure 4.4. (a) Cerebral blood flow (CBF) and oxygen metabolic rate (CMRO₂); and (b) Oxygen extraction fraction (OEF) in Group II piglets (N=4) at each cerebral temperature under isoflurane or propofol/N₂O anesthetic regimes. Values are shown as mean ± SD; * *p*<0.05 versus at 38°C with isoflurane.....106

Figure 4.5. (a) Cerebral blood flow (CBF) and oxygen metabolic rate (CMRO₂), (b) Oxygen extraction fraction (OEF) in Group III piglets (N=3) at each cerebral temperature under isoflurane or propofol/Xe anesthetic regimes. Values are shown as mean ± SD; * *p*<0.05 versus at 38°C with isoflurane.....107

Figure A.1. Schematic diagram of the airway model.	125
Figure A.2. Schematic representation of the cooling circuit used for pulmonary cooling.	129
Figure A.3. (a) Maximum cooling rate for brain as a function of groups and theoretical predictions; (b) Brain temperature measurements over time for experimental and theoretical model. * signifies a statistically significant difference between pulmonary cooling group versus control group ($P<0.05$).	131
Figure A.4. Effects of (a) blood perfusion level; (b) air velocity, and (c) metabolic rate across respiratory tract response on blood temperature. Calculation were carried out with thermal conductivity $k = 0.5 \text{ w.m}^{-1}.\text{°C}^{-1}$, flowing air temperature $T_{in} = 5\text{°C}$, metabolic rate $Q_m = 420 \text{ w.m}^{-3}$, local mean longitudinal air velocity $V = 30 \text{ cm}^3.\text{s}^{-1}$ and blood perfusion rate $\omega_b = 50 \text{ ml. min}^{-1}.\text{100 g}^{-1}$ as a default values for each simulations.	133
Figure B.1. Maximum cooling rate for brain as a function of different conditions in Nasal cooling.....	141
Figure B.2. Changes in the brain-rectal temperature over time for intra-nasal cooling method with setting the air flow rate to 14-15 L.min^{-1} for (a) piglets with average weight of $\approx 2\text{-}3\text{kg}$; and (b) juvenile pig with average weight of $\approx 16\text{kg}$	142

List Of Tables

Table 2.1. Physiological parameters measured at different times during SBC with different methods.	54
Table 3.1. Absorption and reduced scattering coefficients measured at three discrete wavelengths as function of temperature in <i>in-vitro</i> (tissue-mimicking phantoms)..	80
Table 3.2. Physiological parameters measured at different brain temperatures.	82
Table 3.3. Absorption and reduced scattering coefficients measured at three discrete wavelengths as function of temperature in <i>in-vivo</i> (newborn piglets brain).....	82
Table 4.1. Physiological parameters measured at different groups.	1022
Table A.1: Base set of parameters used in heat sink thermal model	127
Table A.2: Physiological parameters measured at different groups.	130
Table A.3: Comparison of some physical properties of O ₂ -Air and O ₂ -Xe at normal atmospheric pressure.....	135

List of Acronyms and Abbreviations

AIF	Arterial Input Function
AMPA	α -Amino-3-hydroxy-5-methyl-4-isoxazolepropionic acid
ANOVA	Analysis Of Variance
AOV	Anglularis Oculi Vein
ASL	Arterial Spin Labeling
ATP	Adenosine Triphosphate
AVDO ₂	Arterial-Venous Difference Of Oxygen
Ca ²⁺	Calcium Cation
CBF	Cerebral Blood Flow
CBV	Cerebral Blood Volume
CEPA	Canadian Environmental Protection
Cl ⁻	Chloride Act
CMR _{glc}	Cerebral Metabolic Rate of Glucose
CMRO ₂	Cerebral Metabolic Rate of Oxygen
CNS	Central Nervous System
CPR	Cardiopulmonary Resuscitation
CPP	Cerebral Perfusion Pressure
CSF	Cerebrospinal Fluid
CT	Computed Tomography
CW	Continuous Wavelength
DCS	Diffuse Correlation Spectroscopy
DOS	Diffuse Optical Spectroscopy

DSC	Dynamic Susceptibility Contrast
EPI	Echo-Planar Imaging
EPSI	Echo-Planar Spectroscopic Imaging
EPO	Erythropoietin
FD	Frequency-Domain
H ₂ O	Water
H&E	Hematoxylin and Eosin
Hb	Deoxyhaemoglobin
HbO ₂	Oxyhaemoglobin
HI	Hypoxia-Ischemia
HIE	Hypoxic-Ischemic Encephalopathy
HR	Heart Rate
HT	Hypothermia
ICA	Internal Carotid Arteries
ICP	Increased Intracranial Pressure
K ⁺	Potassium
KS	Kolmogorov–Smirnov
MAP	Mean Arterial Pressure
MFP	Mean Free Path
MgSO ₄	Magnesium Sulfate
MR	Magnetic Resonance
MRI	Magnetic Resonance Imaging
MRS	Magnetic Resonance Spectroscopy

MRSI	Magnetic Resonance Spectroscopy Imaging
MWR	Microwave Radiometry
N ₂ O	Nitrous Oxide
Na ⁺	Sodium
NAC	N-Acetylcysteine
NICU	Neurointensive Care Units
NIRS	Near-Infrared Spectroscopy
NMDA	N-Methyl-D-Aspartate
NO	Nitric Oxide
NOS	Nitric Oxide Synthase
OEF	Oxygen Extraction Fraction
PBS	Phosphate Buffer Saline
PCA	Principal Component Analysis
PCR	Principal Component Regression
PCT	Perfusion Computed Tomography
PET	Positron Emission Tomography
PFC	Perfluorocarbon
PRF	Proton Resonance Frequency
<i>p</i> _a O ₂	Arterial Oxygen Tension
ROI	Region Of Interest
ROS	Reactive Oxygen Species
ROSC	Return Of Spontaneous Resuscitation
SBC	Selective Brain Cooling

SD	Standard Deviation
SI	Spectroscopic Imaging
SNR	Signal-to-Noise Ratio
SOS	Speed Of Sound
TBI	Traumatic Brain Injury
TCD	Transcranial Doppler
TH	Therapeutic Hypothermia
TR	Time Resolved
TR-NIR	Time Resolved Near Infrared
TM	Tympanic Membrane
TPSF	Temporal Point Spread Function
Xe	Xenon
XeCT	Xenon-enhanced computed tomography
WHO	World Health Organization
ZHF	Zero-Heat-Flux

Chapter 1

Introduction

1.1 Overview

The central nervous system (CNS) has a high metabolic rate and depends on a continuous blood supply of oxygen and nutrients and clearance of metabolic end-products. In the event of interruption of circulation, function quickly fails, and if circulation is not restored in a short time, irreversible damage to neurons occurs. The most common causes of energy crisis are a severe drop in cerebral perfusion or ischemia from arterial occlusion due to vasospasm or increased intracranial pressure from brain edema/herniation and a reduction in the oxygen content of blood referred to as cerebral hypoxia. Cerebral hypoxia refers to a lack of oxygen in the brain, even though blood flow and pressure may be normal. It can be caused by many conditions including near-drowning, strangling, carbon monoxide and other poisonous gas exposures, choking, compression of the trachea, cardiac arrest, diseases which have paralyzed the respiratory muscles, and birth asphyxia.

Clinical studies have shown that mild (32-35°C) and moderate hypothermia improves neurological outcome and reduces mortality for a variety of acute brain injuries following severe head trauma, cardiac arrest, stroke and neonatal asphyxia. However, cooling the whole body below 33-34°C can induce severe complications including sclerema, skin erythema, renal failure, coagulopathy, pulmonary hypertension, and even death. Such complications along with other ones offset the benefits accrued from the neuroprotective effects of hypothermia. In response to the aforementioned complications, selective brain cooling (SBC) methods have been proposed to alleviate the complications associated with systemic hypothermia by selectively cooling the brain while maintaining normal core body temperature. However, SBC requires a non-invasive method that can measure local brain temperature, since core measurements may not reflect brain

temperature. Improved cooling and monitoring technologies are still necessary to take in the full potential of this therapy.

The next section of this chapter will introduce neonatal hypoxic-ischemic encephalopathy (HIE) and describe the pathophysiology of the brain injury arising from and the clinical management of this condition. The chapter will then focus on discussing therapeutic hypothermia as the most promising neuroprotectant against hypoxic-ischemic (HI) brain injury. The chapter ends with an overview of current techniques to measure brain temperature and a discussion of near-infrared spectroscopy (NIRS) and its application for measuring tissue temperature and cerebral hemodynamics and metabolism. Finally, the objective and scope of the thesis are described to introduce the work performed for chapters 2 through 5.

1.2 Neonatal Hypoxia-Ischemia

Neonatal HI is still one of the most important causes of disability and death throughout the world.¹ Approximately four million babies die every year in the neonatal period, and one quarter of these deaths are attributed to HI.² HI has an overall incidence of 3-5 in 1000 births, and accounts for a large proportion of admissions to neonatal intensive care; 10-15% of cases will die in the neonatal unit. Of the survivors, 10-15% will develop cerebral palsy and up to 40% will have other significant disabilities.³ Undoubtedly, this clinical event is increasingly becoming a burden not only for the patients, but also for the families and communities that care for them. This problem is a financial issue as much as it is a health complication. The lifelong projected costs for cerebral palsy alone are estimated at \$11.5 billion dollars in the United States.⁴

HI triggers a cascade of events characterized by a reduction in cerebral blood flow (CBF) and oxygen delivery. This phase is referred to as *primary energy failure* which is associated with the reduction in high energy phosphate reserve, loss of membrane ionic homostasis, excitotoxicity, an increase in intracellular calcium and the inhibition of protein synthesis. Primary energy failure is followed by cell death. *Secondary energy*

failure, which occurs during reperfusion and reoxygenation several hours after the initial event and lasts for days. Secondary energy failure initiates a cascade of biochemical events, which involve nitric oxide synthases activation, the production of cytotoxic free-radicals, inflammation, membrane dysfunction and apoptosis, among others. The time interval between primary and secondary energy failure is thought to be a latent phase where therapies to reduce brain damage can be applied. This time interval is referred to as "therapeutic window".

1.3 Pathophysiology of HI

The principal mechanism underlying neurological damage resulting from HI is the deprivation of oxygen supply, which causes a primary energy failure. This energy failure forces the cells to generate oxygen independent energy via glycolysis through anaerobic respiration, which causes lactate production to increase (acidic bi-product of glycolysis in the absence of available oxygen) and creates an acidic environment for the cells in CNS.⁵ The deleterious effect of this primary energy failure impairs vascular autoregulation (i.e. the inability of the cerebral vasculature to maintain adequate CBF during systemic hypotension), and the low pH halts the activity of cellular enzymes.⁶ The sodium potassium (Na^+/K^+) adenosine triphosphate (ATP) pump will then begin to fail, and will cause an intracellular accumulation of sodium (Na^+), chloride (Cl^-) and calcium ions (Ca^{2+}).⁷ The intracellular accumulation of these ions will cause the neurons to depolarize and release a large amount of excitatory amino acid including glutamate. Glutamatergic actions are mediated by two major receptors: N-methyl-D-aspartate (NMDA) and α -Amino-3-hydroxy-5-methyl-4-isoxazolepropionic acid (AMPA). These receptors when activated open agonist-operated ion channels, which allow ions to cross the membrane. Extracellular glutamate can magnify intracellular concentrations of Ca^{2+} by opening NMDA- Ca^{2+} and AMPA- and kainate- Na^+ channels. Other effects of increased intracellular Ca^{2+} include the generation of free-radicals and nitric oxide (NO). As reperfusion occurs, glutamate levels return to normal, however; the glutamate receptors may remain active as an important cause of brain cell death.

During the reperfusion period, free-radical damage will be initiated and the reactive oxygen species (ROS) will combine with the nitric oxide synthase (NOS) from glutamate receptor activation to form toxic oxidants.⁸ Furthermore, calcium ion accumulation will activate a series of enzymes which lead to oxidative degradation of lipids and proteins and DNA damage.⁹ These damaging pathways will initiate the apoptotic and necrotic cascade which will cause neurons to die. The releasing of pro-inflammatory cytokines by resident immune cells of the CNS, and peripheral immune cells extravasating to the area of injury will initiate the inflammatory response¹⁰, all of which contribute to cerebral edema, subsequently leading to neuronal death. The continuum of neuronal death extends from early which is typically necrotic to delayed apoptotic cell death.¹¹ Apoptosis occurs over days as a result of a less severe insult, thus is a potential therapeutic target.

1.4 Clinical Management of HI

Many potential neuroprotective drugs that target specific pathways of HI brain injury have been investigated. These therapies operate at different times after the HI insults, depending on their mechanisms of action (Figure 1.1). The main goals of these interventions are decreasing the formation of toxic free-radicals to reduce cerebral damage, and inhibiting the excessive influx of calcium into neurons to minimize cerebral oedema.¹²

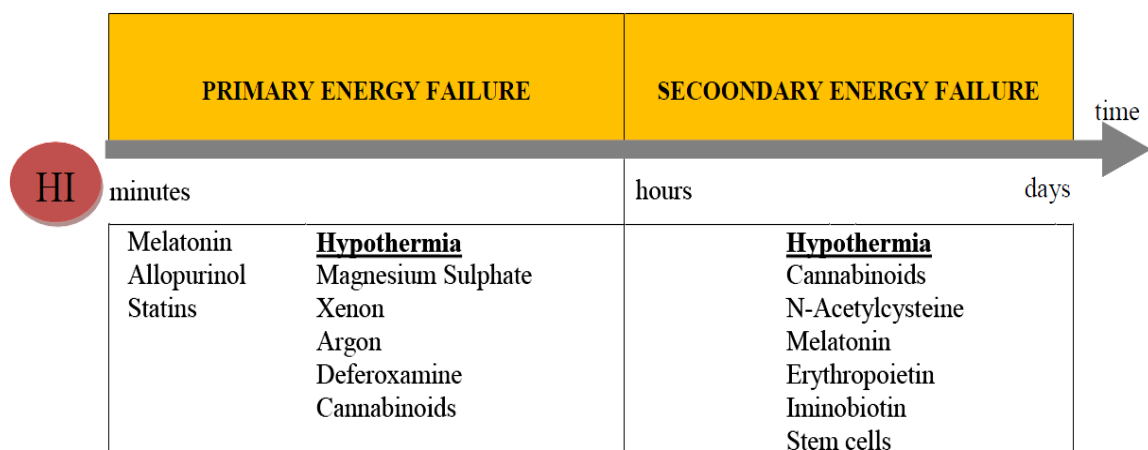


Figure 1.1: Neuroprotective therapies and their optimal moment of administration, according to their mechanisms of action.

Figure adapted from Cerio *et al.*¹²

Some interventions that have been investigated in animal and/or human trials include: anti-oxidant interventions that could reduce free-radical formation after the HI event such as *allupurinol*, *statins*, *N-acetylcysteine (NAC)*, *melatonin*, *cannabinoids*, *erythropoietin*, *deferoxamine* and *hypothermia*.¹² Apart from producing an antioxidant effect, *NAC*, *cannabinoids*, *melatonin* and *hypothermia* can also modulate the inflammatory responses. Furthermore, administration of *magnesium sulfate (MgSO₄)* has been shown to be neuroprotective. *MgSO₄* is an NMDA receptor antagonist, which prevents excitotoxic calcium-induced injury through the inhibition of NMDA receptor.¹³ Moreover, *MgSO₄* may also have direct actions on mitochondrial activity, have anticonvulsant properties and beneficial haemodynamic effects by increasing cerebral blood flow.

Likewise, the nontoxic anesthetic gas *Xenon (Xe)* has been shown to be an effective neuroprotectant in a variety of neuronal injury models. *Xe* is a potent NMDA antagonist, and has additional mechanisms of action such as inhibition of other subtypes of glutamate receptors, reduction of neurotransmitter release, inhibition of Ca^{2+} /calmodulin-dependent protein kinase II, and protection against excitotoxicity.¹⁴ Furthermore, *Xe* is an attractive adjunct to hypothermia due to its lack of chemical reactivity and toxicity, ease of reversibility and rapid brain penetration. It has been shown

that neuroprotection significantly increased from ~35% with HT alone to ~70% when HT was combined with 50% inhaled Xe gas.¹⁵ The major disadvantage of this intervention is that Xe is very expensive and its administration is rather complicated, since it requires intubation and ventilation of the patient as well as a large volume of expensive Xe gas. Recently, Dingley *et al.* have developed a relatively straightforward rebreathing closed circuit system suitable for cost effective delivery of Xe to mechanically ventilated neonates as a potential neuroprotectant after perinatal asphyxia.¹⁶

Erythropoietin (EPO) has also shown great promise as a neuroprotectant against HI brain injury.¹⁷ It was found to play a variety of roles in the modulation of inflammatory responses and has vasogenic effects.¹⁸ It may activate antioxidant enzymes, decrease excitotoxic damage, induce anti-apoptotic and anti-inflammatory factors and inhibit lipid peroxidation.¹⁹ Another neuroprotectant is *iminobiotin* which has been shown to inhibit both nNOS and iNOS in experimental studies.²⁰

During HI brain injury, neurons, glia and endothelial cells are damaged causing a reduction of their functionality or death. Recent advances in regenerative medicine suggest that stem cell transplantation may improve repair of the damaged brain.²¹ It has been shown that HI induced brain damage can be treated with Mesenchymal stem cells, easily recovered from bone marrow, placental tissue, and umbilical cord stroma without ethical problems.

Compared to the treatments discussed above, hypothermia appears to be a more reliable intervention available at the moment for reducing the risk of death or disability with brain injury²², as discussed in detail in the following section.

1.4.1 Therapeutic Hypothermia

Hypothermia can be classified as mild (32-35°C), moderate (28-32°C), severe (20-28°C) and profound at less than 20°C. Clinical studies indicate that the temperature range associated with better outcomes appears to be 33-35°C.²³ Systemic adverse effects

of hypothermia in general appear to be relative to the degree of cooling, occurring at core temperatures $< 34^{\circ}\text{C}$.²⁴ The current practice of hypothermia intervention in HI is to maintain a cerebral temperature of approximately $33\text{-}34^{\circ}\text{C}$ for about 48-72 h²², commencing as soon as possible after resuscitation.

a) Neuroprotective Mechanism

Hypothermia is thought to interfere with different damaging cascades, being protective both by itself and in prolonging the window for effective application of other neuroprotective strategies such as anti-oxidant, anti-apoptotic, or anti-inflammatory drug treatments.

Research has elucidated two distinct therapeutic windows for clinical use of hypothermia. In the early intra-ischemia window, hypothermia modulates abnormal cellular free radical production, poor calcium management, and poor pH management. In the more delayed post-reperfusion window, hypothermia modulates the downstream necrotic, apoptotic, and inflammatory pathways that cause delayed cell death. A schematic illustration of these processes is provided in Figure 1.2.

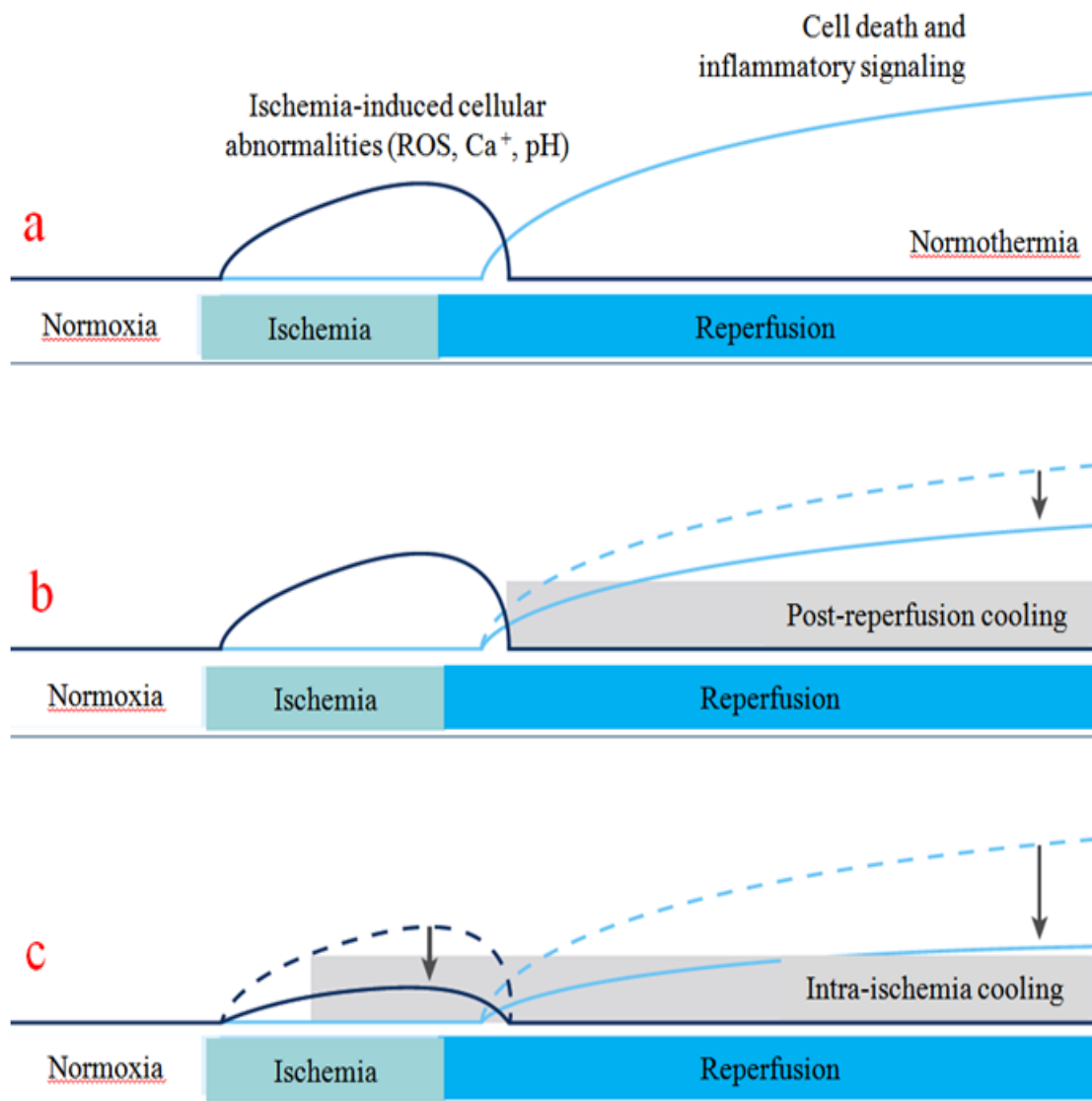


Figure 1.2: Schematic illustrating the effects of hypothermia on ischemia/reperfusion injury. Figure adapted from Lampe *et al.*²⁵ Post-reperfusion cooling (b) is thought to target only the later cell death and inflammatory signaling. Intra-ischemia protection shown in (c) is thought to target both ischemia-induced cellular abnormalities and post-reperfusion cell signaling.

There are a number of possible mechanisms by which mild hypothermia might improve neurological functions which include at least the following: (i) reduction in brain metabolic rate, (ii) reduction in free radicals, (iii) blockade of excitotoxic mechanisms, (iv) calcium antagonism, (v) preservation of protein synthesis, (vi) modulation of the inflammatory response, (vii) apoptosis and mitochondrial dysfunction, (viii) early gene activation, and (ix) decrease in edema formation.

(i). Reduction in Brain Metabolic Rate

It was originally believed that hypothermia's sole protective benefit was due to its ability to reduce cerebral metabolism. For every 1°C reduction in body temperature, there is a 6 to 10% decrease in cerebral metabolism.²⁶ This temperature dependent decrease in metabolism results in a decreased demand for oxygen and glucose in the brain.²⁷ The reduction in glucose and oxygen consumption helps prevent injury caused by a limited supply of oxygen. While there is a decrease in metabolism with hypothermia, we now know that this is only one of the many mechanisms of hypothermia.

(ii). Reduction in Free-Radicals

In the section 1.3, the idea that energy failure and consequential increases in intracellular Ca^{2+} lead to the production of free radicals was introduced. Free radicals are compounds with an uneven number of electrons in the outermost orbital, and as a result, are highly reactive. The effects of free radicals are magnified upon reperfusion when free radicals can interact with the renewed supply of oxygen to create reactive oxygen species (ROS), such as superoxide (O_2^-), which are more destructive. This effect is again magnified with the presence of NO, which is also made more abundant by increased intracellular Ca^{2+} . Superoxide can combine with NO to generate the highly toxic free radical species, peroxynitrite (NO_2^-), which is able to rapidly diffuse across cell membranes and affect surrounding cells. It also inactivates enzymes including mitochondrial ATPase, inhibiting mitochondrial electron transport, which leads to cells inability to sustain homeostasis and eventually apoptosis.

Under hypothermia condition, the release of free radicals is considerably decreased allowing endogenous anti-oxidative mechanisms to prevent or attenuate oxidative damage to cells²⁸ by prevention of mitochondrial failure, reduction in excitotoxicity and neutrophil accumulation, interleukin-1 (IL-1) mRNA upregulation and NOS activity.

(iii). Blockade of Excitatory Neurotransmitters

The injured tissue releases massive amounts of glutamate which leads to the activation of NMDA receptors and concomitant influx of Ca^{2+} into the cell, inducing what is known as excitotoxic brain damage. Hypothermia significantly reduces extracellular levels of both glutamate and glycine.^{28, 29} Neuroprotective properties of hypothermia may be partly due to its ability to prevent increases in the extracellular concentrations of amino acids that enhance the activity of the NMDA glutamate receptors and block the sustained elevation of the extracellular glycine concentration in response to brain ischemia.²⁹ Glycine is an inhibitory neurotransmitter in the brain stem and spinal cord. The NMDA receptor channel cannot be activated in the absence of glycine.³⁰ Reducing NMDA receptor activation prevents the excessive influx of Ca^{2+} into the cell, thereby preventing Ca^{2+} -mediated neuronal damage.

(iv). Hypothermia As a Calcium Antagonist

Intracellular calcium concentration is increased when energy fails. Calcium is involved in the regulation of many enzyme systems inside the cell such as Ca^{2+} /calmodulin-dependent protein kinase II, a multifunctional enzyme complex that mediates many of calcium's effects and also regulates protein kinase C which plays a pivotal role in neurotransmitter release. Reduced calcium influx might be one of the key mechanisms underlying hypothermia-induced neuroprotection. {Sahuquillo, 2007 #613}

(v). Protein Synthesis Preservation

The ubiquitin-proteasome proteolytic system is present in all eukaryotic cells and is responsible for the selective degradation of misfolded or damaged proteins. Consequently, ubiquitin plays an essential role in maintaining proper cellular functions. Ischemia and other brain insults provoke ubiquitin depletion. One consequence of ubiquitin deficit is excessive accumulation of abnormal proteins induced by brain injury or secondary ischemic events. Hypothermia has been shown to promote ubiquitin

recovery in experimental models of ischemia and could be one of the protective mechanisms against delayed neuron death.³¹

(vi). Modulation of the Inflammatory Response

In most brain injuries, an inflammatory response begins about 1 hour after ischemia-reperfusion and persists for up to 5 days.³² Large amounts of pro-inflammatory mediators are released inducing inflammatory and immune responses which can cause additional-injuries. Hypothermia has been shown to suppress these reactions.³³ Interrupting the inflammatory cascade can significantly attenuate the extent of brain injury and infarct size.

(vii). Apoptosis and Mitochondrial Dysfunction

Following neuronal injuries such as ischemia, cells may recover, become necrotic, or enter a pathway leading to programmed cell death, or apoptosis. Several studies have shown that hypothermia can interrupt the early stages of the apoptotic pathway, thereby preventing cellular injury from progressing to cell death. Hypothermia appears to reduce apoptosis by inhibiting caspase enzyme activation³⁴ and preventing mitochondrial dysfunction.³⁵

(viii). Early Gene Activation

Hypothermia stimulates early gene activation which is part of the protective cellular stress response to injury and promotes production of cold shock proteins that can be cytoprotective in the presence of ischemic and traumatic injury.²⁷ The relatively fast induction of the immediate early genes such as *fosB*, *junB* and *c-jun*, following hypothermia reflect a faster continuation of normal intracellular signaling, enhancing neuronal recovery.¹²⁶

(ix). Decrease in Edema Formation

Increased intracranial pressure (ICP) is the leading cause of death after severe traumatic brain injury (TBI). This increased ICP reduces cerebral perfusion pressure (CPP) and is one of the main causes of brain ischemia. Furthermore, many of the secondary injuries progress to dysregulation of intracellular and extracellular water content and consequently to brain edema, which both increases ICP and reduces CPP, which ends in cell death. Hypothermia decreases the detrimental effects of injury on the blood brain barrier and consequently decreases the formation of edema and reduces vascular permeability.³⁶

b) Current Methods of Hypothermia Induction

There are two main approaches used to induce hypothermia. The first approach is systemic or whole body cooling. The second approach is selective cooling where the damaged tissue is cooled, while maintaining the normal core body temperature.

(i) Whole Body Cooling

Systemic cooling induces hypothermia by lowering the core body temperature, often by using a blanket to cool the skin surface, which has been a relatively simple and popular method. Other whole body cooling approaches include immersing the body into cold water, packing the body with ice, or inserting an endovascular cooling catheter. Surface cooling cannot always be readily applicable in a clinical setting because of the large surface area of the human body and shivering-related complications introduced with surface cooling that may be difficult to control.³⁷

The use of endovascular cooling eliminates complications associated with shivering since it directly cools the blood supply while maintaining a normal skin surface temperature. A cooling catheter can be inserted quickly, between 10-25 minutes, and the target core body temperature, 33-34°C, can be reached more quickly than when

hypothermia was induced using a cooling blanket.³⁸ However, the major disadvantage of this method for systemic cooling is that it requires invasive surgical techniques for catheter insertion and success is highly dependent on the skills of the surgeon.

(ii) Potential Side Effects of Whole-Body Cooling

Large decreases in the core body temperature, which are often associated with systemic hypothermia, can lead to dangerous complications, such as development of sclerema, skin erythema, acrocyanosis, pulmonary hemorrhage, renal failure, increased blood viscosity, disseminated intravascular coagulation, hypoglycemia, acid-base and electrolyte disturbances, increased risk of infections, significant cardiovascular disturbances, and even death.^{39, 40} Sudden cardiac arrest and ventricular tachyarrhythmia including fibrillation have also been reported in infants who were hypothermic with rectal temperatures of less than 34.5°C during exchange transfusion with cold blood. Even mild hypothermia of 34-35°C has been reported to cause a marked decrease in myocardial contractility⁴¹, which can lead to conduction disturbances, hypotension and cardiac arrhythmia as seen in adults and newborn infants.^{42, 43} Moreover, hypothermia may result in decreased leukocyte mobility and phagocytosis, and increased risk of infection, especially pneumonia, as reported in adults.⁴⁴

A recent study correlating degree of therapeutic hypothermia with fatality and physiological disorders reported mortality rates of 39%, 52%, and 80%, respectively with mild, moderate, and severe therapeutic hypothermia.⁴⁵ Therefore, in order to avoid the complications associated with systemic hypothermia, it may be more beneficial to apply selective cooling. This method allows the core body temperature to remain within 36-37°C while the targeted tissue temperature is reduced.

(iii) Selective Brain Cooling

Methods for selective brain cooling (SBC) include using a cooling helmet, epidural cooling, packing the head with ice, forced convection, nasopharyngeal cooling,

and directly cooling the blood supplied to the brain. It has been shown that perfusing cold saline (4°C) in the epidural space of the brain for 6 hours provided rapid and deep cooling to the brain tissue. The brain temperature decreased to $\approx 27\text{-}30^\circ\text{C}$ within 5 minutes, while the normal core body temperature remained constant.⁴⁶ Using a cooling helmet with circulating cold water (4°C) reduced the average brain temperature 2-4°C within 2 hours^{47, 48}, while maintaining normal rectal temperatures. Placing a cooling device ($\approx 18^\circ\text{C}$) on the carotid arteries provided a 2.4°C reduction in the brain temperature of rats, while maintaining a constant core body temperature.⁴⁹

Nasopharyngeal cooling has the potential to overcome some of the limitations of current cooling methods. Based on anatomical features, cooling the nasal cavity may offer the capability to cool the brain selectively by cooling blood in both internal carotid arteries (ICAs) via counter-current heat exchange mechanism with the neighboring cavernous sinuses which collect cold venous blood from the mucosal linings of the nasal cavities. Furthermore, cerebrospinal fluid (CSF) chilled at the basal cistern cools the whole brain through the CSF circulation. Dohi *et al.*, achieved a lower cooling rate of $\approx 2.5^\circ\text{C/h}$ by blowing 24-26°C air at a flow rate of 8-12 L.min⁻¹ directly into the nasal cavities of two patients with Foley catheters adjunct with surface cooling.⁵⁰ Furthermore, Covaciu *et al.*, demonstrated selective cooling of the brain ($\approx 3^\circ\text{C/h}$) by circulating cold (8-10°C) saline in balloon catheters placed into the nasal cavities of pigs.⁵¹ A recent study employed transnasal evaporative cooling by spraying room temperature perfluorocarbon liquid (perfluorohexane, PFH; F2 Chemicals) into the nasal cavities with compressed oxygen to achieve average intra-nasal cooling rate of $\approx 4^\circ\text{C/h}$.⁵² However, use of perfluorocarbon raises environmental and health issues. It is a greenhouse gas and depletes the ozone layer and is listed as a toxic substance under the Canadian Environmental Protection Act (CEPA).⁵³ Another safety concern is the risk of coolant aspiration which might cause lung damage over prolonged periods since neural protection therapy may involve mild hypothermia being maintained for 72 hours.

c) **Rewarming**

Rewarming is a delicate phase of therapeutic hypothermia. Adverse consequences of whole body rewarming may lead to secondary injury seriously limiting the protective effects of hypothermia. Many studies demonstrated that a slow rewarming rate (0.1-0.4°C/hr⁵⁴) improves clinical outcome, while rapid rewarming may impair thermoregulation and exacerbate cell damage⁵⁵, and have unfavorable effects on basic hemodynamic variables.⁵⁶ Significant decreases in jugular venous oxygen saturation have been reported during rapid rewarming of patients following cardiac surgery under hypothermic conditions, indicating hypoxia of the brain⁵⁷; more slow rewarming led to a decrease in the incidence and severity of jugular bulb desaturations. Rapid rewarming was also recognized to cause a rebound in intracranial pressure⁵⁸, as well as cause a mismatch between increases of cerebral metabolic rate of oxygen (CMRO₂) and cerebral blood flow.⁵⁹ Rapid rewarming may open the permeability transition pore in the mitochondrial membrane, and hence result in mitochondrial dysfunction.⁶⁰ Following the rewarming phase, another important concept is the maintenance of strict normothermia, as fever is independently linked to adverse outcome in all types of neurological injuries.

In summary, optimal cooling duration and cooling depth still remain inconsistent and require further investigations. The general agreements among clinicians are early cooling initiation within the treatment window after injury and gradual rewarming. These approaches usually yield maximum neuroprotection and avoid adverse effects.

1.5 Current Methods of Brain Temperature Measurement

Once the brain is damaged, whether by brain ischemia or physical injury, brain temperature rises above body temperature. A typical elevation is between 1°C and 2°C.^{61, 62} As a result, core body temperature is not reflective of the actual brain temperature or the efficiency of therapeutic management; therefore, having a method to measure brain temperature non-invasively is extremely useful and important during hypothermia

treatment. Moreover, SBC requires a method that can measure local brain temperature rather than body temperature as the latter may not reflect the actual brain temperature. Several approaches have been developed to assess brain temperature. Brain temperature can be measured using infrared tympanic thermometer, zero-heat-flux thermometry, microwave radiometry, magnetic resonance spectroscopy, and ultra-sound thermometry.

1.5.1 Tympanic Membrane Thermometry

The tympanic membrane (TM) is the boundary between the outer and middle ears, commonly known as the eardrum and its location is proximal to the internal carotid (ICA) artery; therefore, tympanic membrane temperature should be the same as that of blood in the ICA supplying the brain. However, in recent publications, TM temperature was shown to differ from brain temperature by as much as 2.5-3°C.^{63, 64} Such differences might be attributable to poor thermal insulation of the measuring probe from the surrounding ear canal and poor contact between the probe and the membrane itself. If the sensor is not correctly positioned it may detect infra-red radiation energy emitted from the ear canal rather than that of the tympanum.



Figure 1.3: Tympanic thermometer.⁶⁵

1.5.2 Zero-Heat-Flow Method

Zero-heat-flux (ZHF) method is another technique to measure tissue temperature by inducing an isothermal zone under the sensor by heating the skin surface in a way that the outward heat flow from the core is matched with inward heat flow from the surface.⁶⁶ The ZHF probe actively heats the tissue until no temperature gradient exists across the probe. When an equilibrium is reached there is a region of tissue below the surface which has a uniform temperature. The thermometer probe consists of two temperature sensors separated by an insulating pad, which also houses a heating element. One of the sensors is in contact with the patient's forehead and the other one faces away from the forehead. A surface heating element is placed on top, along with another layer of insulation, switching on or off depending on the direction of the temperature gradient between the two sensors. The temperature on both sides of the layer is continuously monitored; when the sensors eventually reach the same temperature, no additional heat can flow out through the pad and the deep body temperature is inferred by the temperature of the skin sensor.

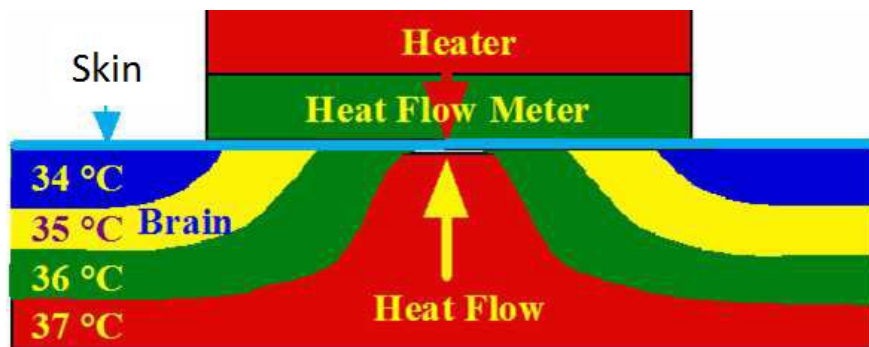


Figure 1.4: Principle of the zero-heat-flux (ZHF) method.

Figure adapted from Dittmar *et al.*⁶⁷

Recently, it has been shown that ZHF method accurately reflects core temperature during mild hypothermia in patients after cardiac arrest with accuracy of $\sim \pm 0.5^\circ\text{C}$ compared to core temperature.^{68, 69} A potentially serious problem is the possibility of inducing an increase in brain temperature during its operation in hypothermia treatment.⁷⁰

1.5.3 Magnetic Resonance Thermometry

The application of magnetic resonance (MR) to noninvasive thermometry of biological tissues is based on the effects of temperature on proton density, relaxation times T_1 and T_2 , the water diffusion coefficient and the water proton resonance frequency (PRF).⁷¹ Among these parameters, the chemical shift of the water proton has been recognized as the most reliable and practical indicator of temperature.⁷² Three methods, phase mapping, single-voxel spectroscopy and spectroscopic imaging (SI), have been proposed for measurement of temperature using proton chemical shift.

In phase-difference PRF thermometry, phase maps acquired before heating/cooling (referred to as the baseline phase maps) are subtracted from phase maps measured after treatment. Temperature differences are calculated based on phase variations with respect to a reference baseline.⁷³ Since there is a temporal delay between the current and the baseline acquisition, this method is very sensitive to motion artifacts. However, referenceless phase-difference methods⁷⁴ were proposed to remove motion artifacts by assuming that the thermal changes are localized to a small and well defined area. The method requires prior knowledge of where the temperature change will occur. Obviously, these assumptions are not applicable in the case of global brain cooling. The second group of PRF techniques uses magnetic resonance spectroscopy (MRS) or magnetic resonance spectroscopic imaging (MRSI) acquisitions to measure changes in water spectral line position. Motion and magnetic susceptibility artifacts can be reduced using an internal temperature-independent metabolite resonance. N-acetylaspartate spectral line at ~2 ppm is most often used for the brain. However, the long measurement time (typically in the order of a several minutes) and poor spatial resolution limit its application, even when applying a fast technique such as echo-planar spectroscopic imaging. Weis *et al* have recently compared two magnetic resonance methods, phase-difference and MRSI methods with high spatial resolution, for monitoring brain temperature changes during cooling on ten healthy volunteers. Mean brain temperature reduction varied in the interval 0.6-3.0°C and 0.7-2.7°C as measured by the MRSI and phase-difference methods, respectively.⁷³ The main advantage of the phase-difference technique is its simplicity and rapid measurement acquisition time. The disadvantage lies

with the phase wrapping that can complicate measurements in the areas containing fat tissue or in those regions with increased magnetic field inhomogeneity. The MRSI technique avoids the phase-wrapping problem and is able to separate water and fat signals for temperature measurement in tissues that contain fat. However, the disadvantage of this technique lies with the prolonged measurement acquisition time, more complicated data processing and the need to transfer patients to imaging facilities.⁷³

1.5.4 Microwave Radiometry

Microwave radiometry (MWR) technique use the tissue temperature-dependence of the power of the natural blackbody thermal radiation emitted from body tissues.⁷⁵ Lossy dielectric materials such as human body tissues are partially transparent to microwave radiation in the frequency range from 1-4 GHz allowing the measurement of temperature at a significant depth within the body.⁷⁶ For brain tissue, the effective depth is tens of millimeters and changes with frequency. By measuring temperatures in several microwave frequency bands, the internal temperature profile can be estimated from the data by solving an inverse problem. Han *et al.*, have developed a five-band microwave radiometer to measure the brain temperature of infants during hypothermia therapy demonstrating an accuracy of $\pm 0.75^{\circ}\text{C}$.⁷⁷ There are several issues in the application of MWR to the measurement of deep brain temperature. These problems include relatively poor temporal and spatial resolution of the measurements and systemic errors arising from inaccuracies in model parameters.⁷⁸

1.5.5 Ultrasound Thermometry

Ultrasound is an attractive modality for temperature monitoring because it is inexpensive and has relatively simple signal processing requirements. This modality may be useful for temperature estimation if a temperature-dependent ultrasonic parameter can be identified, measured and calibrated. The use of echo shifts has received the most attention in the last decade. It has been shown that by measuring the time shift of received

echoes and tracking scattering volumes, the temperature from a region of interest can be predicted. However, prior knowledge of both the speed of sound and thermal expansion coefficients are necessary, which limits this technique for temperature measurement.⁷⁹ Moreover, acoustic attenuation is also dependent on temperature, but with significant changes occurring only at temperatures above 50°C.⁸⁰ Minimal change in attenuation below this temperature range reduces its attractiveness for use in clinical applications. The major disadvantage of this technique is inducing temperature increase, which limits the protective effects of hypothermia. Fater *et al.* demonstrate a good correlation of tissue heating and transcranially transmitted ultrasound of mid-kilohertz range (340 kHz). They showed that brain temperature increased within 2 to 5 minutes of insonation with average elevation of 0.9°C with 7 W/cm².⁸¹

1.6 Near-Infrared Spectroscopy

Optical methods are a promising alternative to the aforementioned techniques since they are safe and the instruments are compact and portable. Biological tissue is relatively transparent to NIR (650-1000 nm) light due to the low optical absorption coefficient in this region. The major absorbing chromophores in the NIR include water (H₂O) and oxy- (HbO₂) and deoxyhaemoglobin (Hb). Figure 1.5 displays the specific absorption spectra of H₂O, HbO₂ and Hb in the NIR range.

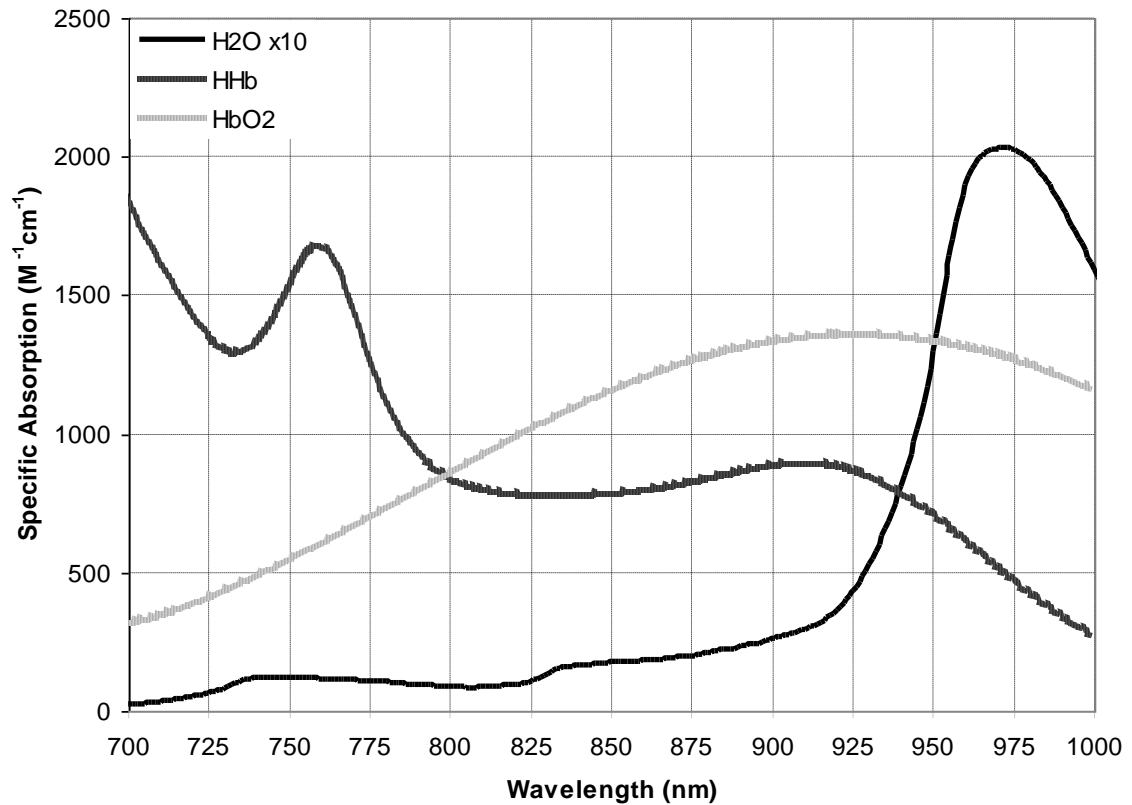


Figure 1.5: Specific absorption spectra of H₂O, Hb, and HbO₂ in the NIR range. Values for H₂O are adjusted by a factor of 10, for illustrative purposes. Extinction coefficients of pure water and oxy- and deoxy-hemoglobin were taken from literature.⁸²

1.6.1 Optical Characteristics of Tissue

Biological tissues are comprised of a vast assortment of molecules organized in different structures and functional units. There are four independent macroscopic parameters that are believed to characterize light propagation in tissue: the index of refraction (n), the absorption coefficient (μ_a), the scattering coefficient (μ_s), and the scattering anisotropy (g).

1.6.2 Light Scattering in Tissue

The ability to perform quantitative spectroscopy is complicated by the high-scatter nature of tissue. Scattering can be defined as the dispersion and redirection of wavelets in the medium of transmission. Scattering and light redirection can occur when light is incident on small particles (Rayleigh scatter), larger structures (Mie scatter), and at interfaces between media of differing indices of refraction (Fresnel reflection). As light propagates through tissue, it interacts with cell membranes, tissue boundaries, and organelles; at each interface, light is reflected and refracted by these objects, and therefore experiences a deviation in trajectory. When NIR light is used to interrogate biological tissue, all three major modes of light redirection can occur multiply and in combination. In fact, scattering events far outnumber absorption events, where the main light scattering components of cerebral tissue are lipoproteins found in cell membranes, followed by mitochondria and other cellular components.⁸³

The definition of mean free path (MFP) is the mean distance that a photon travels in the medium of tissue before it is absorbed, (absorption MFP: l_a) or scattered (scattering MFP: l_s). The reciprocal of a MFP is the corresponding of absorption or scattering coefficient ($\mu_a = 1 / l_a$, and $\mu_s = 1 / l_s$).

The anisotropy factor g is defined as:

$$g = \langle \cos \theta \rangle = \int_0^\pi p(\theta) \cos \theta 2\pi \sin \theta d\theta \quad (1-1)$$

where $\int_0^\pi p(\theta) \cos \theta 2\pi \sin \theta d\theta = 1$, and $p(\theta)$ is the distribution pattern of possible deflection angles of a photon scattered by a particle. These optical parameters should provide some information about the biomedical properties as well as the morphological and structural configurations of tissue. The reduced scattering coefficient μ'_s is then defined as:

$$\mu'_s \equiv \mu_s(1 - g) \quad (1-2)$$

The purpose of μ'_s is to describe the diffusion of photons in a random walk of step size of $1/\mu'_s$ where each step involves isotropic scattering. It follows that the transport attenuation coefficient is the sum of both absorption and reduced scattering coefficients: $\mu_t \equiv \mu_a + \mu'_s$. In NIR range, since $\mu'_s \gg \mu_a$, it is usually assumed that $\mu_t \equiv \mu'_s$. In addition, the wavelength dependence of μ'_s is well approximated by the so called power law:

$$\mu'_s(\lambda) \equiv A\lambda^{-b} \quad (1-3)$$

where A and b are constants either empirically determined or predicted by Mie theory, depending on the application.⁸⁴

1.6.3 Light Absorption in Tissue

The absorption coefficient (μ_a) describes the effectiveness of light absorption by a chromophore. When light radiation is incident on matter composed of discrete electrical charges, the charges are forced to oscillate at the frequency of the incident electric field. When infrared radiation is incident on a system of matter, resonance will occur, whereby energy is transferred from the incident field to the system and its amplitude of vibration is greatly increased. The excited state of the atoms or molecules usually lose their energy by colliding with one another within 10^{-12} seconds, thereby raising the kinetic energy of the other particles involved in the collisions. Hence, the energy associated with the incident field is most often dissipated as heat within the medium. This process is known as absorption.

The overall effect of absorption is a reduction in the intensity of the light beam travelling the medium. A relationship between the absorption of light in a purely absorbing medium and the thickness of the medium was first determined as the Beer-Lambert law

$$\begin{aligned} I &= I_0 e^{-\alpha.C.L} = I_0 e^{-\mu_a.L} \text{ in base of } e \text{ or} \\ I &= I_0 10^{-\epsilon.C.L} \text{ in base on } 10 \end{aligned} \quad (1-4)$$

where I_0 is the incident intensity, I is the transmitted intensity, (the log ratio of which is the attenuation of light), C is the chromophore concentration, L is the path length of light through the medium, and α and ϵ is known as the specific absorption coefficient for base of e and 10 , respectively. The ability to perform spectroscopy *in-vivo* relies on the fact that there are few absorbers of NIR light in biological tissue allowing adequate light penetration of the tissue. The chief endogenous absorbers are water, oxygenated hemoglobin, deoxygenated hemoglobin and lipids.

a) Water

The average water content of neonatal brain is estimated to be 85 % of the mass of the brain and 80 % of the adult brain.⁸⁵ Because of its high concentration in most biological tissues, water is considered to be one of the most important chromophores in tissue spectroscopy measurements. The extinction coefficient for water shows a general trend of increase with increasing wavelength. Between 600 and 900 nm there exists a region of relatively low absorption. Within this NIR range (600-900 nm), water has two distinct features in its absorption spectrum: one at 740 nm and another at 840 nm. Above 900 nm the absorption coefficient increases fairly rapidly to a peak at about 970 nm. In fact, for wavelengths of light greater than 900 nm, absorption by water is strong enough to limit the propagation of light to less than 1 centimeter, effectively forming the upper-limit on what is termed the "optical window" of NIR. Within tissue, water binds to a variety of molecules such as other water molecules, proteins (collagen, myosin, actin), mineral deposits in bone and phospholipids bilayers. The hydrogen bonding with these molecules changes the NIR spectral features derived from O-H vibrations.

b) Hemoglobin

Hemoglobin is the strongest endogenous absorber of NIR light. Hemoglobin is a large iron-containing protein found only in the blood, and constitutes approximately 40-45% of the whole blood. It is responsible for delivering oxygen from the lungs to body

tissues and returning waste gases, such as carbon dioxide, to the lungs to be exhaled. Carbon dioxide is transported in the blood from the tissue to the lungs by one of three methods⁸⁶: (i) About 5-7% is dissolved directly into the blood (ii) 10% binding to proteins, particularly haemoglobin; and (iii) 85% carried as a bicarbonate ion. Both Hb and HbO₂ exhibit strong absorptions at wavelengths shorter than 600 nm: effectively placing a lower-limit constraint on the range of wavelengths suitable for tissue interrogation. Another feature to note is the isosbestic point where the specific extinction coefficients of these two forms of hemoglobin are the same. Within the NIR range, the specific absorption spectra of Hb and HbO₂ cross at 800 nm but the marked differences between them at other NIR wavelengths have allowed the determination of tissue blood oxygenation with NIRS. The temperature-dependent changes of the hemoglobin NIR absorption spectra have been investigated^{87, 88}. It has been shown that by increasing the temperature in the range of 20-40°C, the amplitude of Hb and HbO₂ decreased by 0.15-0.18% °C⁻¹ and less than 0.05% °C⁻¹ and shifted by 0.08 nm °C⁻¹ (red-shifted for 760nm) and 0.15 nm °C⁻¹, respectively.⁸⁷ The amplitude changes in Hb are likely to have more significant effect on the total absorption in the range of interest than those for HbO₂.

c) **Lipids and Other Absorbing Compounds**

Lipids constitute about 5% of the total wet weight of a newborn infant's brain. This percentage increases to 8% of the grey matter and 17% of the white matter in adulthood. The specific absorption of NIR light by lipids is similar in magnitude to that of water. Lipid will not significantly add to the overall extinction coefficient of brain tissue as it is only present at approximately one tenth the proportion compared to water. Other negligible absorbers include some other enzymes involved in cellular respiration and some proteins found in blood plasma, none of which are abundant enough to contribute significantly to *in-vivo* spectroscopy.

1.6.4 *in-vivo* spectroscopy

The aim of NIR spectroscopy is to quantify the concentrations of these chromophores in tissue, and this requires the ability to separate the effects of absorption from those of scattering. Fundamentally, the coefficients of absorption (μ_a) and reduced scattering (μ'_s) can be determined by a series of reflectance measurements performed in one of three domains, namely, time⁸⁹ (with a fast pulse of light), frequency⁹⁰ (with a sinusoidal modulated source of light), and steady state or continuous wave (CW)⁹¹ (with a source of constant intensity). These three techniques are illustrated schematically in Figure 1.6.

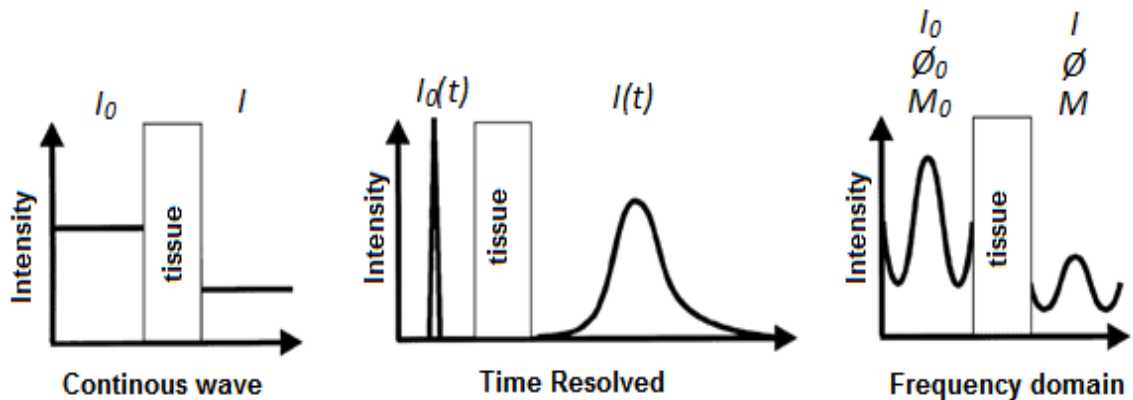


Figure 1.6: Schematic illustration of the three main types of NIRS instrumentation.
Figure adapted from Delpy *et al.*⁹²

Associated with each type of instrumentation is an equally wide range of types of measurements that can be made with them. Quantitative NIRS of the brain can essentially be separated into four subfields: spatially resolved spectroscopy, second derivative NIRS, frequency-domain and time-resolved spectroscopy. For a complete review of these techniques see Delpy *et al.*⁹² In spatially resolved spectroscopy simultaneous measurements of attenuation at multiple distances are combined to obtain sufficient information, to separate absorbance and scattering properties at spatially resolved locations.⁹³ Derivative of light attenuation with respect to optode spacing can be used to derive the product of the optical properties, i.e., μ_a and μ'_s . If the wavelength dependence of the reduced scattering coefficient is known for the tissue of interest then the absorption

coefficient can be calculated and presumably used to calculate absolute concentrations of chromophores.

Second derivative spectroscopy technique can estimate chromophore concentrations from an attenuation spectrum, by approximating a linear relationship between the measured attenuation and absorption of the medium. The dominant term in the second-order derivative of attenuation spectrum with respect to wavelength is the product of the differential pathlength, and the second derivative of the chromophore absorption spectra. Regressing the derivative chromophore spectra on to the derivative attenuation spectrum will yield the product of pathlength, and concentration for each chromophore. Concentrations of chromophores can be evaluated based on two assumptions: that the water concentration of the tissue of interest is constant and the tissue is homogeneous.⁹⁴

Frequency-domain (FD) techniques modulate the intensity of a light source at radio frequencies to produce the diffuse photon density wave that propagates through the tissue.⁹⁵ The phase and amplitude of this wave are measured at the detector which allows calculation of the optical pathlength and enables conversion of changes in attenuation to changes in absorber concentrations. Time-resolved NIR methods are photon counting techniques that use a laser light source to emit pulses of monochromatic light and fast detectors to measure the time-of-flight of each detected photon (i.e., the time required for a photon to travel from the laser to the photomultiplier tube). This process is repeated, typically at a frequency of around 80 MHz until about 10^7 photons are measured, and temporal point spread function (TPSF) is generated. Furthermore, by fitting the TPSF to an appropriate model of light transport, values for both the absorption and reduced scattering coefficients can be estimated and absolute concentrations of absorbers can be calculated. Time-resolved spectroscopy was the technique of choice for the work completed in this thesis. This section will be followed by reviewing the previous studies which have utilized NIRS to measure temperature.

1.6.5 Temperature Monitoring by Near-Infrared Spectroscopy

There are a number of studies that have investigated the temperature dependent effects on tissue water NIR spectra. As pure water is heated the fraction of hydrogen bonds are reduced through thermal agitation of the water molecules, which overcomes the force of the hydrogen bonds. This in turn produces a blue-shift of the water absorption peak. The water NIR absorption peaks around 740, 840 and 970 nm decreases in amplitude by approximately $0.5\text{-}0.8\%^\circ\text{C}^{-1}$, and shifts towards higher wavelengths with decreasing temperature; an approximate shift of 5-10 nm (easiest to see in the 970 nm band) has been reported over the range 30-40°C.⁹⁶ Water absorption spectra as a function of temperature are shown in Figure 1.7. These temperature dependent spectral shifts are due to decreases in the extent of intermolecular hydrogen bonding by water molecules with increasing temperature.

Hollis *et al.* investigated the use of an optical technique to measure tissue temperature. They used a broadband CW technique to measure reflectance over the spectral range of 650-980 nm. Within this spectral window water absorption peaks are located at ~740, ~840 and ~976 nm. The primary focus of their work was on the absorption peaks at 740 and 840 nm because the lower absorption of these peaks relative to the 976 nm peak allows for deeper penetration of light. They used the technique of principal component regression (PCR) to calibrate the temperature response of pure water spectra in order to determine dominant spectral features associated with temperature changes that could then be used for fitting the tissue temperature. Measurements performed on an adult forearm had a standard error of prediction of $\sim 1.2^\circ\text{C}$ for the recovered temperature. Hollis concluded that in order to improve results scattering should be accounted for and that using the water peak at ~976 nm would provide more contrast although it would limit the light penetration depth in the tissue.⁹⁶ Chung *et al.* have also demonstrated a method that employs broadband diffuse optical spectroscopy (DOS) to measure tissue temperature based on resolving water vibration frequency shifts in NIR water absorption spectra that occur with changes in temperature and macromolecular binding state. DOS acquires scattering-separated absorption spectra, typically from 650 to 1000 nm, using a combination of frequency domain and steady-state reflectance and

provides an absolute measure of absorption, unlike conventional reflectance methods. The method focuses on the ~ 976 nm water peak for greater contrast in temperature and uses the temperature isobestic point at 996nm, in which the specific absorption spectra of water at different temperature is constant, to separate the macromolecular bound water contribution from the thermally induced spectral shift which requires quantifying subtle changes in the NIR water absorption features and a high-resolution calibrated spectrometer. This method has been tested in tissue simulating intralipid phantoms. The average difference between optical and thermistor measurements was $\sim 1.1 \pm 0.91^\circ\text{C}$ in the temperature range of 28-48°C.^{97, 98}

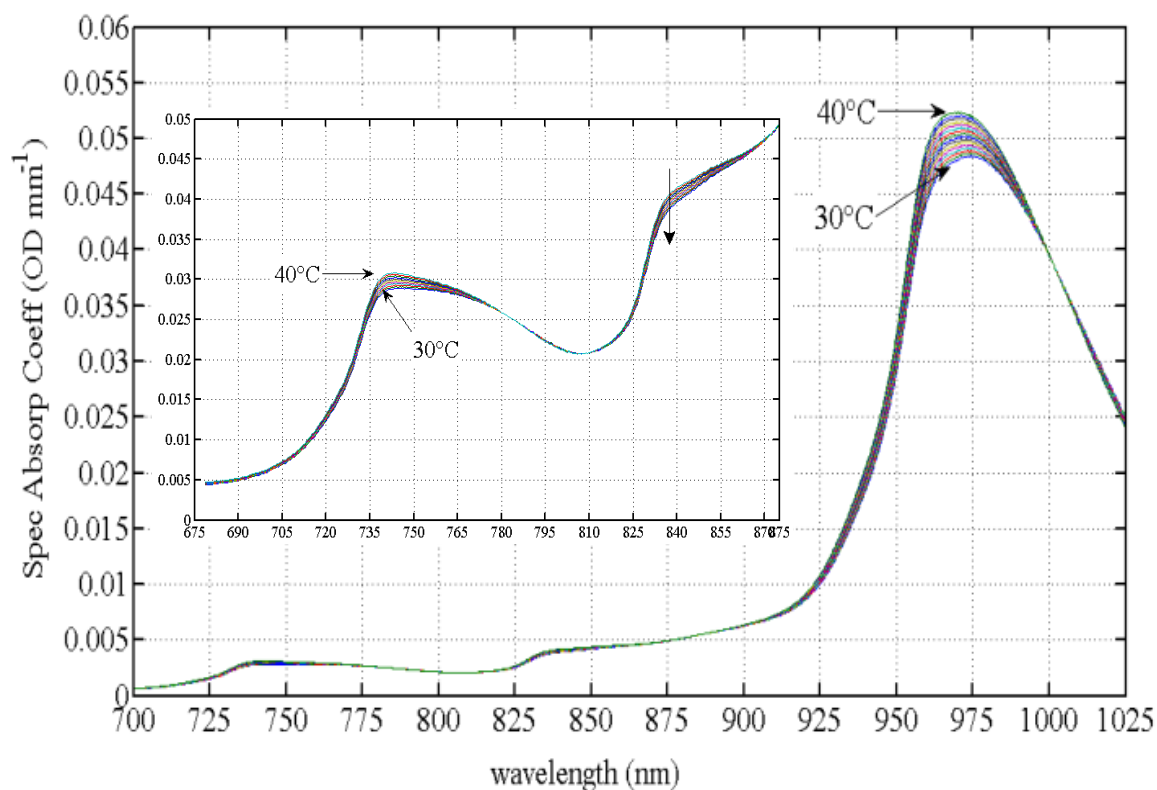


Figure 1.7: NIR absorption spectra of pure water at various temperatures. Extinction coefficients of pure water as function of temperature were taken from literature.⁸²

1.7 Cerebral Blood Flow and Cerebral Metabolic Rate of Oxygen

As discussed in detail in the section 1.4.1, one of the important mechanism of HT-induced neuroprotection is the preservation of brain ATP levels resulting from a reduction in cerebral metabolism or metabolic rate of oxygen (i.e. $CMRO_2$).⁹⁹ The effects of HT on CBF are a consequence of the well-accepted phenomenon that $CMRO_2$ is closely coupled to CBF and therefore, a reduction in the former is coupled to a reduction in the latter.^{100, 101} Preserving the coupling between CBF and $CMRO_2$ is an important factor in the control of the cerebral circulation, connecting the change in metabolic demands with the supply of substrates by blood flow. As a consequence of this balance between flow and metabolism, the oxygen extraction fraction (OEF) indicates any regional variation in brain. As such, it is critical to measure these key physiological parameters throughout therapeutic hypothermia, particularly during rewarming phase. Rapid rewarming of the injured brain commonly leads to a mismatch between cerebral metabolism and perfusion⁵⁹ and can cause in rebound intracranial pressure elevations⁵⁸, cerebral venous desaturation¹⁰², and brain ischemia. It is suggested that controlling the rewarming rate as low as 0.1-0.4°C/hour is preferred to reduce the neurological risks.⁵⁴ Therefore, predicting and managing possible systemic side effects of rewarming is also important for guaranteeing HT efficacy.

1.7.1 Current Techniques

CBF can be defined as the blood volume travelling through a given amount of brain tissue in a given amount of time. All methodologies require the use of a tracer, whether introduced or endogenous, diffusible or intravascular with the various imaging modalities that include positron emission tomography (PET), Xe-enhanced computed tomography (XeCT), perfusion CT (PCT), and magnetic resonance imaging (MRI).

PET is diagnostic tool that provides quantitative information on a variety of hemodynamic parameters such as CBF, cerebral blood volume (CBV), OEF and glucose metabolism. PET has evolved to be considered the gold standard for studying cerebral hemodynamics. Tracers are being used for CBF measurements are $^{15}\text{O}_2$, C^{15}O_2 and H_2^{15}O .¹⁰³ The other tracer is ^{18}F in fluorodeoxyglucose which is used to monitor glucose consumption in cancer evaluation.¹⁰⁴ Data acquisition takes typically 5-10 minutes and it takes another 5-10 minutes to obtain a processed CBF map. The main advantage of PET is the accuracy and reproducibility of its results. However, PET imaging involves the injection of radioactive tracers, which limits its repeatability and application in healthy volunteers. Among other limitations are low temporal and spatial resolution, low signal-to-noise ratio (SNR), as well as the requirement for a cyclotron. PET allows quantification of CBF by measuring either the delivery or clearance of radioactively labeled water. To measure the delivery of the agent with PET, ^{15}O -labeled water is injected into the subject's blood stream and emission data is acquired. To measure agent clearance, the subject breathes ^{15}O -labeled CO_2 . When CO_2 is absorbed in the blood, the ^{15}O exchanges with oxygen of water, and this ^{15}O -labeled water perfuse the brain tissue. Upon cessation of the CO_2 inhalation, the clearance of the agent is measured several minutes. Tracer clearance occurs by radioactive decay of the labeled water and physical clearance by means of the local blood flow.

XeCT is a diffusible tracer technique that provides quantitative CBF by administering Xe via inhalation and using the time-dependent concentration of Xe in tissue as a measure of perfusion. After Xe is inhaled, it crosses the blood-brain barrier and diffuses into cerebral tissue.¹⁰⁵ CBF is then measured by determining the Xe clearance rate from the brain using the Kety-Schmidt model¹⁰⁶, which describes the relationship of CBF to the tracer blood/brain partition coefficient and tracer concentration in the brain and arterial blood. Because XeCT requires specialized equipment, is expensive, and necessitates that an anesthetist be present during the procedure¹⁰⁷, perfusion CT (PCT) is more often used clinically.

PCT measurements depend on the injection rate and cardiac output¹⁰⁸ and have proven to be clinically useful for analysis of CBF, CBV, and mean transit time.¹⁰⁹ When

combined with acetazolamide, perfusion CT can yield analysis of the cerebral vascular reserve (CVR), thus enabling an extensive evaluation of cerebral hemodynamics.¹¹⁰ PCT can accurately give a quantitative index of CBF that is comparable with the gold standard, PET. Compared with PET, PCT provides for shorter examination times¹¹¹, offers higher spatial resolution¹⁰³, and provides a simple acquisition.

The two types of MRI measurement of blood flow are arterial spin labeling (ASL) MRI¹¹² and dynamic susceptibility contrast (DSC) MRI¹¹³. In DSC imaging a paramagnetic material such as gadolinium-DTPA produces dephasing in a small area around the tracer in its first pass and as it moves in vessels it affects the T_2^* in adjoining tissues. Perfusion can be measured based on the change in the MR signal. To measure absolute quantitative values, the arterial input function (AIF) is required. AIF is the concentration-time curve of the tracer in the artery supplying the tissue. The technique requires fast imaging sequences such as echo planar imaging (EPI). Images are taken in the rate of 500 ms to 2 seconds per single image. The major drawback to produce quantifiable data is the lack of robust arterial input and venous output functions. The difficulties with obtaining robust measurements of arterial or venous curves in perfusion MRI relate back to the problems of signal-to-noise, image contrast, spatial resolution. ASL uses water as an endogenous diffusible tracer. In this technique, arterial blood water protons are labeled proximal to the region of interest by applying radiofrequency pulses to invert the spins. The labeled water then travels throughout the vasculature into the capillary bed, where it exchanges with tissue water. Thus the tissue water is partially saturated when the voxel is imaged, causing a reduction in the signal intensity proportional to the amount of labeled water in that voxel. By subtracting the labeled image from a control image, in which there is no labeling of water spins, the relative CBF can be determined for each voxel in the imaging plane. The difference between labeled and control acquisitions is about 1% of the control signal intensity. The method suffers from low signal to noise ratio.

Bedside techniques for monitoring CBF include transcranial Doppler (TCD) ultrasonography¹¹⁴, and thermal diffusion¹¹⁵ and laser Doppler flowmetries.¹¹⁶ However, TCD ultrasonography is used for global CBF investigation and limited to observations of

large vessel flow velocities, which do not necessarily reflect microvascular perfusion in patients with cerebrovascular disease¹¹⁷, and both thermal diffusion and laser Doppler flowmetries are invasive. Furthermore, one technique that is commonly used in animal studies makes use of microspheres. Microspheres are small polymer or ceramic beads, typically labeled with radioactive material, which are injected into the blood stream. By creating microspheres that are smaller than the diameter of arterioles, but larger than the capillary diameter, the microspheres become trapped in the capillary bed. In animal models, the tissue can be sectioned, and the detected radioactivity from each tissue section is proportional to the CBF.

Optical methods are promising alternatives to these current techniques since they are safe, the instruments are compact, portable and can provide physiological measurements at the bedside of patients. The methods employed for measuring CBF and CMRO₂ in this thesis rely on the administration of a non-diffusible, intravascular tracer. Consequently a review of the theory behind this technique is warranted.

1.7.2 Cerebral Blood Flow Measurement by NIRS

The NIRS technique presented in this thesis to measure hemodynamic information rely on a bolus injection of a contrast agent. The transport of the tracer through the microvasculature of the tissue can be described by constructing a kinetic model and applying it to time-dependent measurements of the tracer concentration. For example, blood flow in brain, *CBF*, can be calculated using an intravascular tracer if the time-dependent concentration of tracer in the brain, $Q(t)$, in the arterial and the venous blood draining the brain, $C_a(t)$ and $C_v(t)$, are measured. In this case, the following expression describes the dynamic behaviour of the tracer

$$Q(t) = CBF \cdot \left[\int_0^t C_a(t) \cdot dt - \int_0^t C_v(t) \cdot dt \right] \quad (1-5)$$

where t represents a dummy time variable to integrate over. Application of equation (1-5) for calculation of CBF is hindered by difficulties associated with measuring $C_v(t)$. Tissue

vascular bed can be considered as a mesh of microvessels supplied by a single input and draining to a single output, where each possible path from the artery to the vein has a specific transit time (amount of time required for tracer to travel from input to output in the tissue region of interest (ROI)). In this case, the concentration of tracer in the tissue at a given time point is a function of its collective path through the capillary bed, as well as the arterial input function. By definition, $h(t)$ is the distribution of transit times of the system. Based on this theory, the venous output can be represented as follows:

$$C_v(t) = \int_0^t C_a(u)h(t-u)du \quad (1-6)$$

where u is a dummy variable in the convolution. Equation of (1-5) can be rearranged as follows:

$$\frac{dQ(t)}{dt} = CBF \cdot (C_a(t) - C_a(t) * h(t)) \quad (1-7)$$

where $*$ represents the convolution operator. The impursed residue function, $R(t)$, can be defined as follows:

$$R(t) = 1 - \int_0^t h(s)ds \quad (1-8)$$

and is the proportion of tracer in the system as a function of time when an impulse function is the input. Substituting $R(t)$ for $h(t)$, equation (1-7) can be rewritten:

$$Q(t) = C_a(t) * [CBF \cdot R(t)] \quad (1-9)$$

$Q(t)$ and $C_a(t)$ are the amount of ICG in the brain and arterial blood, respectively, and $[CBF \cdot R(t)]$ is the flow-scaled impulse residue function or $R(t)$. The function $CBF \cdot R(t)$ can be extracted from the arterial and tissue contrast concentration curves using a deconvolution algorithm.¹¹⁸ The initial height of the derived function is CBF, since by definition $R(0)=1$, and the area under the curve is the cerebral blood volume (CBV).¹¹⁹

1.7.3 Cerebral Metabolic Rate of Oxygen Measurement by NIRS

Measurements of $CMRO_2$ were calculated¹²⁰ using Fick's principle as follows:

$$CMRO_2 = CBF \cdot ([O_2]_a - [O_2]_v) \quad (1-10)$$

The difference between the arterial concentration of oxygen, $[O_2]_a$, and the cerebral venous concentration of oxygen, $[O_2]_v$, is commonly referred to as the arterial-venous difference of oxygen (AVDO₂), or the difference between the O₂ concentration of the arterial blood feeding the tissue of interest and O₂ concentration of the venous blood draining the tissue of interest. Equation (1-10) can be further expanded as follows¹²¹:

$$CMRO_2 = CBF \cdot 1.39 \cdot [tHb] \cdot (S_aO_2 - S_vO_2) \quad (1-11)$$

where $[tHb]$ is total hemoglobin concentration which can be measured from arterial blood samples. S_aO_2 and S_vO_2 are arterial and venous O₂ saturation, respectively. The constant 1.39 is the O₂ carrying capacity of hemoglobin measured in milliliters per gram of Hb. Note that the dye densitometer also provides continuous measurements of S_aO_2 , while S_vO_2 was determined indirectly from the NIRS measurements of average tissue cerebral blood oxygen saturation, $(SO_2)_{tissue}$. This technique relies on the assumption that there exists a stable arterial-venous blood ratio in the CBV, i.e.

$$(SO_2)_{tissue} = \alpha S_aO_2 + (1 - \alpha) S_vO_2 \quad (1-12)$$

where α represents the fraction of arterial blood in CBV. The relative distribution of arterial and venous compartments is generally accepted to be approximately 25% and 75% in the total CBV, therefore to measure S_vO_2 , α was set to 0.25.^{122, 123} To obtain tissue cerebral blood oxygen saturation, i.e., $(SO_2)_{tissue}$, cerebral hemoglobin (HbO₂, Hb) concentrations can be calculated with the NIRS technique. $(SO_2)_{tissue}$ can then be calculated as follows:

$$(SO_2)_{tissue} = \frac{HbO_2}{HbO_2 + Hb}. \quad (1-13)$$

Using this relationship, a new expression for $CMRO_2$ can be derived that is independent of S_vO_2 :

$$CMRO_2 = CBF \cdot 1.39 \cdot [tHb] \cdot \left(\frac{S_aO_2 - (SO_2)_{tissue}}{1 - \alpha} \right) \quad (1-14)$$

The fraction of oxygen extracted from arterial blood into the brain, OEF, can be calculated with the method described by Brown *et al*¹²⁰:

$$OEF = \frac{CMRO_2}{CBF \cdot [O_2]_a}. \quad (1-15)$$

The tight coupling of CBF and $CMRO_2$ in the normal brain leads to a fixed level of OEF around ~33%.¹²⁴ A decoupling of the two, signifies oxidative stress, as in ischemia, and would lead to an increase in OEF beyond the normal value of ~33%.¹²⁵

1.8 Thesis objectives

The objectives of the work presented in this thesis are to develop a neuroprotection method for neurological emergencies by inducing brain hypothermia quickly and selectively to avoid adverse complications from whole body cooling and NIRS methods for monitoring the brain temperature and neuroprotective effects of hypothermia during cooling.

This work comprised of the following projects whose goals are to

- (i). Develop an effective, safe, simple and fast nasopharyngeal cooling method to selectively reduce and maintain brain temperature in the range of mild hypothermia (32-35°C) while maintaining the whole body (rectal) temperature above 35°C.

- (ii). Develop a TR-NIR technique to measure local brain temperature which can be used at the bedside of patients.
- (iii). Evaluate the utility of TR-NIR for measuring cerebral blood flow (CBF) and cerebral metabolic rate of oxygen (CMRO₂) and in particular their ratio oxygen extraction efficiency (OEF) as a surrogate marker of oxidation status of the brain during hypothermia and investigates the effects of different anesthetic regimes and temperatures on CMRO₂:CBF in the normal brain.

1.9 References

1. Kurinczuk JJ, White-Koning M, Badawi N. Epidemiology of neonatal encephalopathy and hypoxic-ischaemic encephalopathy. *Early Hum Dev.* 2010;86:329-338
2. Lawn JE, Cousens S, Zupan J. 4 million neonatal deaths: When? Where? Why? *Lancet.* 2005;365:891-900
3. Al-Macki N, Miller SP, Hall N, Shevell M. The spectrum of abnormal neurologic outcomes subsequent to term intrapartum asphyxia. *Pediatr Neurol.* 2009;41:399-405
4. Derrick M, Drobyshevsky A, Ji X, Tan S. A model of cerebral palsy from fetal hypoxia-ischemia. *Stroke.* 2007;38:731-735
5. Verklan MT. The chilling details: Hypoxic-ischemic encephalopathy. *J Perinat Neonatal Nurs.* 2009;23:59-68; quiz 69-70
6. Johnston MV, Trescher WH, Ishida A, Nakajima W. Neurobiology of hypoxic-ischemic injury in the developing brain. *Pediatr Res.* 2001;49:735-741
7. Barks JD, Silverstein FS. Excitatory amino acids contribute to the pathogenesis of perinatal hypoxic-ischemic brain injury. *Brain Pathol.* 1992;2:235-243
8. Lai MC, Yang SN. Perinatal hypoxic-ischemic encephalopathy. *J Biomed Biotechnol.* 2011;2011:609813
9. Ankarcrona M, Dypbukt JM, Bonfoco E, Zhivotovsky B, Orrenius S, Lipton SA, Nicotera P. Glutamate-induced neuronal death: A succession of necrosis or apoptosis depending on mitochondrial function. *Neuron.* 1995;15:961-973

10. Iadecola C, Anrather J. Stroke research at a crossroad: Asking the brain for directions. *Nat Neurosci.* 2011;14:1363-1368
11. Northington FJ, Ferriero DM, Martin LJ. Neurodegeneration in the thalamus following neonatal hypoxia-ischemia is programmed cell death. *Dev Neurosci.* 2001;23:186-191
12. Cerio F. Neuroprotective therapies after perinatal hypoxic-ischemic brain injury. *Brain Sci.* 2013;3
13. Spandou E, Soubasi V, Papoutsopoulou S, Augoustides-Savvopoulou P, Loizidis T, Pazaiti A, Karkavelas G, Guiba-Tziampiri O. Neuroprotective effect of long-term mgso4 administration after cerebral hypoxia-ischemia in newborn rats is related to the severity of brain damage. *Reprod Sci.* 2007;14:667-677
14. Petzelt CP, Kodirov S, Taschenberger G, Kox WJ. Participation of the ca(2+)-calmodulin-activated kinase ii in the control of metaphase-anaphase transition in human cells. *Cell Biol Int.* 2001;25:403-409
15. Hobbs C, Thoresen M, Tucker A, Aquilina K, Chakkarapani E, Dingley J. Xenon and hypothermia combine additively, offering long-term functional and histopathologic neuroprotection after neonatal hypoxia/ischemia. *Stroke.* 2008;39:1307-1313
16. Chakkarapani E, Thoresen M, Hobbs CE, Aquilina K, Liu X, Dingley J. A closed-circuit neonatal xenon delivery system: A technical and practical neuroprotection feasibility study in newborn pigs. *Anesth Analg.* 2009;109:451-460
17. Gonzalez FF, McQuillen P, Mu D, Chang Y, Wendland M, Vexler Z, Ferriero DM. Erythropoietin enhances long-term neuroprotection and neurogenesis in neonatal stroke. *Dev Neurosci.* 2007;29:321-330
18. Gonzalez FF, Ferriero DM. Therapeutics for neonatal brain injury. *Pharmacol Ther.* 2008;120:43-53
19. Elmahdy H, El-Mashad AR, El-Bahrawy H, El-Gohary T, El-Barbary A, Aly H. Human recombinant erythropoietin in asphyxia neonatorum: Pilot trial. *Pediatrics.* 2010;125:e1135-1142
20. Nijboer CH, Groenendaal F, Kavelaars A, Hagberg HH, van Bel F, Heijnen CJ. Gender-specific neuroprotection by 2-iminobiotin after hypoxia-ischemia in the neonatal rat via a nitric oxide independent pathway. *J Cereb Blood Flow Metab.* 2007;27:282-292

21. van Velthoven CT, Kavelaars A, van Bel F, Heijnen CJ. Regeneration of the ischemic brain by engineered stem cells: Fuelling endogenous repair processes. *Brain Res Rev.* 2009;61:1-13
22. Azzopardi D, Strohm B, Edwards AD, Halliday H, Juszczak E, Levene M, Thoresen M, Whitelaw A, Brocklehurst P, Steering G, participants TCR. Treatment of asphyxiated newborns with moderate hypothermia in routine clinical practice: How cooling is managed in the uk outside a clinical trial. *Arch Dis Child Fetal Neonatal Ed.* 2009;94:F260-264
23. Guidelines for the management of severe traumatic brain injury. *J Neurotrauma.* 2007;24 Suppl 1:S1-106
24. Thoresen M. Supportive care during neuroprotective hypothermia in the term newborn: Adverse effects and their prevention. *Clin Perinatol.* 2008;35:749-763, vii
25. Lampe JW, Becker LB. State of the art in therapeutic hypothermia. *Annu Rev Med.* 2011;62:79-93
26. Rosomoff HL, Holaday DA. Cerebral blood flow and cerebral oxygen consumption during hypothermia. *Am J Physiol.* 1954;179:85-88
27. Polderman KH. Mechanisms of action, physiological effects, and complications of hypothermia. *Crit Care Med.* 2009;37:S186-202
28. Globus MY, Alonso O, Dietrich WD, Busto R, Ginsberg MD. Glutamate release and free radical production following brain injury: Effects of posttraumatic hypothermia. *J Neurochem.* 1995;65:1704-1711
29. Baker AJ, Zornow MH, Grafe MR, Scheller MS, Skilling SR, Smullin DH, Larson AA. Hypothermia prevents ischemia-induced increases in hippocampal glycine concentrations in rabbits. *Stroke.* 1991;22:666-673
30. Warner DS. Pharmacologic protection from ischemic neuronal injury. *J Neurosurg Anesthesiol.* 2004;16:95-97
31. Yamashita K, Eguchi Y, Kajiwara K, Ito H. Mild hypothermia ameliorates ubiquitin synthesis and prevents delayed neuronal death in the gerbil hippocampus. *Stroke.* 1991;22:1574-1581
32. Schmidt OI, Heyde CE, Ertel W, Stahel PF. Closed head injury--an inflammatory disease? *Brain Res Brain Res Rev.* 2005;48:388-399

33. Kimura A, Sakurada S, Ohkuni H, Todome Y, Kurata K. Moderate hypothermia delays proinflammatory cytokine production of human peripheral blood mononuclear cells. *Crit Care Med.* 2002;30:1499-1502
34. Adachi M, Sohma O, Tsuneishi S, Takada S, Nakamura H. Combination effect of systemic hypothermia and caspase inhibitor administration against hypoxic-ischemic brain damage in neonatal rats. *Pediatr Res.* 2001;50:590-595
35. Ning XH, Chen SH, Xu CS, Li L, Yao LY, Qian K, Krueger JJ, Hytti OM, Portman MA. Hypothermic protection of the ischemic heart via alterations in apoptotic pathways as assessed by gene array analysis. *J Appl Physiol (1985).* 2002;92:2200-2207
36. Smith SL, Hall ED. Mild pre- and posttraumatic hypothermia attenuates blood-brain barrier damage following controlled cortical impact injury in the rat. *J Neurotrauma.* 1996;13:1-9
37. Steinberg GK, Ogilvy CS, Shuer LM, Connolly ES, Jr., Solomon RA, Lam A, Kassell NF, Baker CJ, Giannotta SL, Cockroft KM, Bell-Stephens TE, Allgren RL. Comparison of endovascular and surface cooling during unruptured cerebral aneurysm repair. *Neurosurgery.* 2004;55:307-314; discussion 314-305
38. Keller E, Imhof HG, Gasser S, Terzic A, Yonekawa Y. Endovascular cooling with heat exchange catheters: A new method to induce and maintain hypothermia. *Intensive Care Med.* 2003;29:939-943
39. Culic S. Cold injury syndrome and neurodevelopmental changes in survivors. *Arch Med Res.* 2005;36:532-538
40. Sarkar S, Barks JD. Systemic complications and hypothermia. *Semin Fetal Neonatal Med.* 2010;15:270-275
41. Greene PS, Cameron DE, Mohlala ML, Dinatale JM, Gardner TJ. Systolic and diastolic left ventricular dysfunction due to mild hypothermia. *Circulation.* 1989;80:III44-48
42. Okada M. The cardiac rhythm in accidental hypothermia. *J Electrocardiol.* 1984;17:123-128
43. Ilija R, Ovsyshcher I, Rudnik L, Gueron M. Atypical ventricular tachycardia and alternating osborn waves induced by spontaneous mild hypothermia. *Pediatr Cardiol.* 1988;9:63-65
44. McIntyre LA, Fergusson DA, Hebert PC, Moher D, Hutchison JS. Prolonged therapeutic hypothermia after traumatic brain injury in adults: A systematic review. *JAMA.* 2003;289:2992-2999

45. Mathur NB, Krishnamurthy S, Mishra TK. Evaluation of who classification of hypothermia in sick extramural neonates as predictor of fatality. *J Trop Pediatr.* 2005;51:341-345
46. Cheng H, Shi J, Zhang L, Zhang Q, Yin H, Wang L. Epidural cooling for selective brain hypothermia in porcine model. *Acta Neurochir (Wien).* 2006;148:559-564; discussion 564
47. Wang H, Olivero W, Lanzino G, Elkins W, Rose J, Honings D, Rodde M, Burnham J, Wang D. Rapid and selective cerebral hypothermia achieved using a cooling helmet. *J Neurosurg.* 2004;100:272-277
48. Liu WG, Qiu WS, Zhang Y, Wang WM, Lu F, Yang XF. Effects of selective brain cooling in patients with severe traumatic brain injury: A preliminary study. *J Int Med Res.* 2006;34:58-64
49. Wang Y. Neck and brain temperature distributions for selectively cooling the arterial blood with an interstitial cooling device. 2008;PhD
50. Dohi K, Jimbo H, Abe T, Aruga T. Positive selective brain cooling method: A novel, simple, and selective nasopharyngeal brain cooling method. *Acta Neurochir Suppl.* 2006;96:409-412
51. Covaciu L, Allers M, Enblad P, Lunderquist A, Wieloch T, Rubertsson S. Intranasal selective brain cooling in pigs. *Resuscitation.* 2008;76:83-88
52. Boller M, Lampe JW, Katz JM, Barbut D, Becker LB. Feasibility of intra-arrest hypothermia induction: A novel nasopharyngeal approach achieves preferential brain cooling. *Resuscitation.* 2010;81:1025-1030
53. Chemicals Management Division of Environment Canada. List of toxic substances managed under cepa (schedule 1), available at: [Http://www.Ec.Gc.Ca/toxiques-toxics/default.Asp?Lang=en&n=98e80cc6-1&xml=aa329670-c3c7-4ad5-a7ab-5fd8a05439f1](http://www.Ec.Gc.Ca/toxiques-toxics/default.Asp?Lang=en&n=98e80cc6-1&xml=aa329670-c3c7-4ad5-a7ab-5fd8a05439f1). 2005;2013
54. Povlishock JT, Wei EP. Posthypothermic rewarming considerations following traumatic brain injury. *J Neurotrauma.* 2009;26:333-340
55. Suehiro E, Povlishock JT. Exacerbation of traumatically induced axonal injury by rapid posthypothermic rewarming and attenuation of axonal change by cyclosporin a. *J Neurosurg.* 2001;94:493-498
56. Vaagenes P, Gundersen Y, Opstad PK. Rapid rewarming after mild hypothermia accentuates the inflammatory response after acute volume controlled haemorrhage in spontaneously breathing rats. *Resuscitation.* 2003;58:103-112

57. Kawahara F, Kadoi Y, Saito S, Goto F, Fujita N. Slow rewarming improves jugular venous oxygen saturation during rewarming. *Acta Anaesthesiol Scand.* 2003;47:419-424
58. Shiozaki T, Sugimoto H, Taneda M, Yoshida H, Iwai A, Yoshioka T, Sugimoto T. Effect of mild hypothermia on uncontrollable intracranial hypertension after severe head injury. *J Neurosurg.* 1993;79:363-368
59. Enomoto S, Hindman BJ, Dexter F, Smith T, Cutkomp J. Rapid rewarming causes an increase in the cerebral metabolic rate for oxygen that is temporarily unmatched by cerebral blood flow. A study during cardiopulmonary bypass in rabbits. *Anesthesiology.* 1996;84:1392-1400
60. Cairns CJ, Andrews PJ. Management of hyperthermia in traumatic brain injury. *Curr Opin Crit Care.* 2002;8:106-110
61. McIlvoy L. Comparison of brain temperature to core temperature: A review of the literature. *J Neurosci Nurs.* 2004;36:23-31
62. Rumana CS, Gopinath SP, Uzura M, Valadka AB, Robertson CS. Brain temperature exceeds systemic temperature in head-injured patients. *Crit Care Med.* 1998;26:562-567
63. Childs C. Human brain temperature: Regulation, measurement and relationship with cerebral trauma: Part 1. *Br J Neurosurg.* 2008;22:486-496
64. Kirk D, Rainey T, Vail A, Childs C. Infra-red thermometry: The reliability of tympanic and temporal artery readings for predicting brain temperature after severe traumatic brain injury. *Crit Care.* 2009;13:R81
65. Ear thermometer, figure is adopted from: [Http://www.Drugs.Com/cg/how-to-take-an-ear-temperature.Html](http://www.Drugs.Com/cg/how-to-take-an-ear-temperature.Html).
66. Fox RH, Solman AJ. A new technique for monitoring the deep body temperature in man from the intact skin surface. *J Physiol.* 1971;212:8P-10P
67. Dittmar A, Gehin C, Delhomme G, Boivin D, Dumont G, Mott C. A non invasive wearable sensor for the measurement of brain temperature. *Conf Proc IEEE Eng Med Biol Soc.* 2006;1:900-902
68. Zeiner A, Klewer J, Sterz F, Haugk M, Krizanac D, Testori C, Losert H, Ayati S, Holzer M. Non-invasive continuous cerebral temperature monitoring in patients treated with mild therapeutic hypothermia: An observational pilot study. *Resuscitation.* 2010;81:861-866

69. Teunissen LP, Klewer J, de Haan A, de Koning JJ, Daanen HA. Non-invasive continuous core temperature measurement by zero heat flux. *Physiol Meas.* 2011;32:559-570
70. Brajkovic D, Ducharme MB. Confounding factors in the use of the zero-heat-flow method for non-invasive muscle temperature measurement. *Eur J Appl Physiol.* 2005;94:386-391
71. Rieke V, Butts Pauly K. Mr thermometry. *J Magn Reson Imaging.* 2008;27:376-390
72. Kuroda K. Non-invasive mr thermography using the water proton chemical shift. *Int J Hyperthermia.* 2005;21:547-560
73. Weis J, Covaciu L, Rubertsson S, Allers M, Lunderquist A, Ortiz-Nieto F, Ahlstrom H. Phase-difference and spectroscopic imaging for monitoring of human brain temperature during cooling. *Magnetic resonance imaging.* 2012
74. Rieke V, Vigen KK, Sommer G, Daniel BL, Pauly JM, Butts K. Referenceless pfr shift thermometry. *Magn Reson Med.* 2004;51:1223-1231
75. Leroy Y. Microwave radiometry and thermography: Present and prospective. *Prog Clin Biol Res.* 1982;107:485-499
76. Karathanasis KT, Gouzouasis IA, Karanasiou IS, Giamalaki MI, Stratakos G, Uzunoglu NK. Noninvasive focused monitoring and irradiation of head tissue phantoms at microwave frequencies. *IEEE Trans Inf Technol Biomed.* 2010;14:657-663
77. Han JW, Van Leeuwen GM, Mizushina S, Van de Kamer JB, Maruyama K, Sugiura T, Azzopardi DV, Edwards AD. Monitoring of deep brain temperature in infants using multi-frequency microwave radiometry and thermal modelling. *Phys Med Biol.* 2001;46:1885-1903
78. Levick A, Land D, Hand J. Validation of microwave radiometry for measuring the internal temperature profile of human tissue. *Meas. Sci. Technol.* 2011;22
79. Sun Z, Ying H. A multi-gate time-of-flight technique for estimation of temperature distribution in heated tissue: Theory and computer simulation. *Ultrasonics.* 1999;37:107-122
80. Towa RT, Miller RJ, Frizzell LA, Zachary JF, O'Brien WD, Jr. Attenuation coefficient and propagation speed estimates of rat and pig intercostal tissue as a function of temperature. *IEEE Trans Ultrason Ferroelectr Freq Control.* 2002;49:1411-1420

81. Fatar M, Stroick M, Griebe M, Alonso A, Hennerici MG, Daffertshofer M. Brain temperature during 340-khz pulsed ultrasound insonation: A safety study for sonothrombolysis. *Stroke*. 2006;37:1883-1887
82. Biomedical optics laboratory, university of london, "specific extinction spectra of tissue chromophores," available from: [Http://www.Medphys.Ucl.Ac.Uk/research/borl/research/nir_topics/spectra/spectra.Htm](http://www.Medphys.Ucl.Ac.Uk/research/borl/research/nir_topics/spectra/spectra.Htm).
83. Cope M. The development of a near infrared spectroscopy system and its application for non-invasive monitoring of cerebral blood and tissue oxygenation in the newborn infant. *PhD thesis, University of London, London*. 1991
84. Wang R. Modelling optical properties of soft tissue by fractal distribution of scatterers. *J Mod Opt*. 2000;47
85. Woodard HQ, White DR. The composition of body tissues. *Br J Radiol*. 1986;59:1209-1218
86. Ganong W. *Review of medical physiology*. 2003.
87. Sfareni R, Boffi A, Quaresima V, Ferrari M. Near infrared absorption spectra of human deoxy- and oxyhaemoglobin in the temperature range 20-40 degrees c. *Biochim Biophys Acta*. 1997;1340:165-169
88. Cordone L, Cupane A, Leone M, Vitrano E. Optical absorption spectra of deoxy- and oxyhemoglobin in the temperature range 300-20 k. Relation with protein dynamics. *Biophys Chem*. 1986;24:259-275
89. Patterson MS, Chance B, Wilson BC. Time resolved reflectance and transmittance for the non-invasive measurement of tissue optical properties. *Appl Opt*. 1989;28:2331-2336
90. Pogue BW, Patterson MS. Frequency-domain optical absorption spectroscopy of finite tissue volumes using diffusion theory. *Phys Med Biol*. 1994;39:1157-1180
91. Farrell TJ, Patterson MS, Wilson B. A diffusion theory model of spatially resolved, steady-state diffuse reflectance for the noninvasive determination of tissue optical properties in vivo. *Med Phys*. 1992;19:879-888
92. Delpy DT, Cope, M. Quantification in tissue near-infrared spectroscopy. *Phil. Trans. R. Soc. Lond. B*. 1997;352:649-659
93. Matcher SJ, Kirkpatrick, P., Nahid, K., Cope, M. & Delpy, D. T. Absolute quantification methods in tissue near infrared spectroscopy. *Proc. SPIE 2389*, 486-495. 1995

94. Cooper CE, Elwell CE, Meek JH, Matcher SJ, Wyatt JS, Cope M, Delpy DT. The noninvasive measurement of absolute cerebral deoxyhemoglobin concentration and mean optical path length in the neonatal brain by second derivative near infrared spectroscopy. *Pediatr Res*. 1996;39:32-38
95. Boas DA, O'Leary MA, Chance B, Yodh AG. Scattering of diffuse photon density waves by spherical inhomogeneities within turbid media: Analytic solution and applications. *Proc Natl Acad Sci U S A*. 1994;91:4887-4891
96. Hollis VS, T. B, T. DD. Non-invasive monitoring of brain tissue temperature by near-infrared spectroscopy. *Proceedings of SPIE*. 2001;4250:470-481
97. Chung SH, Cerussi AE, Merritt SI, Ruth J, Tromberg BJ. Non-invasive tissue temperature measurements based on quantitative diffuse optical spectroscopy (dos) of water. *Phys Med Biol*. 2010;55:3753-3765
98. Chung SH, Mehta R, Tromberg BJ, Yodh AG. Non-invasive measurement of deep tissue temperature changes caused by apoptosis during breast cancer neoadjuvant chemotherapy: A case study. *J Innov Opt Health Sci*. 2011;4:361-372
99. Erecinska M, Thoresen M, Silver IA. Effects of hypothermia on energy metabolism in mammalian central nervous system. *J Cereb Blood Flow Metab*. 2003;23:513-530
100. Sakoh M, Gjedde A. Neuroprotection in hypothermia linked to redistribution of oxygen in brain. *Am J Physiol Heart Circ Physiol*. 2003;285:H17-25
101. Ehrlich MP, McCullough JN, Zhang N, Weisz DJ, Juvonen T, Bodian CA, Griep RB. Effect of hypothermia on cerebral blood flow and metabolism in the pig. *Ann Thorac Surg*. 2002;73:191-197
102. van der Linden J, Ekroth R, Lincoln C, Pugsley W, Scallan M, Tyden H. Is cerebral blood flow/metabolic mismatch during rewarming a risk factor after profound hypothermic procedures in small children? *Eur J Cardiothorac Surg*. 1989;3:209-215
103. Kudo K, Terae S, Katoh C, Oka M, Shiga T, Tamaki N, Miyasaka K. Quantitative cerebral blood flow measurement with dynamic perfusion ct using the vascular-pixel elimination method: Comparison with h2(15)o positron emission tomography. *AJNR Am J Neuroradiol*. 2003;24:419-426
104. Wintermark M, Sesay M, Barbier E, Borbely K, Dillon WP, Eastwood JD, Glenn TC, Grandin CB, Pedraza S, Soustiel JF, Nariai T, Zaharchuk G, Caille JM, Dousset V, Yonas H. Comparative overview of brain perfusion imaging techniques. *Stroke*. 2005;36:e83-99

105. Sase S, Honda M, Machida K, Seiki Y. Comparison of cerebral blood flow between perfusion computed tomography and xenon-enhanced computed tomography for normal subjects: Territorial analysis. *J Comput Assist Tomogr.* 2005;29:270-277
106. Kety SS. The theory and applications of the exchange of inert gas at the lungs and tissues. *Pharmacol Rev.* 1951;3:1-41
107. Mullins ME. Stroke imaging with xenon-ct. *Semin Ultrasound CT MR.* 2006;27:219-220
108. Kang KH, Kim HS, Kim SY. Quantitative cerebrovascular reserve measured by acetazolamide-challenged dynamic ct perfusion in ischemic adult moyamoya disease: Initial experience with angiographic correlation. *AJNR Am J Neuroradiol.* 2008;29:1487-1493
109. Coles JP. Imaging after brain injury. *Br J Anaesth.* 2007;99:49-60
110. Vagal AS, Leach JL, Fernandez-Ulloa M, Zuccarello M. The acetazolamide challenge: Techniques and applications in the evaluation of chronic cerebral ischemia. *AJNR Am J Neuroradiol.* 2009;30:876-884
111. Kamath A, Smith WS, Powers WJ, Cianfoni A, Chien JD, Videen T, Lawton MT, Finley B, Dillon WP, Wintermark M. Perfusion ct compared to h(2) (15)o/o (15)o pet in patients with chronic cervical carotid artery occlusion. *Neuroradiology.* 2008;50:745-751
112. Liu TT, Brown GG. Measurement of cerebral perfusion with arterial spin labeling: Part 1. Methods. *J Int Neuropsychol Soc.* 2007;13:517-525
113. Dittrich R, Kloska SP, Fischer T, Nam E, Ritter MA, Seidensticker P, Heindel W, Nabavi DG, Ringelstein EB. Accuracy of perfusion-ct in predicting malignant middle cerebral artery brain infarction. *J Neurol.* 2008;255:896-902
114. Evans DH. Doppler ultrasound and the neonatal cerebral circulation: Methodology and pitfalls. *Biol Neonate.* 1992;62:271-279
115. Vajkoczy P, Roth H, Horn P, Lucke T, Thome C, Hubner U, Martin GT, Zapletal C, Klar E, Schilling L, Schmiedek P. Continuous monitoring of regional cerebral blood flow: Experimental and clinical validation of a novel thermal diffusion microprobe. *J Neurosurg.* 2000;93:265-274
116. Kirkpatrick PJ, Smielewski P, Czosnyka M, Pickard JD. Continuous monitoring of cortical perfusion by laser doppler flowmetry in ventilated patients with head injury. *J Neurol Neurosurg Psychiatry.* 1994;57:1382-1388

117. Reinhard M, Wehrle-Wieland E, Grabiak D, Roth M, Guschlbauer B, Timmer J, Weiller C, Hetzel A. Oscillatory cerebral hemodynamics--the macro- vs. Microvascular level. *J Neurol Sci.* 2006;250:103-109
118. Cenic A, Nabavi DG, Craen RA, Gelb AW, Lee TY. Dynamic ct measurement of cerebral blood flow: A validation study. *AJNR Am J Neuroradiol.* 1999;20:63-73
119. Zierler KL. Equations for measuring blood flow by external monitoring of radioisotopes. *Circ Res.* 1965;16:309-321
120. Brown DW, Hadway J, Lee TY. Near-infrared spectroscopy measurement of oxygen extraction fraction and cerebral metabolic rate of oxygen in newborn piglets. *Pediatr Res.* 2003;54:861-867
121. Roche-Labarbe N, Carp SA, Surova A, Patel M, Boas DA, Grant PE, Franceschini MA. Noninvasive optical measures of cbv, sto(2), cbf index, and rcmro(2) in human premature neonates' brains in the first six weeks of life. *Hum Brain Mapp.* 2010;31:341-352
122. Mchedlishvili G. Arterial behavior and blood circulation in the brain. *New York: Consultants Bureau.* 1986
123. Watzman HM, Kurth CD, Montenegro LM, Rome J, Steven JM, Nicolson SC. Arterial and venous contributions to near-infrared cerebral oximetry. *Anesthesiology.* 2000;93:947-953
124. Nozari A, Rubertsson S, Gedeberg R, Nordgren A, Wiklund L. Maximisation of cerebral blood flow during experimental cardiopulmonary resuscitation does not ameliorate post-resuscitation hypoperfusion. *Resuscitation.* 1999;40:27-35
125. Powers WJ. Cerebral hemodynamics in ischemic cerebrovascular disease. *Ann Neurol.* 1991;29:231-240
126. Kamme F. Biphasic expression of the fos and jun families of transcription factors following transient forebrain ischaemia in the rat. Effect of hypothermia. *European Journal of Neuroscience.* 1995;7:2007-2016

Chapter 2

Feasibility of Selective Brain Cooling Using a Nasopharyngeal Method in Piglets

This chapter is adapted from the work entitled “Feasibility of Selective Brain Cooling Using a Nasopharyngeal Method in Piglets” by M Fazel Bakhsheshi, EE Stewart, JH Tai, L Keenlside and TY Lee, submitted to the *Journal of Critical Care Medicine*. The focus of this paper is to investigate the feasibility of cooling selectively the brain of normal new-born piglets with developed temperature regulation by spraying normal or humidified cooled air into the nasal cavities.

2. Introduction

Clinical investigators have reported that mild and moderate hypothermia can be neuroprotective to reduce brain injury and decrease death and disability for a variety of acute brain injuries following severe head trauma, cardiac arrest, stroke and neonatal asphyxia.¹⁻³ The neuroprotective benefits of hypothermia have been linked to the time to initiate cooling after injury, depth of cooling and re-warming rate.^{4, 5} Clinical studies indicate that the temperature range associated with better outcomes appears to be 32-35°C^{6, 7} and has to be achieved as quickly as possible.^{8, 9} However, cooling the whole body below 34°C can cause complications including , shivering, sclerema, skin erythema, renal failure, coagulopathy, pulmonary hypertension and increased mortality.^{10, 11} Moreover, it may decrease perfusion and oxygenation by impairing myocardial contractility, reducing cardiac output and making myocardial muscle more prone to arrhythmia^{12, 13}; as well as causing pulmonary vasoconstriction and increasing blood viscosity.^{14, 15} Such complications along with other ones offset the benefits accrued from the neuroprotective effects of hypothermia. Therefore, in order to avoid the complications associated with systemic hypothermia, it is very important to develop a selective brain cooling (SBC) approach that can be initiated as early as possible to reduce the temperature of the brain tissue uniformly.

Based on anatomical features, blowing cold air into the nasopharynx may offer the capability to cool the brain selectively by cooling blood in both internal carotid arteries via counter-current heat exchange mechanism with the neighboring cavernous sinuses which collect cold venous blood from the mucosal linings of the nasal cavities. Furthermore, cerebrospinal fluid (CSF) chilled at the basal cistern cools the whole brain through the CSF circulation (Figure 2.1). In the present study, we evaluate the feasibility and efficiency of nasopharyngeal SBC by blowing room temperature or cold air (medical air) into the nostrils at two different flow rates on normal new-born piglets with developed thermal regulation.

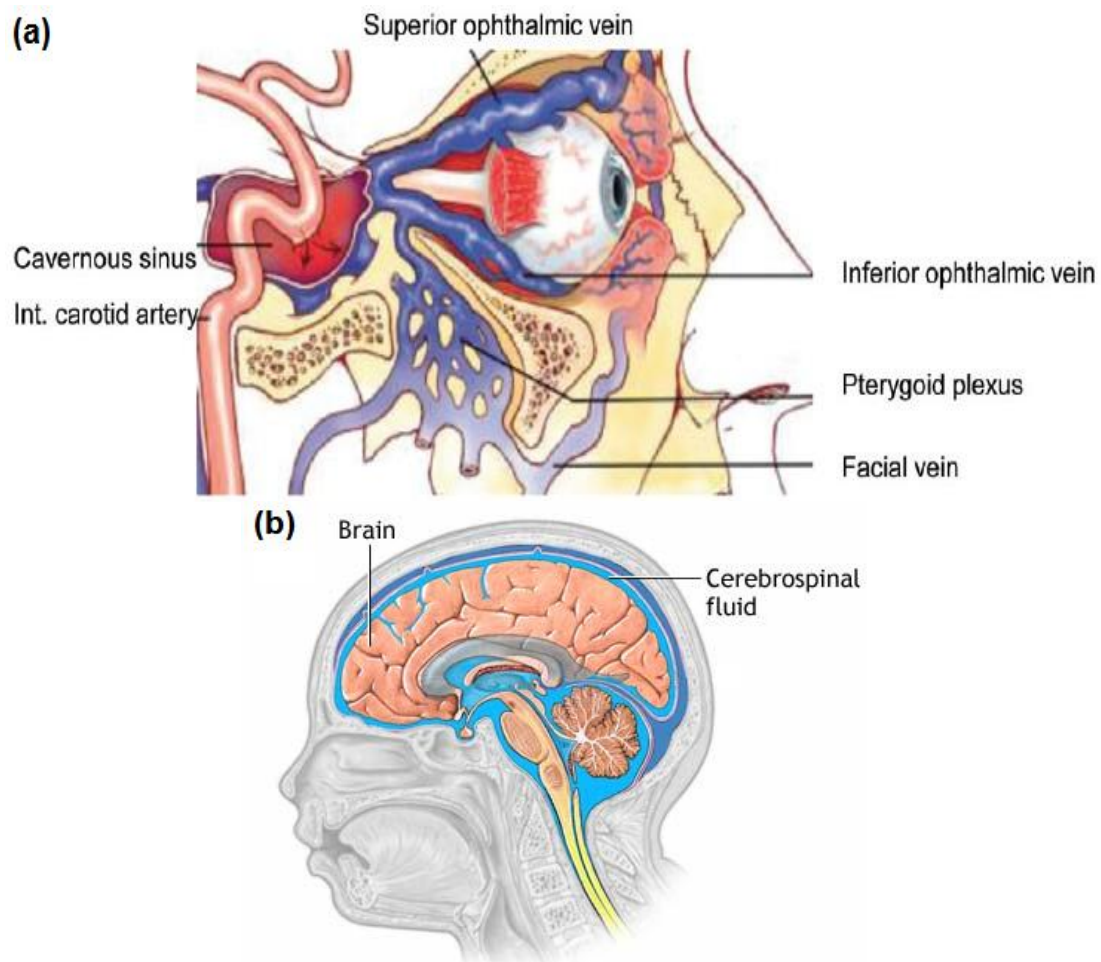


Figure 2.1. (a) Cerebral blood and brain are chilled by heat exchange between internal carotid arteries and cavernous sinuses and; (b) cerebrospinal fluid also cools the whole brain through the circulation.

Figure (a) adapted from Bhatti *et al.*¹⁶

2.1 Materials and Methods

2.1.1 Animals preparation and experimental procedure

Experiments were conducted on thirty-two piglets. All animal experiments were approved by the Animal Use Subcommittee of the Canadian Council on Animal Care at the University of Western Ontario. Newborn Duroc cross piglets were obtained from a local supplier on the morning of the experiment. Piglets were anesthetized with 3-4% isoflurane during preparatory surgery. A tracheotomy was performed and the piglet was ventilated with a volume-controlled mechanical ventilator to deliver oxygen/medical air mixture (2:1). A femoral artery was catheterized to monitor heart rate (HR) and mean arterial blood pressure (MAP) and to intermittently collect arterial blood samples for gas ($p_a\text{CO}_2$, $p_a\text{O}_2$), pH and glucose analyses. Arterial CO_2 tension ($p_a\text{CO}_2$) was monitored throughout the experiment, either directly by blood gas measurements or by the end-tidal CO_2 tension, and maintained at normocapnia between 37-42 mmHg by adjusting the breathing rate and volume. Arterial oxygen tension ($p_a\text{O}_2$) was maintained at a level between 90-130 mmHg by adjusting the ratio of oxygen to medical air. Blood glucose was monitored intermittently and if it fell below 4.5 mmol/L, a 1-2 ml infusion of 25% glucose solution was administered intravenously. Rectal temperature was recorded from a rectal probe inserted to 3-4 cm from the anal margin. Deep brain temperature was also measured continuously with a thermocouple probe. A burr hole 1.5 cm posterior to the bregma along the mid-line was made in the skull with a Dremel tool. The needle thermocouple probe was inserted through the burr hole into the brain to a depth of 2 cm from the brain surface to measure brain temperature. After surgery, each piglet together with a recirculating heated water blanket were wrapped with linen blankets, maintained on 1-2% isoflurane, and randomized to receive one of four different nasopharyngeal cooling treatments which involved blowing either room or cold air at either one of two flow rates into both nostrils of piglets:

- I. Room temperature at a flow rate of 3-4 L.min⁻¹(n=6);
- II. $-1 \pm 2^\circ\text{C}$ at a flow rate of 3-4 L.min⁻¹(n=6);

- III. Room temperature at a flow rate of 14-15 L.min⁻¹(n=6);
- IV. $-8 \pm 2^{\circ}\text{C}$ at a flow rate of 14-15 L.min⁻¹ (n=9)

To control for the normal thermal regulatory response of piglets without nasopharyngeal cooling, a control group of piglets (n=5) had their brain temperature monitored without nasopharyngeal cooling.

2.1.2 Method of nasopharyngeal brain cooling

Nasopharyngeal brain cooling was achieved by directing room temperature or cooled air via a catheter in each nostril into the nasal cavities. Each catheter was lubricated with 2% lidocaine gel for anaesthesia and inserted 4-5 cm into each nostril. Air was delivered into the nasal catheters from a pressurized tank through a flow regulator, a pump and a cooling unit (Polyscience refrigerated/heated circulating bath). The circuit was customized by replacing the pump tube with a double-walled tube with circulating cooling liquid (Ethylene glycol) in the outer tube and directing air through the inner tube (Figure 2.2). Before starting the cooling process, the cooling unit was set to -25°C with a temperature stability of $\pm 0.05^{\circ}\text{C}$ over 30-45 min; the same settings were kept during the entire experiment. Induction of hypothermia was initiated by directing air at the required temperature, either $-1 \pm 2^{\circ}\text{C}$ or $-8 \pm 2^{\circ}\text{C}$ measured at the tip of the nasal catheter and flow rate, either 3-4 or 14-15 L.min⁻¹, into the nasal catheters. Once the brain temperature stabilized, the flow rate was decreased to 0.5-1.5 L.min⁻¹ to maintain the lower temperature reached. Before the onset of hypothermia induction, the core temperature of all animals was stabilized at $38 \pm 0.5^{\circ}\text{C}$ for an hour by turning the recirculating heated water blanket on and off.

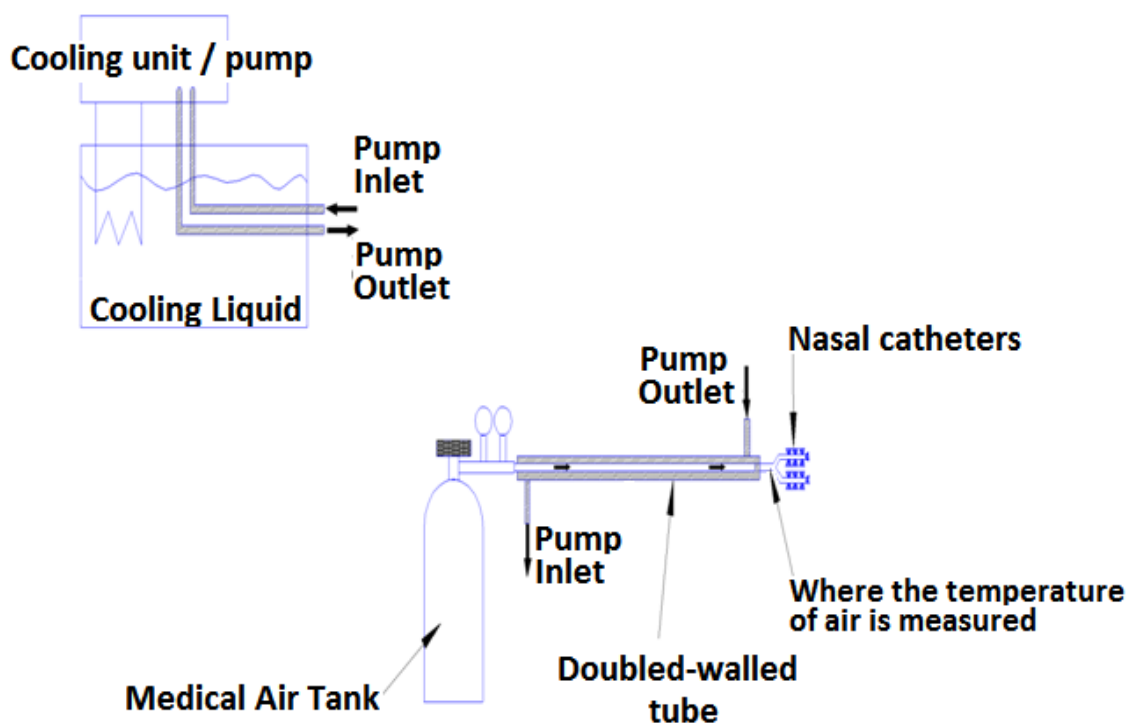


Figure 2.2. Schematic representation of the cooling circuit used for nasal cooling. The 7 Litre container was filled with a cryogenic cooling liquid (Ethylene glycol).

2.1.3 H&E histopathological examination

The piglets were sacrificed at the end of the experiment by intravenous injection of potassium chloride (1-2 ml/kg) while on 5% inhaled isoflurane. For each piglet, the brain and the snout were excised. Coronal sections of the brain (cut into the 4-5 mm-thick sections) and the snout (at the region of the premolar tooth) were obtained. The tissue sections were fixed in 10% neutral buffered formalin for 24~48 hr, and then transferred into a phosphate buffer saline (PBS) solution for preservation. These tissue fragments were then paraffin-embedded, cut into 5 μm -thick sections and stained with Hematoxylin and Eosin (H&E) for histopathological examination.

2.1.4 Statistical analysis

SPSS 17.0.0 (SPSS, Inc, Chicago, IL) was used for all statistical analyses. Normality of the distribution of the measurements was verified using Kolmogorov–Smirnov (KS) test. Analysis of variance (ANOVA) was used to check the difference between the groups. Comparisons between time-based measurements within the groups were performed with analysis of variance repeated measurements. Statistical significance was based on p -value < 0.05 . All data are presented as mean \pm standard deviation (SD) unless otherwise noted.

2.2 Results

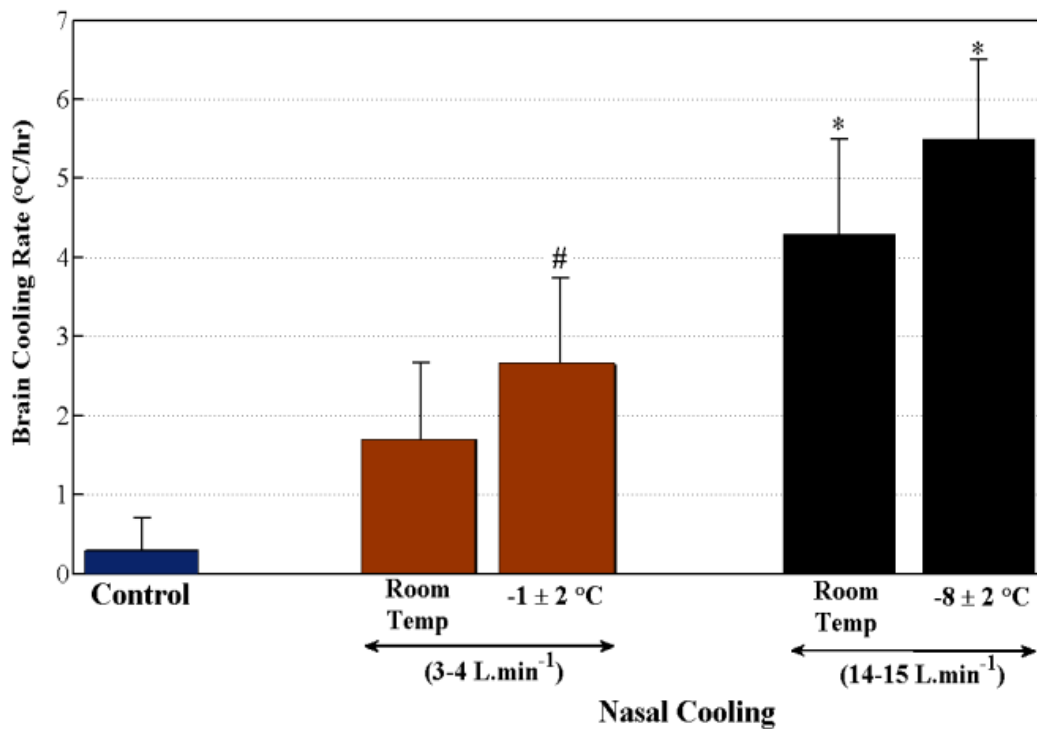
Experiments were conducted on thirty-two piglets (17 females and 15 males), divided into four cooling groups and one control group as described in Section 2.1.1, with an average age of 47 ± 14 hours and an average weight of 2.7 ± 1.5 kg. Table 2.1 presents the summary of the physiologic parameters of the piglets (MAP, HR, p_aO_2 and p_aCO_2) in Group I to IV and controls during cooling. All monitored physiological parameters showed decreasing trends during cooling but only HR and MAP decreased significantly ($p < 0.05$) at the higher flow rate of $14\text{-}15 \text{ L}\cdot\text{min}^{-1}$ and lower temperature of $-8 \pm 2^\circ\text{C}$.

Table 2.1. Physiological parameters measured at different times during SBC with different methods.

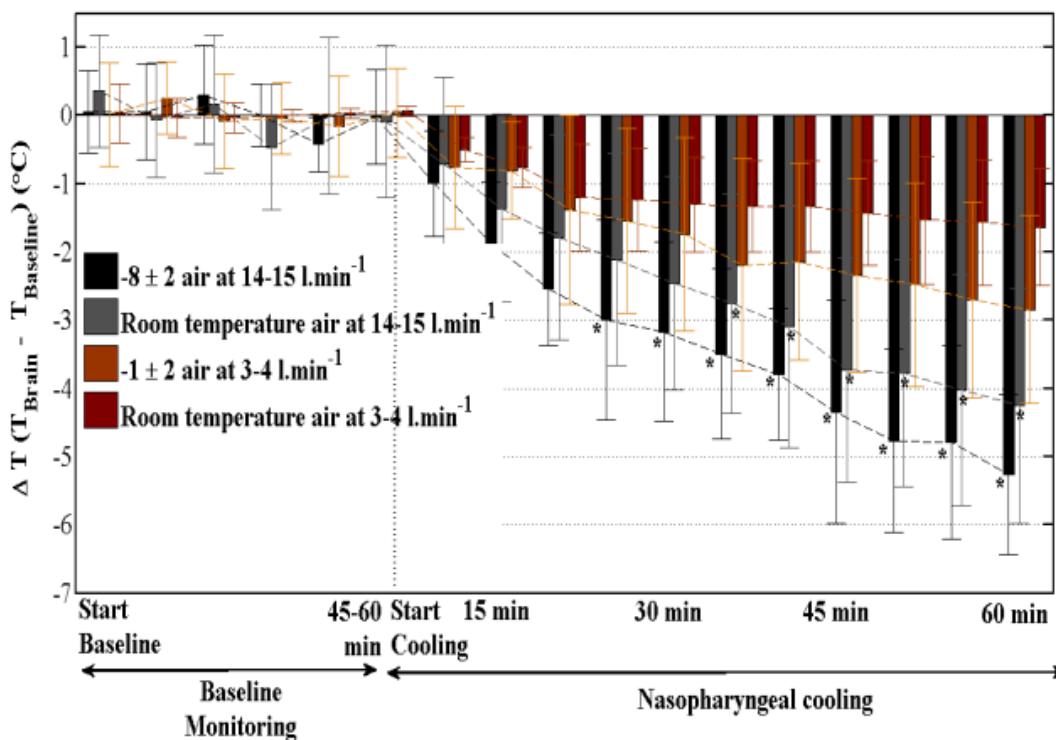
		Baseline	Cooling	
		1-60min	30 min	1 hr
<i>MAP</i> (mmHg)	<i>Control</i>	36 ± 7	34 ± 6	36 ± 7
	<i>Group I: 3-4 L.min⁻¹ at RT</i>	40 ± 2	37 ± 1	35 ± 3
	<i>Group II: 3-4 L.min⁻¹ at -1±2°C</i>	33 ± 3	30 ± 2	28 ± 5
	<i>Group III: 14-15 L.min⁻¹ at RT</i>	41 ± 4	39 ± 3*	36 ± 5*
	<i>Group IV: 14-15 L.min⁻¹ at -8±2°C</i>	35 ± 7	32 ± 6*	30 ± 6*
<i>HR</i> (bpm)	<i>Control</i>	162 ± 16	163 ± 15	162 ± 16
	<i>Group I: 3-4 L.min⁻¹ at RT</i>	139 ± 10	132 ± 9	128 ± 21
	<i>Group II: 3-4 L.min⁻¹ at -1±2°C</i>	158 ± 16	154 ± 22	143 ± 25
	<i>Group III: 14-15 L.min⁻¹ at RT</i>	149 ± 15	135 ± 22*	125 ± 25*
	<i>Group IV: 14-15 L.min⁻¹ at -8±2°C</i>	164 ± 15	145 ± 16*	133 ± 19*
<i>p_aCO₂</i> (mmHg)	<i>Control</i>	39 ± 3	40 ± 3	39 ± 3
	<i>Group I: 3-4 L.min⁻¹ at RT</i>	40 ± 2	38 ± 2	39 ± 1
	<i>Group II: 3-4 L.min⁻¹ at -1±2°C</i>	40 ± 2	39 ± 2	38 ± 4
	<i>Group III: 14-15 L.min⁻¹ at RT</i>	39 ± 2	39 ± 2	37 ± 1
	<i>Group IV: 14-15 L.min⁻¹ at -8±2°C</i>	40 ± 3	39 ± 2	38 ± 2
<i>p_aO₂</i> (mmHg)	<i>Control</i>	131 ± 44	133 ± 32	125 ± 30
	<i>Group I: 3-4 L.min⁻¹ at RT</i>	129 ± 19	99 ± 20	93 ± 14
	<i>Group II: 3-4 L.min⁻¹ at -1±2°C</i>	117 ± 15	110 ± 7	92 ± 13
	<i>Group III: 14-15 L.min⁻¹ at RT</i>	103 ± 24	95 ± 19	94 ± 30
	<i>Group IV: 14-15 L.min⁻¹ at -8±2°C</i>	129 ± 3	111 ± 2	104 ± 2

RT: Room Temperature; * a statistically significant ($P < 0.05$) difference compared to the baseline.

Figure 2.3 displays the average cooling rates achieved with different nasopharyngeal cooling methods and the brain temperature as a function of time for each method. At the low flow rate of 3-4 L.min⁻¹ mean brain cooling rate was significantly greater ($p < 0.05$) with $-1 \pm 2^\circ\text{C}$ than room temperature air. Using either room temperature or chilled air ($-1 \pm 2^\circ\text{C}$ or $-8 \pm 2^\circ\text{C}$), there was statistically significant ($P < 0.05$) greater brain cooling rate with high (14-15 L.min⁻¹) than low (3-4 L.min⁻¹) flow rate. In the control group, both rectal and brain temperature did not drop more than 0.5°C (brain: $0.35 \pm 0.3^\circ\text{C}$; rectal: $0.35 \pm 0.3^\circ\text{C}$).



(a)

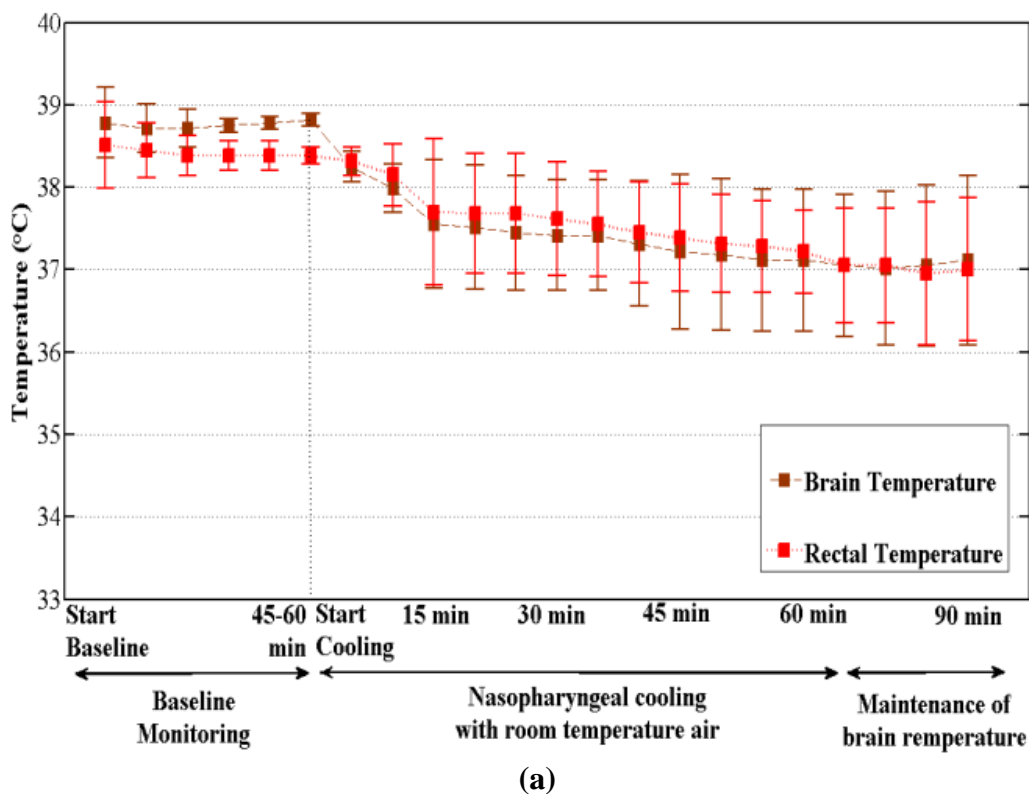


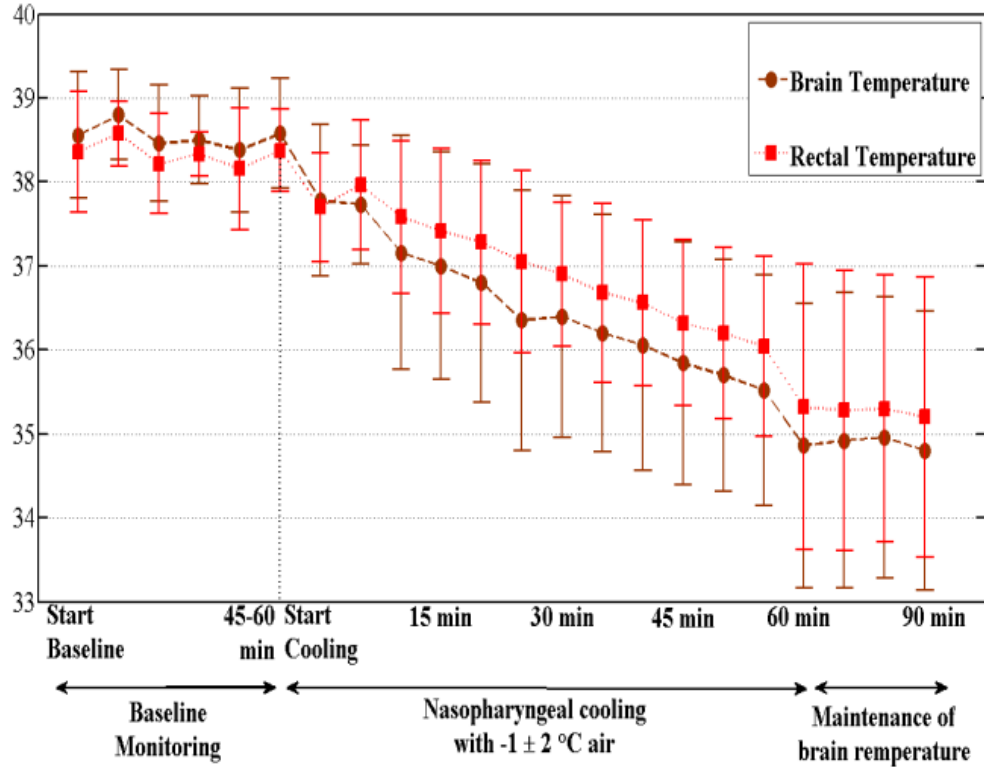
(b)

Figure 2.3. (a) Mean brain cooling rate with different nasopharyngeal cooling methods; (b) Changes in brain temperature over time for each method in Figure 2.3(a). * signifies a statistically significant ($P < 0.05$) difference between high flow rate versus low flow rate at both cold and room temperature; #

signifies a statistically significant ($P<0.05$) difference between cold temp versus room temp at low flow rate ($3-4 \text{ L}\cdot\text{min}^{-1}$).

Following 60 minutes of baseline to demonstrate relatively constant brain ($38.8 \pm 0.2^\circ\text{C}$) and rectal ($38.4 \pm 0.2^\circ\text{C}$) temperature over this period, brain temperature started falling immediately after the initiation of nasopharyngeal cooling with room temperature air at a flow rate of $3-4 \text{ L}\cdot\text{min}^{-1}$. One hour post cooling, the brain and rectal temperatures were $37.1 \pm 0.9^\circ\text{C}$ and $37.2 \pm 0.5^\circ\text{C}$ which resulted in mean brain cooling rates of $1.7 \pm 0.9^\circ\text{C}/\text{h}$ and $1.4 \pm 0.9^\circ\text{C}/\text{h}$, respectively as displayed in Figure 2.4(a).





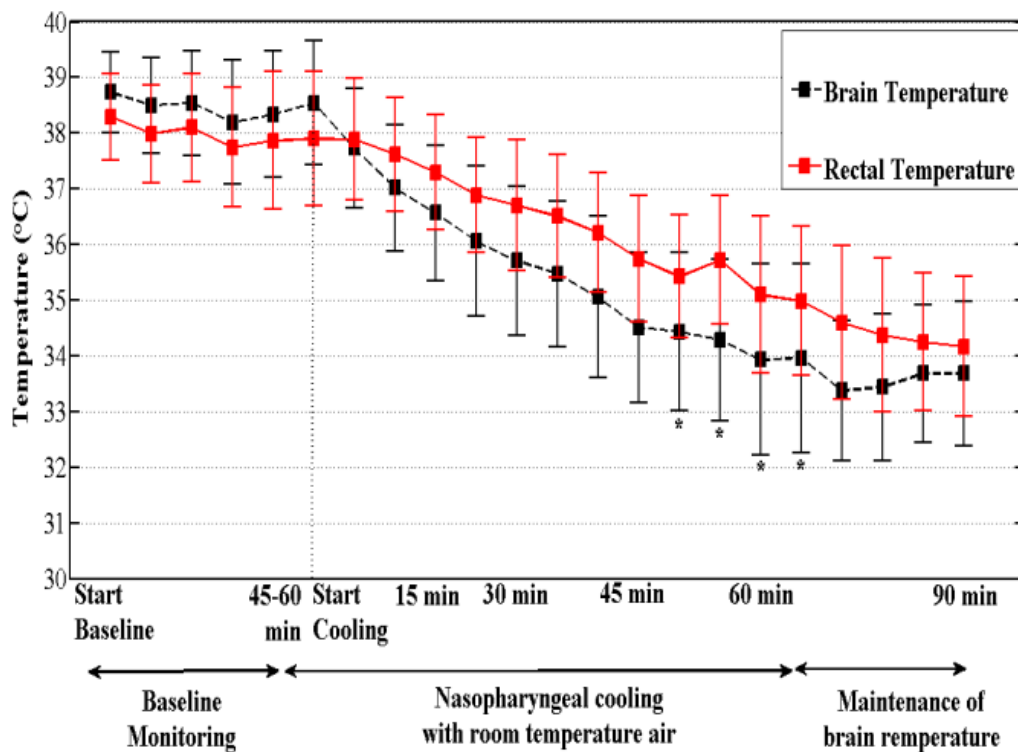
(b)

Figure 2.4. Brain and rectal temperature over time for nasopharyngeal cooling method with (a) room temperature and (b) $-1 \pm 2^\circ\text{C}$ air at a flow rate of $3-4 \text{ L}\cdot\text{min}^{-1}$.

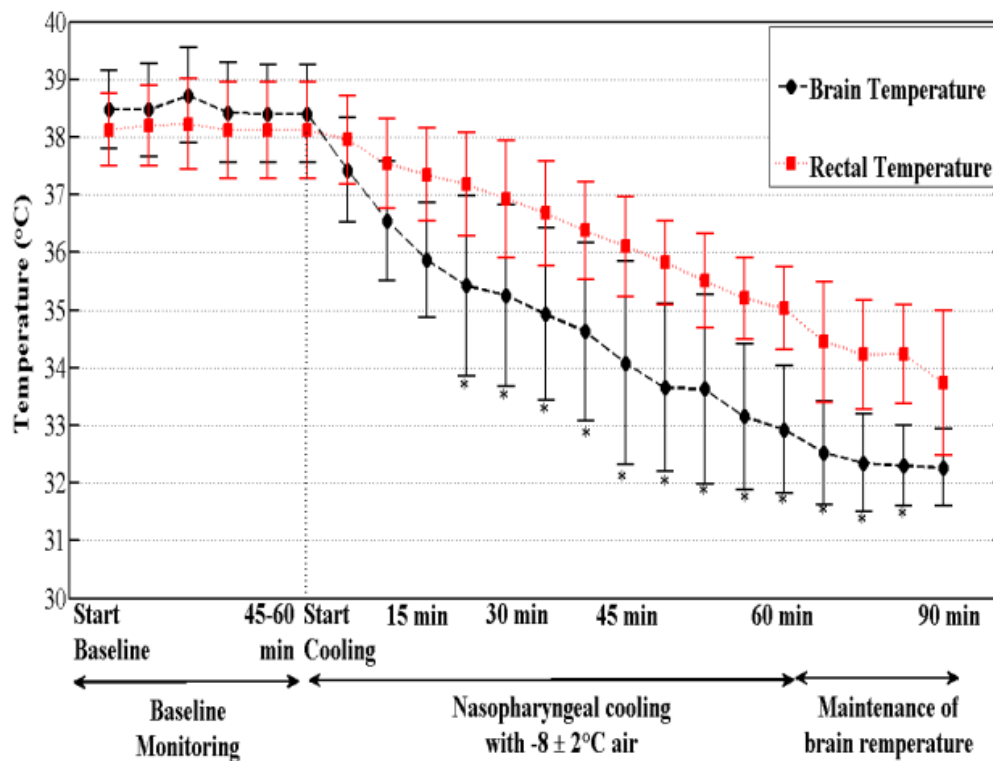
With the air flow rate at $3-4 \text{ L}\cdot\text{min}^{-1}$, the brain and rectal cooling rates were increased by decreasing the air temperature to $-1 \pm 2^\circ\text{C}$ by circulating cryogenic cooling liquids in the outer tube of the double-walled pump tube. Figure 2.4(b) shows both brain and rectal temperature decreased from $38.4 \pm 0.7^\circ\text{C}$ and $38.2 \pm 0.7^\circ\text{C}$ to $34.8 \pm 1.7^\circ\text{C}$ and $35.3 \pm 1.7^\circ\text{C}$ which corresponded to cooling rates of $2.6 \pm 1.1^\circ\text{C}/\text{h}$ and $1.8 \pm 0.6^\circ\text{C}/\text{h}$, respectively. Figure 2.4 shows that it was possible to maintain brain at the temperature arrived at after an hour of cooling with a variation of $0.35 \pm 0.45^\circ\text{C}$ by decreasing the air flow rate to $0.5-1.5 \text{ L}\cdot\text{min}^{-1}$. No significant differences were found between brain and rectal cooling rates for either air temperature at the flow rate of $3-4 \text{ L}\cdot\text{min}^{-1}$. During the baseline monitoring period, brain and rectal temperatures variations were the same (brain: $0.4 \pm 0.4^\circ\text{C}$; rectal: $0.4 \pm 0.5^\circ\text{C}$).

By increasing flow rate to $14-15 \text{ L}\cdot\text{min}^{-1}$ at room temperature, Figure 2.5(a) demonstrates that brain and rectal temperature could be reduced more rapidly at mean rates of $4.3 \pm 1.2^\circ\text{C}/\text{h}$ and $3.7 \pm 1.2^\circ\text{C}/\text{hr}$ respectively. Mean brain temperature decreased

to $33.7 \pm 1.7^\circ\text{C}$ within approximately 60 min of cooling from baseline ($38.2 \pm 1.1^\circ\text{C}$). Figure 4.5(b) shows even greater cooling rate by using $-8 \pm 2^\circ\text{C}$ air at the same flow rate. Both brain and rectal temperature decreased from $38.4 \pm 0.8^\circ\text{C}$ and $38.1 \pm 0.8^\circ\text{C}$ to $32.8 \pm 1.1^\circ\text{C}$ and $35.1 \pm 0.7^\circ\text{C}$ which corresponded to a $5.5 \pm 1.1^\circ\text{C/h}$ and $3.2 \pm 0.7^\circ\text{C/h}$, respectively. At this higher air-flow rate of $14\text{-}15 \text{ L}\cdot\text{min}^{-1}$, there were significant differences between brain and rectal temperature during cooling for either room temperature or $-8 \pm 2^\circ\text{C}$ air. After cooling with room temperature or $-8 \pm 2^\circ\text{C}$ air at a flow rate of $14\text{-}15 \text{ L}\cdot\text{min}^{-1}$ (but not with $3\text{-}4 \text{ L}\cdot\text{min}^{-1}$), the rectal temperature continued to decrease during the following 30 minutes when the air flow rate was decreased to $0.5\text{-}1.5 \text{ L}\cdot\text{min}^{-1}$ to maintain the brain temperature (Fig. 2.5 vs Fig. 2.4).



(a)



(b)

Figure 2.5. Brain and rectal temperature over time for nasopharyngeal cooling method with (a) room temperature and (b) $-8 \pm 2^{\circ}\text{C}$ air at a flow rate of $14\text{-}15 \text{ L}\cdot\text{min}^{-1}$. * signifies a statistically significant ($P<0.05$) difference between brain and rectal temperature.

Brain-body temperature gradient, calculated as the difference between brain and rectal temperature, for room temperature or $-8 \pm 2^{\circ}\text{C}$ air at the flow rate of $14\text{-}15 \text{ L}\cdot\text{min}^{-1}$ over the baseline and the cooling period is shown in Figure 2.6. The temperature gradient reached $-1.75 \pm 0.7^{\circ}\text{C}$ after 20 minutes of cooling and remained significant ($p<0.05$) during the rest of cooling period (Figure 2.6(b)).

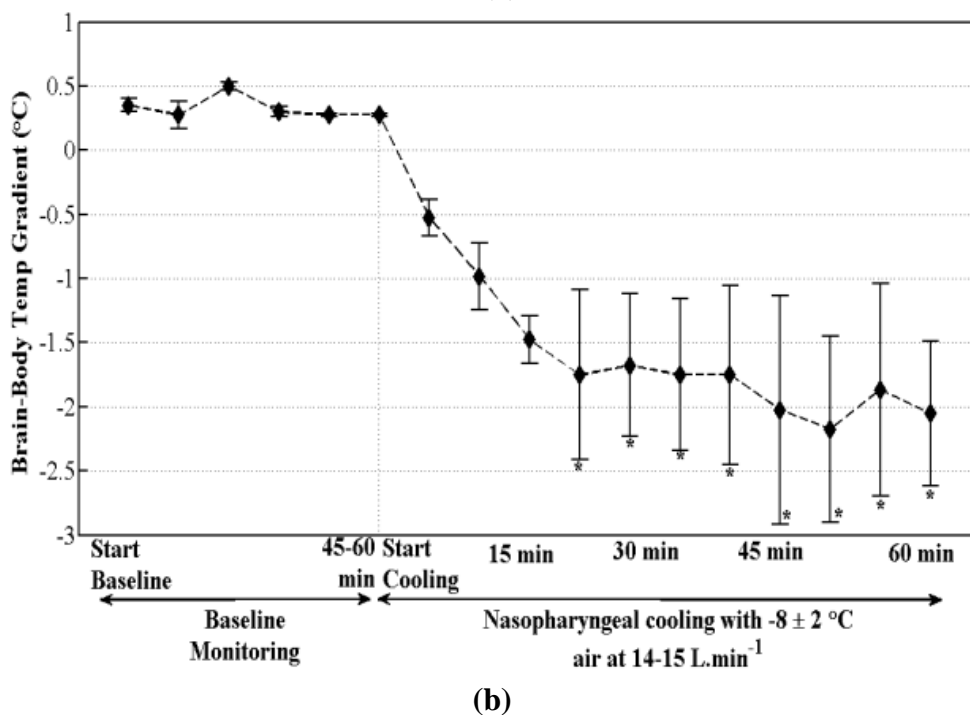
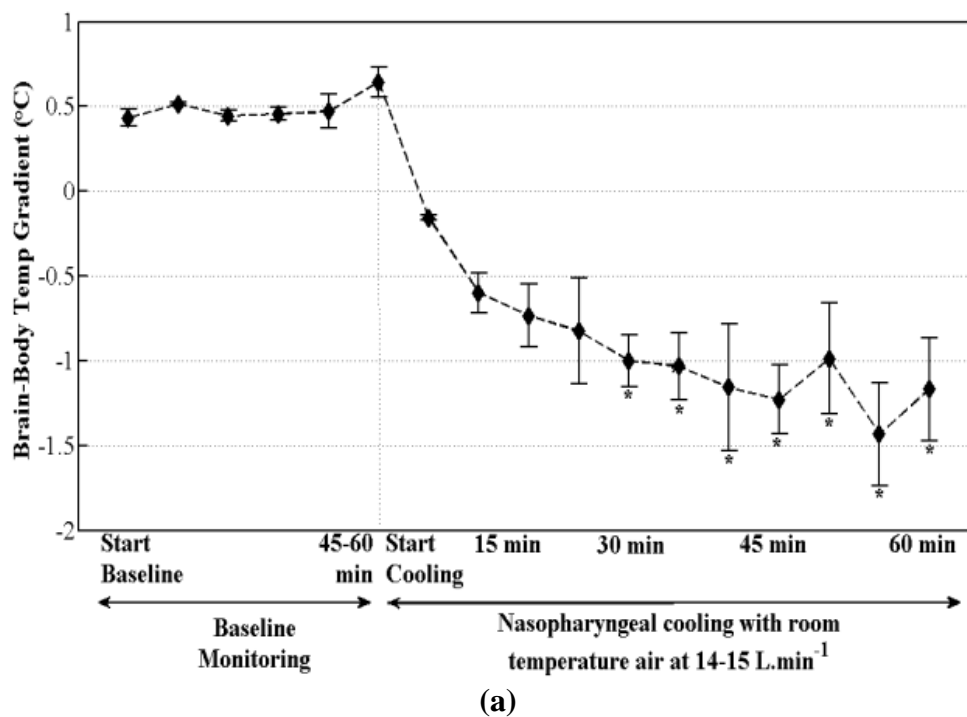


Figure 2.6. Changes in the brain-rectal temperature over time for intra-nasal cooling method with setting the air flow rate to 14-15 L.min⁻¹ at (a) room temperature and (b) cold temperature. * a statistically significant ($P < 0.05$) difference compared to the baseline.

Figure 2.7 (a) to (c) show H&E histopathological examination results of the frontal lobe of the brain and nasal conchae (turbinates) from the nasal cavity of a piglet. There were no pathological findings of bleeding, erythema and blister in the turbinates and of

necrosis in the frontal lobe of brains in both gross and H&E histopathological examinations.

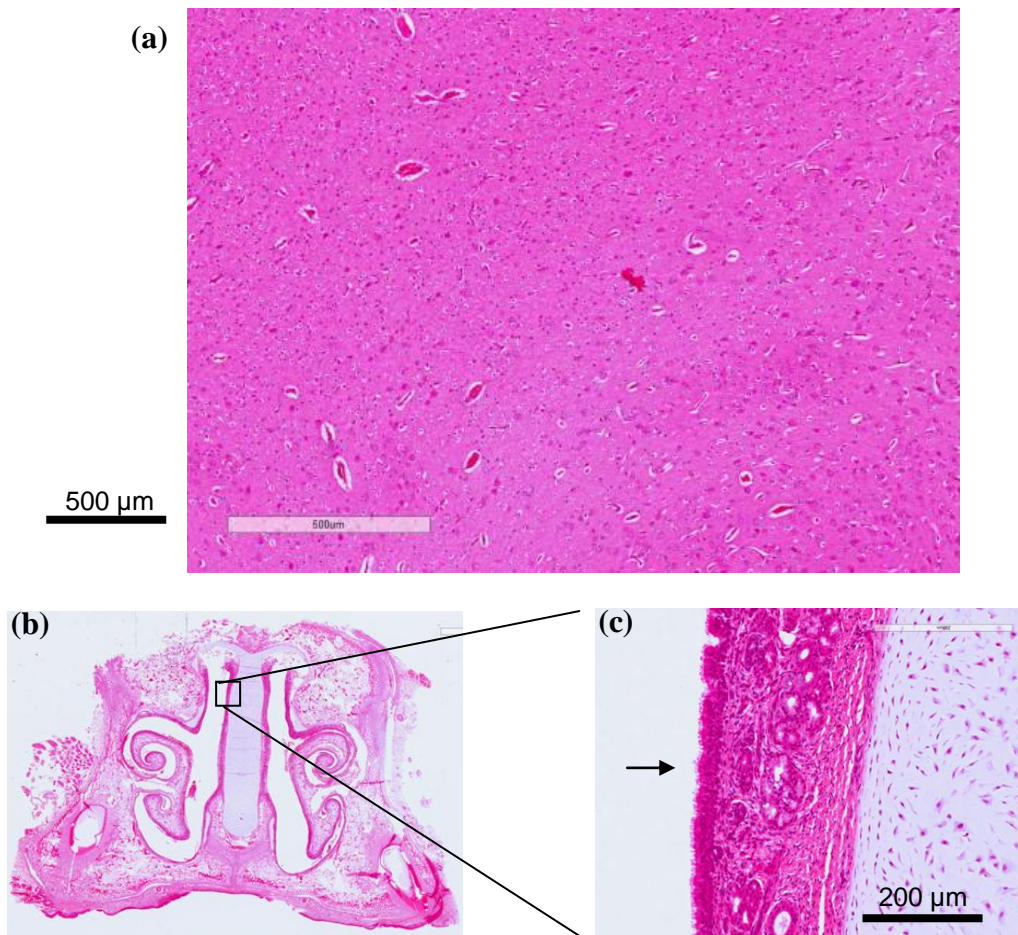


Figure 2.7. Representative H&E histology shows (a) normal brain cells in grey and white matter of the frontal lobe and (b) & (c) intact pseudostratified cilia and conchae (turbinate) cells in the nasal cavity after the nasal cooling process.

2.3 Discussion

Hypothermia in the porcine brain can be achieved via three mechanisms: surface cooling of superficial venous blood which in turn cools the arterial blood supply to the brain; cooling of head skin, from which cooled venous blood in the scalp flows via diploic and emissary veins to the brain (venous sinuses); and heat loss from the upper airway.¹⁷⁻²⁰ The latter two are thought to be mechanisms of SBC, i.e. lowering brain temperature locally or as a whole below core trunk temperature.²¹ In particular, veins in

the nasal mucosa of the upper airway drain into the cavernous sinus, a plexus (network) of thin-walled veins, which closely intertwines with the carotid rete mirabile. Carotid rete represents a vast vascular network at the base of the brain arising from branches of the carotids before entering the circle of Willis. This intricate network comes into close contact with the cavernous sinus which receives cool blood from the mucosa surfaces of the nose. Furthermore, in species with carotid rete, it has been shown that blood flow in the angularis oculi vein (AOV), which is responsible for up 80% of SBC, increases with low nasal temperature.²² In non-human species that do not have carotid rete, the large surface of cavernous sinus, which is in close contact with the base of the brain, was shown to provide the necessary heat exchanger and to make regional cooling of the brain possible.^{23, 24}

When the nasal cavity is cooled down as in our study, SBC is achieved via heat exchange at the cavernous sinus between cold venous blood from nasal mucosa and warm arterial blood in the carotid rete mirabile on route to the brain.²⁵ Based on this heat exchange method, we showed that SBC can be achieved by blowing $-8 \pm 2^\circ\text{C}$ air at a flow rate of $14\text{-}15 \text{ L}\cdot\text{min}^{-1}$ into the nasal cavity: the brain temperature dropped from $38.1 \pm 0.8^\circ\text{C}$ to $32.8 \pm 1.1^\circ\text{C}$ in 60 minutes or a cooling rate of $5.5 \pm 1.1^\circ\text{C}/\text{h}$ while the body temperature as measured by the rectal temperature probe was $> 35^\circ\text{C}$ during cooling. Similarly, Covaciu *et al.*, demonstrated the method of selectively cooling the brain ($\approx 3^\circ\text{C}/\text{h}$) with cold saline ($8\text{-}10^\circ\text{C}$) circulating in balloon catheters placed into the nasal cavities of large pigs.²⁶ Likewise, Wolfson *et al.*, employed transnasal evaporative cooling system by spraying of perfluorocarbon liquid (perfluorohexane, PFH; F2 Chemicals) at room temperature which was driven by compressed oxygen into the nasal cavities to achieve average intra-nasal brain cooling rate of $\approx 4^\circ\text{C}/\text{h}$ in sheep.²⁷ The influence of nasopharyngeal cooling on brain temperature under different range of circulatory states such as untreated cardiac arrest ("no-flow") or during normal circulation ("normal-flow") and cardiopulmonary arrest (CPR) situation ("low-flow") was also shown in a porcine model in a study by Boller *et al.*²⁸ Nasopharyngeal cooling device, RhinoChill (BeneChill, Inc, SanDiego, Ca, USA), shows that the brain is preferentially cooled compared with the other compartments of the body with a average cerebral temperature decrease of -4.7°C for normal flow, -4.3°C for no flow and -3.4°C for low

flow after 60 minutes.²⁸ However, the brain-body temperature gradient was greatest in "no-flow" group which was nearly 4°C, while the smallest gradient was 2°C during normal blood flow.²⁸ Intranasal cooling was beneficial even after prolonged cardiac arrest in a porcine model, where it significantly improved the return of spontaneous resuscitation (ROSC) rate and reduced CPR duration.^{29, 30} The administration of cold nasal airflow and intranasal cooling were both tested in human studies.^{19, 31-34} These methods proved to be feasible, safe and improved the neurological outcome. However, evaluating the effect of selective cooling methods on the human brain is challenging because direct measurements of the brain temperature cannot be made without the need for surgery. Furthermore, invasive temperature measurements do not inform on the intracerebral distribution of temperature changes induced by these methods.

In humans, it was argued that the face and the surface of nasal mucosa as source of cool venous blood are small in relation to the mass of the brain and the carotid rete, where heat exchange might occur, does not exist.²⁰ Moreover, a substantial fraction of the blood supply to the brain is via the vertebral arteries, which have no direct contact with cool venous blood. Because humans do not have a carotid rete, some have suggested that there is no counter-current heat exchange in the cavernous sinus and, as a result, human SBC is not possible. Yet the rete is not prerequisite for SBC because several other mammals without carotid rete clearly demonstrate SBC.^{24, 35} Consequently, lack of a carotid rete does not preclude the existence of SBC in humans or other mammals. The internal carotid artery in humans is tightly surrounded by the venous plexus caroticus and thereafter immersed in the cavernous sinus, and the vertebral arteries surrounded by a plexus of veins where they course through the transverse foramina.²⁰ The blood temperature of the cavernous sinus decreases in response to chilled venous blood and selectively cools the brain by means of heat exchange mechanism with the arterial blood. Other components of the SBC system in humans are also thought to be cooling of head skin via emissary and angular veins, CSF circulation and the upper respiratory tract.^{18, 36, 37} Mariak *et al.* directly demonstrated that increases or decreases in upper airway ventilation gave proportional changes of intracranial temperatures supporting the existence of this mechanism of brain cooling in human.³³ Moreover, It has been shown that the nasal mucosa blood flow increases 3-fold during hyperthermia conditions in

humans and the cold venous blood flows via the angularis oculi vein to the brain, as in other species.^{38, 39} A continuous and cold nasal airflow in patients was found to reduce brain temperatures between 0.15-0.8°C.^{19, 33} Similarly, Dohi *et al.*, achieved a lower cooling rate of $\approx 2.5^\circ\text{C}/\text{h}$ by blowing 24-26°C air at a flow rate of 8-12 L.min⁻¹ directly into the nasal cavities of two patients with Foley catheters adjunct with surface cooling.³⁴ Recently, feasibility of preclinical transnasal evaporative cooling was successfully tested in patients after cardiac arrest.^{31, 32} Castrén *et al.* demonstrated that the RhinoChill intranasal cooling device was effective to reduce of tympanic temperature within the Pre-ROSC Intranasal Cooling Effectiveness trial (PRINCE trial).³² This method was able to show a significant decrease of tympanic temperature in the treatment group on arrival at hospital (34.2°C versus 35.5°C). However, benefit towards survival and neurological outcome was observed in the subgroup of cooling patients in whom CPR was initiated within 10 minutes after collapse, although the design of the study was not conceived for outcome analysis. In summary, prehospital treatment of patients with a cardiac cause of the arrest may increase the rate of favorable outcome at hospital discharge.

The RhinoChill device vaporises perfluorchlorcarbon along with oxygen at flow rate of 60-80 L.min⁻¹ with a catheter system into the nasal cavity leading to a fast induction of hypothermia first to the brain as main target organ and second to the body with a slight delay.³² However, Perfluorocarbons raise environmental and health issues. They are powerful greenhouse gases and deplete the ozone layer and are listed as toxic substances under the Canadian Environmental Protection Act (CEPA).⁴⁰ Another safety concern is the risk of coolant aspiration which might cause lung damage over prolonged periods since neural protection therapy may involve mild hypothermia being maintained for a period of 72 hours.⁴¹ Therefore, new cooling methods should be effective in terms of safety, fast cooling rates and easy to apply in the pre-clinical setting. We explored a method of nasopharyngeal cooling by continuously blowing room temperature or humidified cold air into the nostrils at different conditions on normal new-born piglets with developed thermal regulation. Piglets were studied because they are commonly used animal model of newborn human neurology.⁴² Thermoregulatory response in newborn piglets were progressively achieved after 48 hours of birth.⁴³ In our study, brain temperature dropped with a mean cooling rate of $1.7 \pm 0.9^\circ\text{C}$ after the start of cooling

procedure, by setting the air-flow rate to 3-4 L.min⁻¹. The rate of brain cooling can be improved by increasing the air-flow rate and/or decreasing the temperature of circulating cryogenic cooling liquids in outer tube of heat exchanger. Brain temperature reduced more rapidly at a rate of $5.6 \pm 1.1^{\circ}\text{C/h}$ with increasing air-flow to 14-15 L.min⁻¹ at cold temperature. Rectal temperature continued to drop till it reached to the brain temperature during maintaining period. The decline in rectal temperature following the brain temperature may be due to the balance between heat production in the rest of the body and heat lost through cold air-flow in nasal cavities. Regardless of cooling conditions, HR and MAP decreased with cooling. The level of gaseous carbon dioxide, or $P_a\text{CO}_2$, in arterial blood depends on the solubility coefficient of this gas, which is dependent on temperature and decreases as temperature decreases.⁴⁴ The CO_2 gas crosses the blood-brain barrier and transmits the induced modifications (e.g., alkalosis in hypothermia)⁴⁵ to the extracellular environment, which regulates the state of arteriolar vascular tone. This explains why hypothermia-induced hypocapnia may cause arteriolar vasoconstriction and a decrease in intracranial pressure.¹⁴

Several factors could have influenced the possibility that the results in the experimental studies could be reproduced in humans. Firstly, in all of the experimental studies anaesthesia was maintained with Isoflurane. All general anaesthetics increase the threshold for sweating and decrease the thresholds for vasoconstriction and shivering.⁴⁶ Secondly, there are anatomical and physiological differences between new-born piglets and humans that are important in this context. The baseline temperature in newborn piglets and humans is different. Pigs differ considerably to humans in their ratio between the size of their nasal cavity and their brain. Importantly, the newborn piglets, in contrast to humans, have a carotid rete that may be a SBC system specific for the pig. Based on the relatively rapid cooling rate achieved in this study by setting the air-flow rate to 14-15 L.min⁻¹, we suggest that nasal cooling with this technique still has great potential for inducing hypothermia on large animal or human by increasing air-flow rate up to 60-80 L.min⁻¹ at cold temperature. In conclusion, we have demonstrated that nasopharyngeal cooling by spraying humidified and cooled air into nasal cavities is an effective, feasible and simple method to selectively reduce and maintain brain temperature of newborn piglets. This method can be easily implemented in hospitals and even on ambulances to

cool down the brain to ameliorate brain damage from hypoxia-ischemia in newborns, cardiac arrest in resuscitated patients, stroke and traumatic injury.

2.4 References

1. Sadaka F, Veremakis C. Therapeutic hypothermia for the management of intracranial hypertension in severe traumatic brain injury: A systematic review. *Brain Inj.* 2012;26:899-908
2. Quinn MW, Munyard PF. Treatment of asphyxiated newborns with moderate hypothermia in routine clinical practice: How cooling is managed in the uk outside a clinical trial. *Arch Dis Child Fetal Neonatal Ed.* 2010;95:F152
3. Uray T, Haugk M, Sterz F, Arrich J, Richling N, Janata A, Holzer M, Behringer W. Surface cooling for rapid induction of mild hypothermia after cardiac arrest: Design determines efficacy. *Acad Emerg Med.* 2010;17:360-367
4. Moore EM, Nichol AD, Bernard SA, Bellomo R. Therapeutic hypothermia: Benefits, mechanisms and potential clinical applications in neurological, cardiac and kidney injury. *Injury.* 2011;42:843-854
5. Povlishock JT, Wei EP. Posthypothermic rewarming considerations following traumatic brain injury. *J Neurotrauma.* 2009;26:333-340
6. Guidelines for the management of severe traumatic brain injury. *J Neurotrauma.* 2007;24 Suppl 1:S1-106
7. Mathur NB, Krishnamurthy S, Mishra TK. Evaluation of who classification of hypothermia in sick extramural neonates as predictor of fatality. *J Trop Pediatr.* 2005;51:341-345
8. Kuboyama K, Safar P, Radovsky A, Tisherman SA, Stezoski SW, Alexander H. Delay in cooling negates the beneficial effect of mild resuscitative cerebral hypothermia after cardiac arrest in dogs: A prospective, randomized study. *Crit Care Med.* 1993;21:1348-1358
9. Behringer W, Prueckner S, Safar P, Radovsky A, Kentner R, Stezoski SW, Henchir J, Tisherman SA. Rapid induction of mild cerebral hypothermia by cold aortic flush achieves normal recovery in a dog outcome model with 20-minute exsanguination cardiac arrest. *Acad Emerg Med.* 2000;7:1341-1348
10. Rogers MC, Greenberg M, Alpert JJ. Cold injury of the newborn. *N Engl J Med.* 1971;285:332-334

11. Culic S. Cold injury syndrome and neurodevelopmental changes in survivors. *Arch Med Res.* 2005;36:532-538
12. Dudgeon DL, Randall PA, Hill RB, McAfee JG. Mild hypothermia: Its effect on cardiac output and regional perfusion in the neonatal piglet. *J Pediatr Surg.* 1980;15:805-810
13. Steen PA, Milde JH, Michenfelder JD. The detrimental effects of prolonged hypothermia and rewarming in the dog. *Anesthesiology.* 1980;52:224-230
14. Vigue B, Ract C, Zlotine N, Leblanc PE, Samii K, Bissonnette B. Relationship between intracranial pressure, mild hypothermia and temperature-corrected paco₂ in patients with traumatic brain injury. *Intensive Care Med.* 2000;26:722-728
15. Benumof JL, Wahrenbrock EA. Dependency of hypoxic pulmonary vasoconstriction on temperature. *J Appl Physiol Respir Environ Exerc Physiol.* 1977;42:56-58
16. Bhatti MT. Orbital syndromes. *Semin Neurol.* 2007;27:269-287
17. Baker MA. Brain cooling in endotherms in heat and exercise. *Annu Rev Physiol.* 1982;44:85-96
18. Zenker W, Kubik S. Brain cooling in humans--anatomical considerations. *Anatomy and embryology.* 1996;193:1-13
19. Harris BA, Andrews PJ, Murray GD. Enhanced upper respiratory tract airflow and head fanning reduce brain temperature in brain-injured, mechanically ventilated patients: A randomized, crossover, factorial trial. *Br J Anaesth.* 2007;98:93-99
20. Cabanac M. Selective brain cooling in humans: "Fancy" or fact? *FASEB J.* 1993;7:1143-1146; discussion 1146-1147
21. Glossary of terms for thermal physiology. Second edition. Revised by the commission for thermal physiology of the international union of physiological sciences (iups thermal commission). *Pflugers Arch.* 1987;410:567-587
22. Maloney SK, Mitchell G. Selective brain cooling: Role of angularis oculi vein and nasal thermoreception. *Am J Physiol.* 1997;273:R1108-1116
23. Fuller CA, Baker MA. Selective regulation of brain and body temperatures in the squirrel monkey. *Am J Physiol.* 1983;245:R293-297
24. Caputa M, Kadziela W, Narebski J. Significance of cranial circulation for the brain homeothermia in rabbits. II. The role of the cranial venous lakes in the defence against hyperthermia. *Acta Neurobiol Exp (Wars).* 1976;36:625-637

25. Gillan LA. Blood supply to brains of ungulates with and without a rete mirabile caroticum. *J Comp Neurol*. 1974;153:275-290
26. Covaciu L, Allers M, Enblad P, Lunderquist A, Wieloch T, Rubertsson S. Intranasal selective brain cooling in pigs. *Resuscitation*. 2008;76:83-88
27. Wolfson MR, Malone DJ, Wu J, Hoffman J, Rozenberg A, Shaffer TH, Barbut D. Intranasal perfluorochemical spray for preferential brain cooling in sheep. *Neurocritical care*. 2008;8:437-447
28. Boller M, Lampe JW, Katz JM, Barbut D, Becker LB. Feasibility of intra-arrest hypothermia induction: A novel nasopharyngeal approach achieves preferential brain cooling. *Resuscitation*. 2010;81:1025-1030
29. Tsai MS, Barbut D, Wang H, Guan J, Sun S, Inderbitzen B, Weil MH, Tang W. Intra-arrest rapid head cooling improves postresuscitation myocardial function in comparison with delayed postresuscitation surface cooling. *Crit Care Med*. 2008;36:S434-439
30. Wang H, Barbut D, Tsai MS, Sun S, Weil MH, Tang W. Intra-arrest selective brain cooling improves success of resuscitation in a porcine model of prolonged cardiac arrest. *Resuscitation*. 2010;81:617-621
31. Busch HJ, Eichwede F, Fodisch M, Taccone FS, Wobker G, Schwab T, Hopf HB, Tonner P, Hachimi-Idrissi S, Martens P, Fritz H, Bode C, Vincent JL, Inderbitzen B, Barbut D, Sterz F, Janata A. Safety and feasibility of nasopharyngeal evaporative cooling in the emergency department setting in survivors of cardiac arrest. *Resuscitation*. 2010;81:943-949
32. Castren M, Nordberg P, Svensson L, Taccone F, Vincent JL, Desruelles D, Eichwede F, Mols P, Schwab T, Vergnion M, Storm C, Pesenti A, Pachl J, Guerisse F, Elste T, Roessler M, Fritz H, Durnez P, Busch HJ, Inderbitzen B, Barbut D. Intra-arrest transnasal evaporative cooling: A randomized, prehospital, multicenter study (prince: Pre-rosoc intranasal cooling effectiveness). *Circulation*. 2010;122:729-736
33. Mariak Z, White MD, Lewko J, Lyson T, Piekarski P. Direct cooling of the human brain by heat loss from the upper respiratory tract. *J Appl Physiol (1985)*. 1999;87:1609-1613
34. Dohi K, Jimbo H, Abe T, Aruga T. Positive selective brain cooling method: A novel, simple, and selective nasopharyngeal brain cooling method. *Acta Neurochir Suppl*. 2006;96:409-412

35. McConaghy FF, Hales JR, Rose RJ, Hodgson DR. Selective brain cooling in the horse during exercise and environmental heat stress. *J Appl Physiol* (1985). 1995;79:1849-1854
36. Nagasaka T, Brinnel H, Hales JR, Ogawa T. Selective brain cooling in hyperthermia: The mechanisms and medical implications. *Med Hypotheses*. 1998;50:203-211
37. White MD, Greiner JG, McDonald PL. Point: Humans do demonstrate selective brain cooling during hyperthermia. *J Appl Physiol* (1985). 2011;110:569-571; discussion 581-562
38. Caputa M, Perrin G, Cabanac M. [reversal of human ophthalmic vein blood flow : Selective cooling of the brain]. *C R Acad Sci Hebd Seances Acad Sci D*. 1978;287:1011-1014
39. White MD, Cabanac M. Nasal mucosal vasodilatation in response to passive hyperthermia in humans. *Eur J Appl Physiol Occup Physiol*. 1995;70:207-212
40. Chemicals Management Division of Environment Canada. List of toxic substances managed under cepa (schedule 1), available at: [Http://www.Ec.Gc.Ca/toxiques-toxics/default.Asp?Lang=en&n=98e80cc6-1&xml=aa329670-c3c7-4ad5-a7ab-5fd8a05439f1](http://www.Ec.Gc.Ca/toxiques-toxics/default.Asp?Lang=en&n=98e80cc6-1&xml=aa329670-c3c7-4ad5-a7ab-5fd8a05439f1). (20 April 2012).
41. Azzopardi D, Strohm B, Edwards AD, Halliday H, Juszczak E, Levene M, Thoresen M, Whitelaw A, Brocklehurst P, Steering G, participants TCR. Treatment of asphyxiated newborns with moderate hypothermia in routine clinical practice: How cooling is managed in the uk outside a clinical trial. *Arch Dis Child Fetal Neonatal Ed*. 2009;94:F260-264
42. Rooney T, Raju TN, Moustogiannis AN. Animal models for the study of perinatal hypoxic-ischemic encephalopathy: A critical analysis. *Early Hum Dev*. 1997;47:115-146
43. Herpin P. Development of thermoregulation and neonatal survival in pigs. *Livestock Production Science*. 2002;78:25-45
44. Tremey B, Vigue B. [changes in blood gases with temperature: Implications for clinical practice]. *Ann Fr Anesth Reanim*. 2004;23:474-481
45. Ream AK, Reitz BA, Silverberg G. Temperature correction of pco2 and ph in estimating acid-base status: An example of the emperor's new clothes? *Anesthesiology*. 1982;56:41-44
46. Sessler DI. Mild perioperative hypothermia. *N Engl J Med*. 1997;336:1730-1737

Chapter 3

Monitoring Brain Temperature by Time-Resolved Near-Infrared Spectroscopy: A Pilot Study

This chapter is adapted from the work entitled “Monitoring Brain Temperature by Time-Resolved Near-Infrared Spectroscopy” by M Fazel Bakhsheshi, M Diop, K St. Lawrence and TY Lee, submitted to the *Journal of Bio-Medical Optics*. The focus of this paper is to investigate the potential of time-resolved near-infrared spectroscopy (TR-NIRS) to measure absolute temperature in tissue-mimicking phantoms (*in-vitro*) and deep brain tissue temperature (*in-vivo*).

3. Introduction

Clinical studies have shown that hypothermia improves neurological outcome and reduces mortality following cardiac arrest, traumatic brain injury, birth asphyxia and ischemic encephalopathy.¹⁻³ Despite its well-documented efficacy, the widespread application of hypothermia in neuro-emergencies has been hampered by the difficulty of noninvasively monitoring brain temperature. As well, cooling the whole body below 33-34°C can induce severe complications including, sclerema, skin erythema, renal failure, coagulopathy, pulmonary hypertension, and even death.⁴ SBC methods, such as using a cooling helmet or nasopharyngeal cooling, have been proposed to alleviate the complications associated with systemic hypothermia by directly cooling the brain while maintaining body temperature to as close to normal as possible.⁵ However, SBC requires a method that can measure local brain temperature rather than body temperature as the latter may not reflect the actual brain temperature.

Several approaches have been developed to assess brain temperature. Local brain temperature can be measured invasively by inserting a thermometer directly into the brain parenchyma, which provides accurate measurements but carries a significant risk of complications. Infrared tympanic thermometer is noninvasive; however, it does not

provide continuous monitoring and is sensitive to positioning errors.^{6, 7} Magnetic resonance spectroscopy (MRS) can be used to measure brain temperature⁸, but its clinical utility is hampered by a long measurement time and by the need to transfer patients to imaging facilities. Brain temperature measurement techniques have also been developed using other modalities such as ultrasound⁹, microwave radiometry¹⁰ and the zero-heat-flux technique.¹¹ However, these techniques suffer from practical issues such as inducing temperature increase, and poor temporal and spatial resolution.

Optical methods are a promising alternative to the aforementioned techniques since they are safe and the instruments are compact and portable. As well, temperature-dependent changes in water absorption spectra have been well characterized by near-infrared spectroscopy (NIRS).¹² The water absorption peaks around 740, 840 and 970 nm shift to shorter wavelengths and increase in intensity with increasing temperature¹²⁻¹⁴, due to decreases in the extent of intermolecular hydrogen bonding among water molecules with increasing temperature. In fact, NIRS thermometry approaches based on broadband continuous wavelengths (CW) and diffuse correlation spectroscopy (DOS) have been developed to predict deep tissue temperature in an adult forearm and breast, respectively.^{12, 15} Chung *et al.* used the water peak at 970 nm to predict temperature in tissue mimicking phantoms and breast tissue.¹⁵ Using this water peak to monitor brain temperature is challenging because of the strong water absorption at this wavelength which limits depth penetration. In this study, the temperature-dependency of the water absorption peaks at ~740 nm and ~840 nm was investigated as an alternative approach for monitoring brain temperature. Although the temperature changes at these features are not as great as at 970 nm, this is compensated by the high water concentration in the brain, 80-90% in the newborn brain.¹⁶ TR-NIRS was used in order to separate the effects of tissue scattering from absorption and to provide better depth sensitivity.¹⁷ The method was validated in tissue-mimicking phantoms by correlating TR-NIRS temperature calculations to simultaneous thermometer measurements, and was subsequently used to monitor brain temperature in newborn piglets during cooling. Deep brain temperature was also measured continuously with a thermocouple probe.

3.1 Materials and Methods

3.1.1 Instrumentation

The light sources of the TR-NIRS system consisted of thermoelectrically cooled picosecond pulsed diode lasers (LDH-P-C, PicoQuant, Germany) emitting at 760, 810 and 830 nm and a computer controlled laser driver (SEPIA PDL 828, PicoQuant, Germany). These emission wavelengths were chosen to quantify tissue chromophores (oxy-hemoglobin, HbO₂ and deoxy-hemoglobin, Hb)¹⁸ and characterize temperature-dependent changes of the water absorption peaks. The lasers' output power and pulse repetition rate were set to 1.4 mW and ~27 MHz, respectively. The individual pulses of the three lasers were temporally separated by sharing the 80 MHz clock of the laser drivers. Light emitted by each diode laser was attenuated by two adjustable neutral density filters (NDC-50-4M, Thorlabs, Newton, NJ) and coupled by a microscope objective lens (NA = 0.25, magnification = 10x) into one arm of a trifurcated fiber bundle (three fibers; NA = 0.22, core 400 μm, Fiber Optics Technology, Pomfret, Connecticut). The distal common end of the bundle (emission probe) was placed on the surface of the phantom (or scalp of the piglets) and held in position by a probe holder. The average power delivered to a subject was attenuated to ~20 μW per laser, which is below ANSI safety limits for skin exposure.¹⁹

Photons emerging from the phantom (piglet scalp) were collected by a 2-m fiber optic bundle (NA = 0.55, 3.6 mm diameter active area, and 4.7-mm outer diameter, Fiber Optics Technology). The other end of the detection probe was secured in front of an electromechanical shutter (SM05, Thorlabs). Light transmitted through the shutter was collected by a Peltier cooled microchannel plate photomultiplier tube (MCP-PMT) (PMC-100, Becker and Hickl, Germany). Detection of a photon generated an electrical pulse (amplitude of 50-200 mV, width = 1.5 ns) that was transmitted to a time-correlated single photon counting (TCSPC) module (SPC-134, Becker and Hickl, Germany) to build the temporal point spread function (TPSF).

3.1.2 Optical Properties Measurement

To quantify tissue optical properties (i.e., the absorption coefficient μ_a and the reduced scattering coefficient μ_s') from the measured TPSFs, the instrument response function (IRF) was measured to account for dispersion by the system.²⁰ The IRF was acquired by placing a thin piece of white paper between the emission fiber and the detection fiber bundle. The paper was coated with black toner to reduce specular reflection.²¹ IRFs were measured at the start and end of each experiment at the same count rate as the TPSFs (~800 kHz). Measurement of the optical properties was obtained using an analytical model of light diffusion.²² The model solution was first convolved with the measured IRF, and then a nonlinear optimization routine (MATLAB function *fminsearch*) was used to fit the convolved model to each measured TPSF to determine optical properties (μ_a and μ_s') and scaling factor which accounts for laser power, any potential drift in the intensity of light source, detection gain, and coupling efficiency.²⁰ The fitting range was set to 80% of the peak value on the leading edge and 20% on the falling edge.²³ The TPSFs measured at baseline (i.e., before initiation of cooling) were averaged and fitted to extract the baseline optical properties as well as the scaling factor. Thereafter, changes in light absorption caused by cooling were characterized by using μ_a as the only fitting parameter; μ_s' and the scaling factor were set to their baseline values to improve the stability of the fitting procedure and reduce errors causing by cross-talk between fitting parameters i.e., μ_a - μ_s' .^{12, 20} However, temperature effects on the reduced scattering coefficients, presented in Table 3.1 and 3.3, determined using only the scaling factor as the fix parameter. Tissue optical properties at each temperature were determined from averaging of 32 TPSFs collected at a sampling interval of 10 s (i.e., 320 s). The maximum count rate was set to 1% of the laser repetition rate (800 kHz), to minimize pile-up effect.²⁴ However, Diop *et al.* showed that the error resulting from distortions in TPSF shape was relatively small by measuring the IRF at the two extremes count rate (400 and 800 kHz).²⁵ Finally, the measured changes in μ_a were used to calculate changes in temperature, as discussed in detail in the section 3.2.

3.1.3 Tissue mimicking Phantom Experiments

Tissue-mimicking phantoms ($N = 7$), composed of solutions of 95% distilled water, 0.8% intralipid and 4.2% whole piglet blood, were used for comparison of TR-NIRS temperature calculations and thermometer measurements. Each solution together with a (magnetic) stirrer were placed in a Pyrex beaker on a heating and stirring plate. The emission and detector probes of the TR-NIRS instrument were positioned on the surface of the solution at a source-detector distance of 2 cm. A thermometer (VWR digital thermometer with 0.1°C precision, VWR International Inc) was also placed in the solution for concomitant TR-NIRS and temperature measurements. The phantom (solution) was stirred before each measurement to ensure homogeneity of both optical properties and temperature. Each experiment was completed within 3 hours during which the sample temperature was raised from ~ 32 to 38°C . The phantom and its container were weighed prior to heating, and again at the end of the experiment; the average total weight loss during the whole experiment was approximately $0.5 \pm 0.3\%$.

3.1.4 Animal Preparation and Experimental Procedure

In-vivo experiments were conducted on eight piglets (6 females and 2 males) whose average age and weight were 1.6 ± 0.7 days and 1.9 ± 0.4 kg, respectively. Animal experiments were approved by the Animal Use Subcommittee of the Canadian Council on Animal Care at Western University and conducted according to its guidelines. Newborn Duroc cross piglets were obtained from a local supplier on the morning of the experiment. Piglets were anesthetized with 1-2% isoflurane (3-4% during preparatory surgery). A tracheotomy was performed and the piglet was ventilated with a volume-controlled mechanical ventilator to deliver oxygen and medical air mixture (2:1). A femoral artery was catheterized to monitor heart rate (HR) and mean arterial blood pressure (MAP), and to intermittently collect arterial blood samples for gas analysis and measure of blood glucose levels. Deep brain temperature was also measured continuously with a thermocouple probe; a burr hole was drilled in the skull with a Dremal tool and a needle

thermocouple probe was inserted laterally through the skull into the brain to a depth of 2 cm vertical from the brain surface and 1.5 cm posterior to the bregma along the mid-line. After surgery, a heated water blanket was used to maintain rectal temperature between 37.5-38.5°C. Normocapnia (37-40 mmHg) was maintained throughout the experiment by adjusting the breathing rate and volume, depending on the arterial CO₂ tension ($p\text{CO}_2$) obtained from the blood samples or from monitoring end-tidal CO₂ tension. Arterial oxygen tension ($p_a\text{O}_2$) was maintained at a level between 90-130 mmHg by adjusting the ratio of oxygen to medical air at ventilator setting. Blood glucose was also monitored and 1-2 ml infusion of 25% glucose solution was administered intravenously if blood glucose concentration fell below 4.5 mmol/L.

The experiment started at a delay of 60 min after the completion of the surgical procedures to allow time for the physiological variables (HR, MAP, $p\text{CO}_2$ and $p_a\text{O}_2$) to stabilize. This delay was also sufficient to minimize any drift artifacts in the TR-NIRS measurements.²⁶ Piglets were placed in the prone position and a custom-made probe holder was strapped to the head to hold the emission and detection probes 2 cm apart, parasagittally, approximately 1.5 cm dorsal to the eyes directly in front of thermometer probe. Temperature was altered by placing plastic ice bags on the surface of the piglet's body until the brain temperature decreased to 31-32°C over ~ 3 to 4 hours. For each experiment, the baseline count rate measured with the TR instrument was adjusted to 800 kHz to match the count rate used to measure the IRF and was fixed for the remaining of the study. Tissue absorption coefficients were determined from reflectance data acquired continuously for 320 s at intervals of 10 s each. The entire experiment was completed within 5 hours. After the last measurement, the animals were sacrificed with intravenous potassium chloride (1-2 ml/kg) infusion. Thereafter, the brain was harvested and placed in paraformaldehyde (PFA) for 24 to 48 hours, and then transferred into a phosphate buffer saline (PBS) solution for preservation. Excised brains were later paraffin-embedded and cut into 5 µm-thick serial sections to verify the position of temperature probe and assess any potential bleeding caused by inserting the probe.

3.2 Data Analysis

A number of approaches have been developed to characterize the temperature dependence of the water absorption spectrum, including Gaussian component, classical and inverse least-squares, hybrid method and principal components analysis (PCA).¹² In this study, TR-NIRS data were analyzed with PCA method to predict tissue temperature. It has been shown that PCA can reduce random errors compared to the other methods and improve the fitting to the model.¹²

3.2.1 Temperature Fitting Algorithm

The workflow to predict the temperature was as follows:

- (i) Hollis *et al.* described the calibration of pure water absorption spectrum against temperature as a combination of components, known as *principal components*, that vary linearly with temperature.¹² As a first step, a data set (X) containing many independent variables was decomposed into two sets of linear variables. In matrix notation, principal component regression (PCR) can be described as follows:

$$\mathbf{X}=\mathbf{S}\cdot\mathbf{P}, \quad (3-1)$$

where the rows of data matrix X ($n \times m$) are the (n) pure water absorption spectra over (m) wavelengths at different temperatures at 0.1°C steps between 25°C and 45°C used in the calibration. The rows of P ($h \times m$) are the principal components of X , S ($n \times h$) contains the components scores and (h) is the number of principal component used in the model. A MATLAB program was written to determine the principal components of the mean-centered data using an eigenvector decomposition technique.²⁷ It has been shown that the first PC accounted for 99% of the total variance of the calibration absorption spectra.¹² The next stage of the PCR calibration was to establish a linear relationship between the components scores and temperature.¹² The model is defined as follows:

$$t=S.v, \quad (3-2)$$

where t is the vector of the known calibration temperatures, v is the calibration vector relating the scores to the temperature. Equations (3-1) and (3-2) provide the principal components (matrix P) and calibration vector (v) that are used to predict the temperature from any spectrum.¹²

(ii) The extinction coefficients of the major chromophores (H_2O , HbO_2 and Hb) were used to recover their concentrations from the absorption coefficients measured at the three wavelengths by TR-NIRS. Since the pure water absorption spectra were mean-centered for the PCR calibration, the mean water absorption coefficients from the calibration must also include to the fitting. Although the mean calibration coefficients could also be subtracted (rather than fitted to) from the measured tissue absorption coefficients:

$$\mu_a(\lambda) = c_{H_2O} \cdot (\bar{\epsilon}_{H_2O}(\lambda) + \sum_i S_i \cdot P_i(\lambda)) + \sum_{i=Hb, HbO_2} c_i \cdot \epsilon_i(\lambda), \quad (3-3)$$

where $\mu_a(\lambda)$ is the absorption coefficient measured at wavelength λ , c_i is the concentration of the i^{th} chromophore, $\epsilon_i(\lambda)$ is the extinction coefficient at λ , $\bar{\epsilon}_{H_2O}(\lambda)$ is the the mean pure water absorption coefficient from the calibration at λ , S_i is the score of the i^{th} loading vector, and $P_i(\lambda)$ is a loading vector of the pure water at λ . In the first step, a least-square optimization algorithm (MATLAB function *fminsearchbnd*²⁸) was used to extract the score of one pure water loading vector, i.e. PC, and concentrations of oxy- and deoxy-hemoglobin at baseline temperature by assuming a known water concentration of 95% and 85% for phantom and tissue experiments, respectively.^{16, 29} The optimization function is bound constrained, where bounds were applied to the recovered values to limits of search for oxy- and deoxy-hemoglobin concentrations to be in the range of 30-60 μM ³⁰ and 5-25 μM ^{31, 32}, respectively. Note, the extinction coefficients of pure water as a function of temperature, oxy- and deoxy-hemoglobin used in this study were taken from literature.^{33, 34}

(iii) Predicted temperature was calculated by multiplying the scores of water

loading vectors found in the previous step by the calibration vector:

$$T_{\text{predicted}} = \sum_i S_{pc_i} \cdot v, \quad (3-4)$$

where v is the calibration vector relating the scores to the temperature obtained in step (i).

(iv) If the initial predicted temperature was different from the known temperature obtained by the thermometer at the beginning of the experiment, the Equation (3-3) from step (ii) was altered to include a constant in order to find the corrected score related to the pure water loading vector corresponding to the initial temperature.

$$\mu_a(\lambda) = c_{\text{H}_2\text{O}}(\bar{\epsilon}_{\text{H}_2\text{O}}(\lambda) + \sum_i S_i P_i(\lambda)) + \sum_{i=\text{Hb}, \text{HbO}_2} c_i \epsilon_i(\lambda) + \text{constant}, \quad (3-5)$$

(v) The magnitude of the constant was determined using an iterative algorithm based on the criterion:

$$\max(\text{diff}) \leq 0.5^\circ\text{C}, \quad (3-6)$$

where

$$\text{diff} = (T_{\text{predicted}} - T_{\text{thermometer}})_{@ \text{initial temp}}. \quad (3-7)$$

(vi) For subsequent temperature predictions, the chromophore fitting was repeated with the constant obtained from the correction for initial temperature, and then tissue temperature was computed as described in step (iii).

3.3 Statistical Analysis

SPSS 17.0.0 (SPSS, Inc, Chicago, IL) was used for all statistical analyses. Normality of the distribution of the measurements was verified using Kolmogorov–

Smirnov test. Physiological parameters between different temperatures were then analyzed using one-way ANOVA. Correlations between the predicted temperatures against the temperatures measured by thermometry were analyzed using parametric linear regression. Finally, the degree of similarity between temperature measurements acquired with the two techniques was evaluated using a Bland-Altman plot.³⁵ Comparisons of optical properties (μ_a and μ_s') at different temperatures were analyzed by a repeated-measures two-way mixed ANOVA to determine statistical differences as a function of temperature for different wavelengths. Statistical significance was based on p -value < 0.05 . All data are presented as mean \pm SD unless otherwise noted.

3.4 Results

Table 3.1 displays the temperature effects on absorption and reduced scattering coefficients for the tissue-mimicking phantom. There was a statistically significant increase in absorption coefficient when temperature increases above 36°C at all three wavelengths. The absorption coefficients were significantly lower at 760 nm than at 810 and 830 nm while the reduced scattering coefficients were significantly higher at 760 nm than at 830 nm. No significant differences were found for reduced scattering coefficients between temperatures.

Table 3.1. Absorption and reduced scattering coefficients measured at three discrete wavelengths as function of temperature in *in-vitro* (tissue-mimicking phantoms). Values are mean \pm SD.

Variable	λ (nm)	(38°C)	(36°C)	(34°C)	(32°C)
μ_a (mm ⁻¹)	830	0.0175 \pm 0.007 ^{*†}	0.0152 \pm 0.006 [†]	0.0147 \pm 0.005 [†]	0.0142 \pm 0.005 [†]
	810	0.0155 \pm 0.005 ^{*†}	0.0134 \pm 0.005 [†]	0.0131 \pm 0.005 [†]	0.0127 \pm 0.004 [†]
	760	0.0118 \pm 0.003 [*]	0.0103 \pm 0.003	0.0101 \pm 0.003	0.0099 \pm 0.003
μ_s' (mm ⁻¹)	830	1.97 \pm 0.19 [†]	1.97 \pm 0.15 [†]	1.99 \pm 0.14 [†]	1.99 \pm 0.12 [†]
	810	2.06 \pm 0.26	2.06 \pm 0.21	2.05 \pm 0.21	2.08 \pm 0.20
	760	2.17 \pm 0.22	2.16 \pm 0.17	2.21 \pm 0.21	2.21 \pm 0.19

* a statistically significant ($P < 0.05$) difference compared to the baseline (32°C). † a statistically significant ($P < 0.05$) difference compared to wavelength of 760 nm.

Figure 3.1 shows the measured against predicted temperature of the tissue-mimicking phantoms. The average slope, intercept and R^2 value from the individual regression analyses were 1.01, -0.16°C, 0.82. From the Bland-Altman analysis in Figure

3.1(b), the mean difference between the predicted and measured temperatures was 0.1°C . The 95% confidence interval of the difference between the two were 2.3°C to -2.1°C .

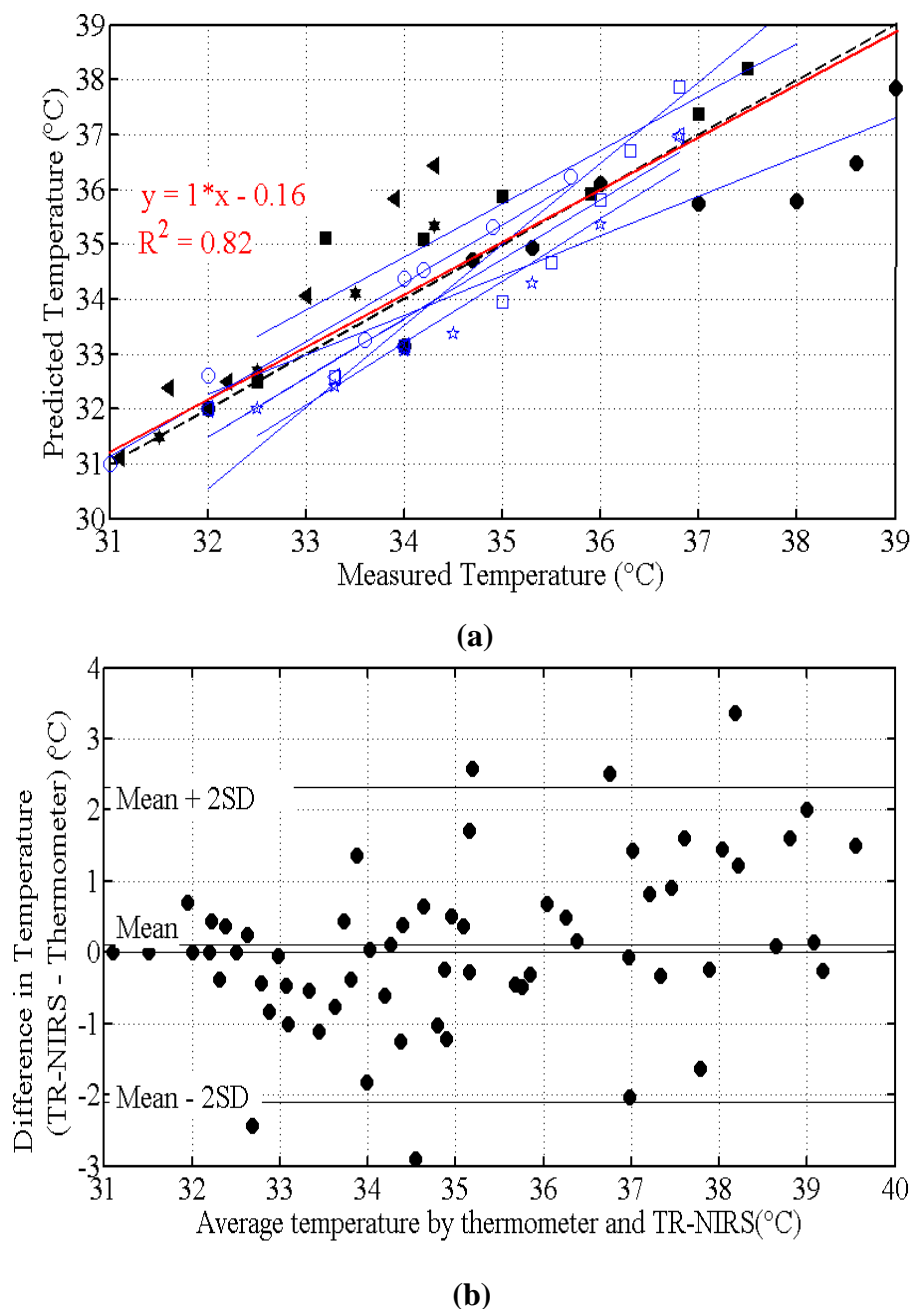


Figure 3.1: (a) Correlation plot comparing temperature in the tissue-mimicking phantom calculated using data acquired by TR-NIRS against temperature measured with a thermometer (labeled Predicted Temperature and Measured Temperature, respectively). Each symbol type represents data from one of seven experiments with the tissue-mimicking phantom. The solid line represents the average of all individual linear regression lines and the dotted line indicates the line of identity (slope =1). (b) Bland-Altman plot comparing Predicted and Measured temperature. The dotted line shows the mean difference and dash-dotted lines show the limits of agreement ($\text{mean} \pm 2 \text{SD}$) between the two temperature measurements.

Table 3.2 provides a summary of the measured physiological parameters in piglets at the different brain temperatures. There was a statistically significant decrease in HR and P_aO_2 when temperature dropped to 34°C and lower. Analysis of the brain tissue sections revealed no gross hemorrhages caused by insertion of the thermometer probe into the brain.

Table 3.2. Physiological parameters measured at different brain temperatures. Values are mean \pm SD.

	(38°C)	(36°C)	(34°C)	(32°C)
MAP (mmHg)	42 \pm 5	41 \pm 4	40 \pm 4	38 \pm 4
HR (bpm)	139 \pm 10	125 \pm 14	109 \pm 11*	94 \pm 13*
pH	7.4 \pm 0.01	7.4 \pm 0.02	7.4 \pm 0.01	7.5 \pm 0.1
p_aCO_2 (mmHg)	39 \pm 1	38 \pm 2	40 \pm 1	38 \pm 1
p_aO_2 (mmHg)	122 \pm 15	93 \pm 7	90 \pm 17*	75 \pm 17*
Hb (μ mol/L)	24.9 \pm 9.2	25.4 \pm 10.8	25.2 \pm 11.2	26.7 \pm 11.1
HbO ₂ (μ mol/L)	63.4 \pm 20.9	62.9 \pm 20.6	63.3 \pm 19.9	61.5 \pm 20.2
tHb (μ mol/L)	88.4 \pm 22.3	88.3 \pm 23.1	88.7 \pm 22	88.9 \pm 21.8

MAP=mean arterial blood pressure; HR=heart rate; tHb=total hemoglobin; Hb=Deoxy-hemoglobin; HbO₂=Oxy-hemoglobin. * a statistically significant ($P<0.05$) difference compared to the baseline (38°C).

Table 3.3 provides the measured μ_a and μ_s' in the piglet brain at three wavelengths and at different temperatures. The absorption coefficient was higher at 830 nm than at 810 and 760 nm and, as expected, the reduced scattering coefficient decreased as wavelength increased.³⁶

Table 3.3. Absorption and reduced scattering coefficients measured at three discrete wavelengths as function of temperature in *in-vivo* (newborn piglets brain). Values are mean \pm SD.

Variable	λ (nm)	(38°C)	(36°C)	(34°C)	(32°C)
μ_a (mm ⁻¹)	830	0.0240 \pm 0.005 [†]	0.0242 \pm 0.005 [†]	0.0225 \pm 0.005 [†]	0.0177 \pm 0.001
	810	0.0214 \pm 0.003	0.0219 \pm 0.004	0.0204 \pm 0.003	0.0168 \pm 0.002
	760	0.0214 \pm 0.002	0.0223 \pm 0.003	0.0212 \pm 0.004	0.0173 \pm 0.002
μ_s' (mm ⁻¹)	830	0.68 \pm 0.08 [†]	0.67 \pm 0.07 [†]	0.67 \pm 0.08 [†]	0.67 \pm 0.05 [†]
	810	0.74 \pm 0.10	0.74 \pm 0.08	0.73 \pm 0.11	0.80 \pm 0.05
	760	0.79 \pm 0.13	0.78 \pm 0.11	0.73 \pm 0.13	0.81 \pm 0.12

[†] a statistically significant ($P<0.05$) difference compared to wavelength of 760 nm.

Figure 3.2(a) shows a correlation plot comparing predicted brain temperature calculated using data acquired from TR-NIRS against temperature measured with a thermometer. Results from regression analysis for each piglet, as well as the average of all experiments are shown in Figure 3.2(a). From the Bland-Altman analysis in Figure 3.2(b), the mean difference between the predicted and measured temperatures was 0.5°C.

The 95% confidence interval of the difference between the two were 2.7°C to -3.6°C. The average slope, intercept and R^2 value from the individual regression analyses were 1.1, -1.6°C, 0.66, respectively.

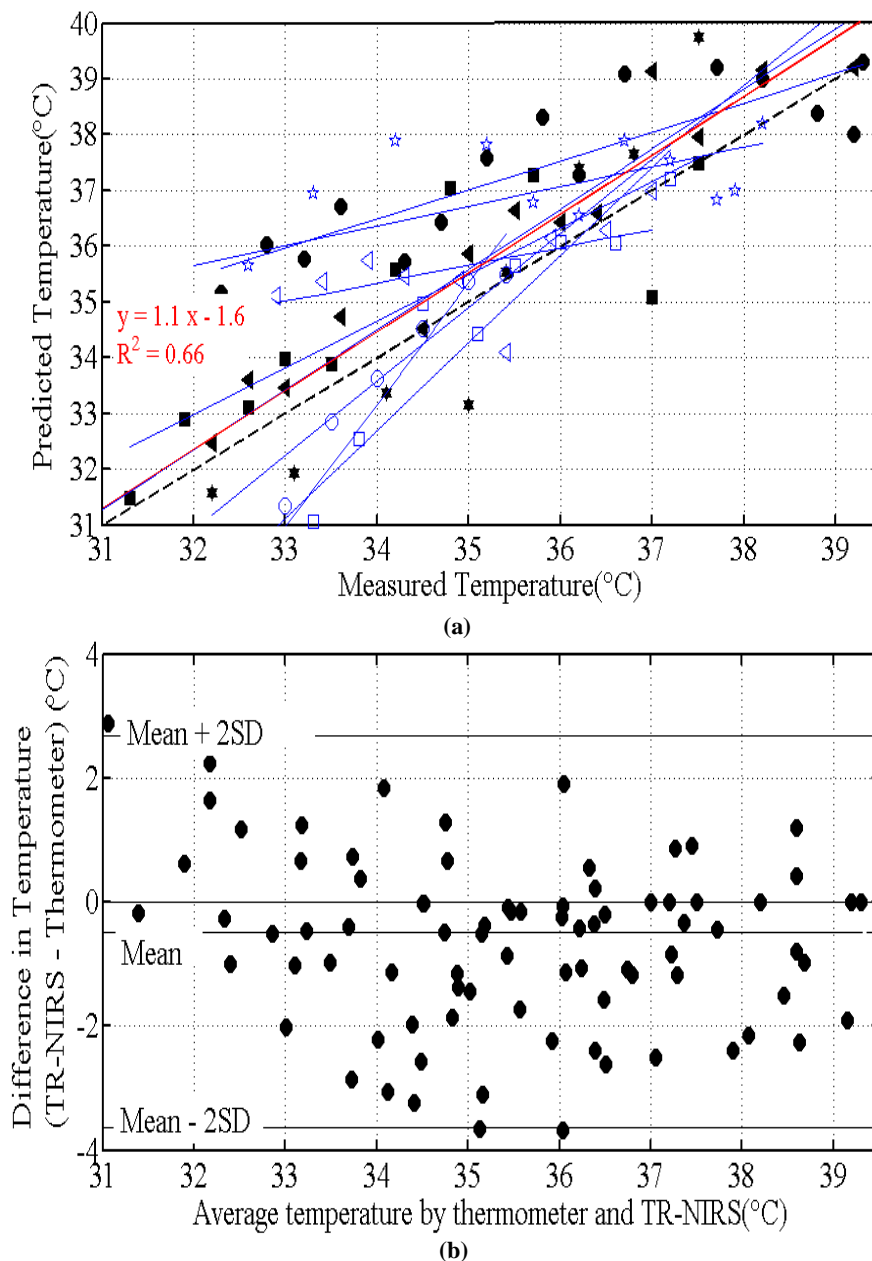


Figure 3.2: (a) Correlation plot comparing temperature in the piglet brain calculated using data acquired by TR-NIRS against temperature measured with a thermometer (labeled Predicted Temperature and Measured Temperature, respectively). Each symbol type represents data from one of eight piglets. The solid line represents the average of all individual linear regression lines and the dotted line indicates the line of identity (slope =1). (b) Bland-Altman plot comparing Predicted and Measured temperature. The dotted line shows the mean difference and dash-dotted lines show the limits of agreement (mean \pm 2SD) between the two temperature measurements.

3.5 Discussion

We investigated the ability of TR-NIRS technique to measure temperature in tissue-mimicking phantoms and newborn piglet's brains using the temperature-dependence of water absorption features around ~740 nm and ~840 nm during heating and cooling, respectively. The TR-NIRS temperature measurements in this study were based on subtle changes in the NIR water absorption characteristics due to macromolecular binding with the following assumptions. First, the concentration of water in the brain is assumed 85% in order to calculate the score of one pure water loading vector, i.e., one PC as well as cerebral hemoglobin concentrations. Second, the initial tissue temperature is known from thermometer to find the corrected score related to the pure water loading vector corresponding to this temperature. Third, to determine optical properties from changes in light absorption caused by cooling, the scaling factor and μ_s' were set to the values determined from the baseline measurements and only μ_a was included as fitting parameter. This approach has been shown to improved the stability of the fitting procedure by limiting the number of fitting parameters as well as reducing cross-talk between parameters.^{12,20} For example, including scaling factor or μ_s' as a fitting parameter along μ_a resulted in a weak correlation of $R^2 = 0.68$ and $R^2 = 0.57$ between the TR-NIRS method and thermometer measurements for phantom experiments, respectively (data not shown). Furthermore, in our calculation, we assumed that the molar extinction coefficient of oxy- and deoxy- hemoglobin are constant over the temperature range of 39-31°C. However, temperature-dependent changes of the hemoglobin NIR absorption spectra have been investigated³⁷; it has been shown that with increasing temperature in the range of 20-40°C the amplitude of Hb and HbO₂ decreased by 0.15-0.18% °C⁻¹ and by less than 0.05% °C⁻¹ and shifted by 0.08 nm °C⁻¹ and 0.15 nm °C⁻¹, respectively.³⁷

The proposed method for calculating temperature were tested against direct thermometer measurement in tissue-mimicking phantom. Results demonstrate that TR-NIRS was sensitive to temperature changes via changes in tissue water absorption coefficient and could measure the temperature of the tissue-mimicking phantom. A strong correlation ($R^2 = 0.82$) of the predicted temperature calculated using TR-NIRS data to the

measured temperature with a thermometer was observed, with a slope of 1.01 indicating the equivalency between the optical and thermometer measurements over the temperature range of 33-38°C. The average difference between the TR-NIRS predicted temperature and the measured temperature was $0.15 \pm 1.1^\circ\text{C}$.

For the *in-vivo* temperature measurement we used piglets because they are commonly used animal model of human newborn neurology³⁸ and signal contamination from the minimal extra-cerebral tissue is relatively negligible, which enables the measured TPSFs to be modeled as the solution of the diffusion equation for a homogeneous semi-infinite geometry.²⁵ A correlation between the thermometer measured and TR-NIRS predicted temperature was obtained ($R^2 = 0.66$) with a slope of 1.1 over the temperature range of 39-31°C. There are thermoregulatory responses to a decline in body temperature, such as the effects of cold-induced vasoconstriction, reduction of mean arterial pressure and cardiac output.³⁹ Vasoconstriction decreases the vascular space during hypothermia⁴⁰, which decrease the volume of blood in the region probed by the TR-NIR light, and hence a reduction in μ_a . Moreover, the red blood cells are known to be a source of light scattering in tissue and typically occupies less than 2% of brain volume⁴¹, therefore a greater values of μ_s' observed in in tissue-mimicking phantom compared with the piglet brain may be explained by higher concentration, i.e. ~4%, of whole blood used in solution.

There are a number of potential sources of error that could contribute to the discrepancy between the TR-NIRS predicted and thermometer measured temperature. One source of error is employing the pure water absorption spectrum and parameters associated with the temperature response that were used for fitting tissue temperature i.e., calibration vector and PCs. The difference in absorption spectrum between tissue and pure water is due to bound water within tissue.⁴² However, in our calculation, the chromophore fitting was performed with the loading vectors obtained from the PCR of the pure water absorption spectrum rather than that of 'tissue water', which resulted in the predicted temperature either underestimating or overestimating the thermometer temperature. A correction was performed using a constant value according to equation (3-3) to make the predicted temperature as close as possible to the true initial temperature,

which was known from the thermometer. We also note that temperature prediction was not improved by the inclusion of more than one water loading vector, i.e. more PCs (only one was used in this study). Another potential source of error could be due to error in the determination of dispersion caused by the TR system (i.e. IRF of the system)²⁵. In general the accuracy of the temperature prediction by our NIRS technique can be improved by having a continuous tissue absorption spectrum which offers better chromophore identification and improved concentration measurement of major tissue chromophores, i.e., water, oxy-, deoxy-hemoglobin and fat, particularly for water peak at 970 nm due to its greater temperature sensitivity and lower scattering in tissue. This can be done by combination of TR and CW spectroscopy, whereas most of the wavelength coverage is provided by a white-light CW measurement, and the TR data are acquired at a few selected NIR wavelengths. Measuring several μ_s' values can be used in a simple function of wavelength to obtain estimates of μ_s' across the entire wavelength range.⁴³ With μ_s' calculated and the measured CW reflectance, coefficients of absorption will be derived from the diffusion equation at all wavelengths in the spectral window of interest.⁴⁴ Another possible way to improve the reproducibility of the predicted tissue temperature by the NIRS technique would be to perform multiple measurements (predictions) at each temperature and calculate the average of the predicted temperatures. The major challenge in adapting this technique to adult patients is the significant signal contamination from superficial tissues. This is not a concern in neonatal applications, where the scalp and skull is negligible and it is reasonable to assume that all the collected light has traveled through brain tissue. However, in the adult subjects, the scalp, skull, and cerebral spinal fluid surrounding the brain can contribute significantly to absorption. In this case, it becomes very difficult to measure absolute concentrations of cerebral chromophores. It has previously been demonstrated that the depth sensitivity of the NIR signal is proportional to the distance separating emitter and detector⁴⁵. This multi-distance, or depth-resolved approach allows the separation of information into superficial and deep components on the basis that light penetration increases with source-detector distance. Consequently, by collecting information at multiple distances simultaneously, it is possible to separate out information in terms of tissue layers, using an optical reconstruction approach.⁴⁶

In conclusion, we have demonstrated a method of monitoring tissue temperature non-invasively using the temperature response of water absorption peaks in the NIR spectral region. The results from tissue-mimicking phantoms show a strong correlation ($R^2 = 0.82$) between the TR-NIRS method and thermometer measurements and we showed the potential of TR-NIRS method to measure temperature *in-vivo* in an animal model of the newborn. Since NIRS is safe and measurements can be obtained at the bedside in only a few minutes, it is believed that this technique could assist in monitoring of brain temperature in the neonatal intensive care unit during hypothermia therapy.

3.6 References

1. Moore EM, Nichol AD, Bernard SA, Bellomo R. Therapeutic hypothermia: Benefits, mechanisms and potential clinical applications in neurological, cardiac and kidney injury. *Injury*. 2011;42:843-854
2. Lampe JW, Becker LB. State of the art in therapeutic hypothermia. *Annu Rev Med*. 2011;62:79-93
3. Quinn MW, Munyard PF. Treatment of asphyxiated newborns with moderate hypothermia in routine clinical practice: How cooling is managed in the uk outside a clinical trial. *Arch Dis Child Fetal Neonatal Ed*. 2010;95:F152
4. Sarkar S, Barks JD. Systemic complications and hypothermia. *Semin Fetal Neonatal Med*. 2010;15:270-275
5. Straus D, Prasad V, Munoz L. Selective therapeutic hypothermia: A review of invasive and noninvasive techniques. *Arq Neuropsiquiatr*. 2011;69:981-987
6. Shibasaki M, Kondo N, Tominaga H, Aoki K, Hasegawa E, Idota Y, Moriwaki T. Continuous measurement of tympanic temperature with a new infrared method using an optical fiber. *J Appl Physiol*. 1998;85:921-926
7. Kirk D, Rainey T, Vail A, Childs C. Infra-red thermometry: The reliability of tympanic and temporal artery readings for predicting brain temperature after severe traumatic brain injury. *Crit Care*. 2009;13:R81
8. Weis J, Covaciu L, Rubertsson S, Allers M, Lunderquist A, Ortiz-Nieto F, Ahlstrom H. Phase-difference and spectroscopic imaging for monitoring of human brain temperature during cooling. *Magn Reson Imaging*. 2012

9. Fatar M, Stroick M, Griebe M, Alonso A, Hennerici MG, Daffertshofer M. Brain temperature during 340-khz pulsed ultrasound insonation: A safety study for sonothrombolysis. *Stroke*. 2006;37:1883-1887
10. Karathanasis KT, Gouzouasis IA, Karanasiou IS, Giamalaki MI, Stratakos G, Uzunoglu NK. Noninvasive focused monitoring and irradiation of head tissue phantoms at microwave frequencies. *IEEE Trans Inf Technol Biomed*. 2010;14:657-663
11. Dittmar A, Gehin C, Delhomme G, Boivin D, Dumont G, Mott C. A non invasive wearable sensor for the measurement of brain temperature. *Conf Proc IEEE Eng Med Biol Soc*. 2006;1:900-902
12. Hollis V. Non-invasive monitoring of brain tissue temperature by near-infrared spectroscopy. *PhD thesis, Department of Medical Physics and Bioengineering, University College London: London*. 2002
13. Langford V. Temperature dependence of the visible-near-infrared absorption spectrum of liquid water. *J Phys Chem A*. 2001;105:8916-8921
14. Kelly J. Tissue temperature by near-infrared spectroscopy. *SPIE Proc*. 2389. 1995:818-828
15. Chung SH, Cerussi AE, Merritt SI, Ruth J, Tromberg BJ. Non-invasive tissue temperature measurements based on quantitative diffuse optical spectroscopy (dos) of water. *Phys Med Biol*. 2010;55:3753-3765
16. White DR, Widdowson EM, Woodard HQ, Dickerson JW. The composition of body tissues (ii). Fetus to young adult. *Br J Radiol*. 1991;64:149-159
17. Selb J, Stott JJ, Franceschini MA, Sorensen AG, Boas DA. Improved sensitivity to cerebral hemodynamics during brain activation with a time-gated optical system: Analytical model and experimental validation. *J Biomed Opt*. 2005;10:11013
18. Okui N, Okada E. Wavelength dependence of crosstalk in dual-wavelength measurement of oxy- and deoxy-hemoglobin. *J Biomed Opt*. 2005;10:11015
19. Ossoff RH. Implementing the ansi z 136.3 laser safety standard in the medical environment. *Otolaryngol Head Neck Surg*. 1986;94:525-528
20. Ntziachristos V, Chance B. Accuracy limits in the determination of absolute optical properties using time-resolved nir spectroscopy. *Med Phys*. 2001;28:1115-1124

21. Liebert A, Wabnitz H, Grosenick D, Macdonald R. Fiber dispersion in time domain measurements compromising the accuracy of determination of optical properties of strongly scattering media. *J Biomed Opt.* 2003;8:512-516
22. Kienle A, Patterson MS. Improved solutions of the steady-state and the time-resolved diffusion equations for reflectance from a semi-infinite turbid medium. *J Opt Soc Am A Opt Image Sci Vis.* 1997;14:246-254
23. Alerstam E, Andersson-Engels S, Svensson T. Improved accuracy in time-resolved diffuse reflectance spectroscopy. *Opt Express.* 2008;16:10440-10454
24. Becker W. Advanced time-correlated single photon counting technique. *Springer.* 2005;New York
25. Diop M, Tichauer KM, Elliott JT, Migueis M, Lee TY, St Lawrence K. Comparison of time-resolved and continuous-wave near-infrared techniques for measuring cerebral blood flow in piglets. *J Biomed Opt.* 2010;15:057004
26. M. Diop JTE, K. M. Tichauer, M. Migueis, T. Y. Lee, and K., Lawrence S. Bedside monitoring of absolute cerebral blood flow by time-resolved nirs. *Proc. SPIE 7555, 1-9.* 2010
27. Shlens J. A tutorial on principal component analysis. *Institute for Nonlinear Science, UCSD.* 2005
28. D'Errico J. "fminsearchbnd, fminsearchcon - file exchange — matlab central [online]," <http://www.Mathworks.Com/matlabcentral/fileexchange/8277-fminsearchbnd> [cit. 2014-01-20].
29. Cooper CE, Elwell CE, Meek JH, Matcher SJ, Wyatt JS, Cope M, Delpy DT. The noninvasive measurement of absolute cerebral deoxyhemoglobin concentration and mean optical path length in the neonatal brain by second derivative near infrared spectroscopy. *Pediatr Res.* 1996;39:32-38
30. Fantini S, Franceschini M, Gratton E, Hueber D, Rosenfeld W, Maulik D, Stubblefield P, Stankovic M. Non-invasive optical mapping of the piglet brain in real time. *Opt Express.* 1999;4:308-314
31. Tichauer KM, Elliott JT, Hadway JA, Lee DS, Lee TY, St Lawrence K. Using near-infrared spectroscopy to measure cerebral metabolic rate of oxygen under multiple levels of arterial oxygenation in piglets. *J Appl Physiol (1985).* 2010;109:878-885
32. Matcher SJ, Cooper CE. Absolute quantification of deoxyhaemoglobin concentration in tissue near infrared spectroscopy. *Phys Med Biol.* 1994;39:1295-1312

33. Matcher SJ, Elwell CE, Cooper CE, Cope M, Delpy DT. Performance comparison of several published tissue near-infrared spectroscopy algorithms. *Anal Biochem.* 1995;227:54-68
34. Biomedical optics laboratory, university of london, “specific extinction spectra of tissue chromophores,” available from: [Http://www.Medphys.Ucl.Ac.Uk/research/borl/research/nir_topics/spectra/spectra.Htm](http://www.Medphys.Ucl.Ac.Uk/research/borl/research/nir_topics/spectra/spectra.Htm).
35. Bland JM, Altman DG. Statistical methods for assessing agreement between two methods of clinical measurement. *Lancet.* 1986;1:307-310
36. Fu Q, Sun W. Mie theory for light scattering by a spherical particle in an absorbing medium. *Appl Opt.* 2001;40:1354-1361
37. Sfarenì R, Boffi A, Quaresima V, Ferrari M. Near infrared absorption spectra of human deoxy- and oxyhaemoglobin in the temperature range 20-40 degrees c. *Biochim Biophys Acta.* 1997;1340:165-169
38. Rooney T, Raju TN, Moustogiannis AN. Animal models for the study of perinatal hypoxic-ischemic encephalopathy: A critical analysis. *Early Hum Dev.* 1997;47:115-146
39. Cavallaro G, Filippi L, Raffaelli G, Cristofori G, Schena F, Agazzani E, Amodeo I, Griggio A, Boccacci S, Fiorini P, Mosca F. Heart rate and arterial pressure changes during whole-body deep hypothermia. *ISRN Pediatr.* 2013;2013:140213
40. Satinoff E. Behavioral thermoregulation in response to local cooling of the rat brain. *Am J Physiol.* 1964;206:1389-1394
41. Cope M. The development of a near infrared spectroscopy system and its application for non-invasive monitoring of cerebral blood and tissue oxygenation in the newborn infant. *PhD thesis, University of London, London.* 1991
42. Chung SH, Cerussi AE, Klifa C, Baek HM, Birgul O, Gulsen G, Merritt SI, Hsiang D, Tromberg BJ. In vivo water state measurements in breast cancer using broadband diffuse optical spectroscopy. *Phys Med Biol.* 2008;53:6713-6727
43. Graaff R, Aarnoudse JG, Zijp JR, Sloot PM, de Mul FF, Greve J, Koelink MH. Reduced light-scattering properties for mixtures of spherical particles: A simple approximation derived from mie calculations. *Appl Opt.* 1992;31:1370-1376
44. Bevilacqua F, Berger AJ, Cerussi AE, Jakubowski D, Tromberg BJ. Broadband absorption spectroscopy in turbid media by combined frequency-domain and steady-state methods. *Appl Opt.* 2000;39:6498-6507

45. Bonner RF, Nossal R, Havlin S, Weiss GH. Model for photon migration in turbid biological media. *J Opt Soc Am A*. 1987;4:423-432
46. Elliott J. On the development of a dynamic contrast-enhanced near-infrared technique to measure cerebral blood flow in the neurocritical care unit. *PhD thesis, Department of Medical Biophysics, Western University: London*. 2013

Chapter 4

Coupling of Cerebral Blood Flow and Oxygen Consumption during Hypothermia under Different Anesthetics in Newborn Piglets Measured by TR-NIRS

This chapter is adapted from the work entitled “Coupling of Cerebral Blood Flow and Oxygen Consumption During Hypothermia Under Different Anesthetics in Newborn Piglets Measured with a Time-Resolved Near-Infrared Technique”, submitted to the *Biomedical Optics Express* by: M Fazel Bakhsheshi, M Diop, K St. Lawrence and TY Lee. The focus of this paper is two-fold: to investigate the sensitivity of the TR-NIR technique to measure CBF during cooling at different temperatures, for validation, CBF was independently measured by CT perfusion at each temperature; and, to investigate the cerebral metabolic activity during hypothermia under different anesthetics.

4. Introduction

Mild hypothermia (HT), in which the brain temperature is lowered to 32-33°C, has been shown to be an effective neuroprotective therapy to reduce brain injury following cardiac arrest, traumatic brain injury and birth asphyxia and ischemic encephalopathy.¹ One of the important mechanisms of HT-induced neuroprotection is the preservation of brain ATP levels resulting from a reduction in cerebral metabolism or metabolic rate of oxygen (i.e. CMRO₂).² The effects of HT on CBF are a consequence of the well-accepted phenomenon that CMRO₂ is closely coupled to CBF and therefore, a reduction in the former is coupled to a reduction in the latter.^{3,4} Preserving the coupling between CBF and CMRO₂ is an important factor in the control of the cerebral circulation, connecting the change in metabolic demands with the supply of substrates by blood flow. As a consequence of this balance between flow and metabolism, the oxygen extraction fraction (OEF) indicates any regional variation in brain. For example under oxidative stress, e.g.

ischemia-hypoxia, the OEF is increased from its basal value of ~30% leading to cerebral venous desaturation.⁵⁻⁷

Clinically, HT is typically induced under anesthesia to minimize brain damage, so it is important to determine whether the combination of anesthesia and HT alters flow-metabolism coupling or deviates OEF from its basal values. Current methods to monitor changes in energy metabolism using PET and blood flow using MRI or CT are hampered by practical issues such as need to transfer patients to imaging facilities and prolonged scanning times, both of which are not practical for unstable patients. Therefore, a non-invasive method that can be available over prolonged periods of cooling and rewarming phases is required since neural protection therapy may involve HT being maintained for periods of 72 hours.^{8, 9} Optical methods are promising alternatives to these current techniques since they are safe, the instruments are compact, portable and can provide physiological measurements at the bedside of patients. We have previously developed a dynamic contrast-enhanced NIR technique for measuring absolute CBF and CMRO₂ based on the Fick's Principle using a light-absorbing dye, indocyanine green (ICG), as an intravascular contrast agent.^{10, 11 12} However, there has been no previous study investigating feasibility of using time-resolved (TR) NIR technique to measure CBF and CMRO₂ during HT. The purpose of the current study is two-fold:

- (i). Validate the TR-NIR CBF measurement against that measured using a CT perfusion technique at different temperatures during HT¹³;
- (ii). Investigate the coupling of CMRO₂ and CBF under HT and different anesthetic combinations that may be used in clinical practice.

In the present study, CBF and CMRO₂ were measured with a TR-NIR technique in newborn piglets in which brain temperature was lowered from ~38° to 33°C under three anesthetic regimes: isoflurane, propofol/nitrous oxide (N₂O) and propofol/35-50% xenon (Xe_{35-50%}). The latter regime (propofol/Xe_{35-50%}) was used in the combined therapy of HT and Xe for neuroprotection in neurointensive care units (NICU)¹⁴; increasing neuroprotection from ~35% with HT_{32°C} only to ~70% when HT_{32°C} was combined with 50% inhaled Xe gas.¹⁵ Although recent study has shown that neonates with (Hypoxic-

Ischemic Encephalopathy) HIE undergoing HT have low CBF and CMRO₂ when compared with healthy age-matched neonates¹⁶, there is no study examine the effect of HT on OEF alternations or flow-metabolism coupling under different anesthetic regimes and temperatures. Understanding how the combination of HT under different anesthetic may alter flow-metabolism coupling or deviates OEF from its basal values in the healthy brain is critical before extending these neuroprotective strategies to the injured brain.

4.1 Materials and Methods

4.1.1 Instrumentation

The light sources of the TR-NIR system are thermoelectrically cooled picosecond pulsed diode lasers (LDH-P-C emitting at 760, 810 and 830 nm, PicoQuant, Germany) activated by a computer controlled laser driver (SEPIA PDL 828, PicoQuant, Germany). The 760 and 830nm emission wavelengths were chosen to quantify tissue chromophores (oxy-hemoglobin, HbO₂ and deoxy-hemoglobin, Hb) which were used to determine the cerebral oxygen saturation, while 810 nm laser coincides with the peak absorption wavelength of ICG in plasma. The output power and pulse repetition rate of the lasers were set to 1.4 mW and ~27 MHz, respectively. The individual pulses of the lasers were temporally separated by sharing the 80 MHz clock of the laser driver among the three lasers. Light emitted by each diode laser was attenuated by two adjustable neutral density filters (NDC-50-4M, Thorlabs, Newton, NJ) and coupled by a microscope objective lens (NA=0.25, magnification=10x) into one arm of a trifurcated fiber bundle (three fibers; NA=0.22, core 400 μm, Fiber Optics Technology, Pomfret, Connecticut). The distal common end of the bundle (emission probe) was placed on the scalp of the animal and held in position by a probe holder. The average power delivered to a subject was attenuated to ~20 μW per laser, which is below ANSI safety limits for skin exposure.¹⁷

Photons emerging from the scalp were collected by a 2-m fiber optic bundle (NA=0.55, 3.6 mm diameter active area, and 4.7-mm outer diameter, Fiberoptics Technology). The other end of the detection probe was secured in front of an

electromechanical shutter (SM05, Thorlabs). Light transmitted through the shutter was collected by a Peltier cooled microchannel plate photomultiplier tube (MCP-PMT) (PMC-100, Becker and Hickl, Germany). Detection of single photons generated electrical pulses (amplitude of 50-200 mV, width=1.5 ns) that were transmitted to a time-correlated single photon counting (TCSPC) module (SPC-134, Becker and Hickl, Germany) to generate the temporal point spread function (TPSF). As described in detail elsewhere¹¹, tissue optical properties (i.e., the absorption coefficient μ_a and the reduced scattering coefficient μ_s') were obtained using analytical solution of light diffusion to model the collected TPSFs .

4.1.2 Determination of Cerebral Blood Flow

CBF was measured using a bolus-tracking method that requires an intravenous bolus injection of ICG (1 ml, 0.2 mg/kg) into a peripheral vein, followed by continuous measurements of the time-varying concentrations of the dye in arterial blood and brain tissue. The arterial concentration, $C_a(t)$, was measured non-invasively by a dye densitometer (model DDG-2001 A/K, Nihon Kohden, Tokyo, Japan) with the probe attached to a front foot. Brain tissue concentration, $C_{icg}(t)$, was determined from reflectance data acquired by the TR-NIRS instrument continually for 76s at a sampling interval of 400 ms. The two concentration curves are related by the following equation:

$$C_{icg}(t) = C_a(t) * [CBF \cdot R(t)] \quad (4-1)$$

where * represents the convolution operator and $[CBF \cdot R(t)]$ is the flow-scaled impulse residue function or $R(t)$. The function $CBF \cdot R(t)$ can be extracted from the arterial and tissue ICG concentration curves using a deconvolution algorithm¹³. The initial height of the derived function is CBF, since by definition $R(0)=1$, and the area under the curve is the cerebral blood volume (CBV).¹⁸ For the TR-NIR data, quantification of the brain concentration of ICG was determined from the measured change in μ_a ¹¹:

$$C_{icg}(t) = [\mu_a(t) - \mu_a(0)] / [\ln(10) \times \varepsilon_{icg}] \quad (4-2)$$

where $\mu_a(0)$ represents the baseline value determined over a 10-second period prior to an injection of ICG, and ε_{ICG} is the extinction coefficient of ICG at 810 nm.

4.1.3 Determination of cerebral metabolic rate of Oxygen

Measurements of $CMRO_2$ were calculated¹⁰ using Fick's principle as follows:

$$CMRO_2 = CBF \cdot ([O_2]_a - [O_2]_v) \quad (4-3)$$

The difference between the arterial concentration of oxygen, $[O_2]_a$, and the cerebral venous concentration of oxygen, $[O_2]_v$, is commonly referred to as the arterial-venous difference of oxygen (AVDO₂), or the difference between the O₂ concentration of the arterial blood feeding the tissue of interest and O₂ concentration of the venous blood draining the tissue of interest. Equation (4-3) can be further expanded as follows¹⁹:

$$CMRO_2 = CBF \cdot 1.39 \cdot [tHb] \cdot (S_aO_2 - S_vO_2) \quad (4-4)$$

where $[tHb]$ is total hemoglobin concentration which can be measured from arterial blood samples. S_aO_2 and S_vO_2 are arterial and venous O₂ saturation, respectively. The constant 1.39 is the O₂ carrying capacity of hemoglobin measured in milliliters per gram of Hb. Note that the dye densitometer also provides continuous measurements of S_aO_2 , while S_vO_2 was determined indirectly from TR-NIRS measurements of average tissue cerebral blood oxygen saturation, $(SO_2)_{tissue}$. This technique relies on the assumption that there exists a stable arterial-venous blood ratio in the CBV, i.e.

$$(SO_2)_{tissue} = \alpha S_aO_2 + (1 - \alpha) S_vO_2 \quad (4-5)$$

where α represents the fraction of arterial blood in CBV. The relative distribution of arterial and venous compartments is generally accepted to be approximately 25% and 75% in the total CBV, therefore to measure S_vO_2 , α was set to 0.25.^{20, 21} To obtain tissue cerebral blood oxygen saturation, i.e., $(SO_2)_{tissue}$, cerebral hemoglobin (HbO_2 , Hb) concentrations were calculated with TR-NIRS which relies on the assumption that there is stable concentration of water in the brain, i.e., ~85%²². These hemoglobin measurements were determined by fitting the tissue absorption coefficients to the extinction coefficients of the major chromophores, i.e., (water, Hb, HbO_2). Tissue absorption coefficients were determined from reflectance data acquired continuously for 160s (i.e. 32 TPSFs) at a sampling interval of 5s. $(SO_2)_{tissue}$ can then be calculated as follows:

$$(SO_2)_{tissue} = \frac{HbO_2}{HbO_2 + Hb} \quad (4-6)$$

Using this relationship, a new expression for $CMRO_2$ can be derived that is independent of S_vO_2 :

$$CMRO_2 = CBF \cdot 1.39 \cdot [tHb] \cdot \left(\frac{S_aO_2 - (SO_2)_{tissue}}{1 - \alpha} \right) \quad (4-7)$$

The fraction of oxygen extracted from arterial blood into the brain, OEF, was calculated with the method described by Brown *et al*¹⁰:

$$OEF = \frac{CMRO_2}{CBF \cdot [O_2]_a} \quad (4-8)$$

The tight coupling of CBF and $CMRO_2$ in the normal brain leads to a fixed level of OEF around ~33%.²³ A decoupling of the two, signifies oxidative stress, as in ischemia, and would lead to an increase in OEF beyond the normal value of ~33%.⁶

4.1.4 Animal Preparation and Experimental Procedure and Groups

Experiments were conducted on fifteen newborn piglets. All animal experiments were approved by the Animal Use Subcommittee of the Canadian Council on Animal Care at our institution. Newborn Duroc cross piglets were obtained from a local supplier on the morning of the experiment. Anesthesia was induced with 1-2% isoflurane which was increased to 3-4% during preparatory surgery. A tracheotomy was performed and the piglet was ventilated with oxygen and medical air mixture. A femoral artery was catheterized to monitor HR and MAP and to intermittently collect arterial blood samples for gas ($p_a\text{CO}_2$, $p_a\text{O}_2$), pH and glucose concentration analysis. A cannula was inserted into an ear vein for infusion of Propofol (AstraZeneca Pharmaceuticals, Canada Inc) and ICG (Sigma-Aldrich, Saint Louis, Missouri). After surgery, piglets were maintained on 1-2% isoflurane at normothermia ($\text{NT}_{37^\circ\text{C}}$). Arterial CO_2 tension ($p_a\text{CO}_2$) was monitored throughout the experiment, either directly by blood gas measurements or by the end-tidal CO_2 tension, and maintained at normocapnia between 37-40 mmHg by adjusting the breathing rate and ventilation volume. Arterial oxygen tension ($p_a\text{O}_2$) was maintained at a level between 90-130 mmHg by adjusting the ratio of oxygen to medical air. Blood glucose was monitored intermittently and if it fell below 4.5 mmol/L, a 1-2 ml infusion of 25% dextrose solution was administered intravenously. Deep brain temperature was also measured with a thermocouple probe. The needle thermocouple probe was inserted laterally into the brain to a depth of 2 cm vertical from the brain surface and 0.5 cm posterior to the bregma. Animals were placed in a prone position and a custom-made probe holder was strapped to the head to hold the TR-NIRS emission and detection probes 2 cm apart, parasagittally, approximately 1.5 cm dorsal to the eyes. The experiments started after a delay of 60 min to allow time for the animals to stabilize following surgery. This delay was also sufficient for the TR-NIR instrument to reach a quasi-equilibrium to minimize drift artifacts in TR-NIR measurements due to temperature changes.²⁴ Piglets were randomized into three groups:

- (i). Group I (N=7) had baseline (normothermia) CT and TR-NIR CBF measurements in the following order: one CT CBF scan, two TR-NIR CBF measurements separated by 10min before and after CT measurements. Following the baseline

(normothermia) CBF measurements, TR-NIR followed by CT CBF measurements were collected at $\sim 2^{\circ}\text{C}$ decrement from the baseline temperature of 38° to 32°C under isoflurane anesthesia; and,

- (ii). Group II (N=4) had two TR-NIRS measurements of CBF and CMRO_2 under inhalational isoflurane (1-2%) anesthesia first and then both measurements were repeated under intravenous infusion of Propofol (9-22.4 mg/kg/h) and ventilation with 70% nitrous oxide (N_2O 70%) and 30% oxygen (O_2 30%) while brain temperature was changed from normo- (38°C) to hypo-thermia (35° and 33°C); and,
- (iii). Group III (N=3) was the same as Group II except that nitrous oxide and oxygen mixture was replaced by xenon/oxygen/nitrogen mixture (Xe 35-50%, O_2 30-40%, N_2 10-20% respectively) using the closed-circuit Xe/O_2 delivery system.²⁵

For propofol (10mg/ml) infusion, the rate was adjusted according to their responses, and change in vital signs such as blood pressure, and pain responsiveness of the piglet. The mean infusion rates were 2.51 ± 1.15 and 2.95 ± 1.11 ml/hr during propofol/ N_2O (Group II) and propofol/ Xe (Group III) anesthesia, respectively. For normothermia, a heated water blanket was used to maintain rectal and brain temperature between 38° - 38.5°C . For induction of HT, brain temperature was altered by exposing the piglet's body to room temperature. For each anesthetic regime, two measurements of CBF and CMRO_2 were collected per brain temperature. Each experiment was completed within 5 hours. After the last measurement, the animals were sacrificed with intravenous potassium chloride (1-2 ml/kg) infusion.

4.1.5 Computed Tomography Measurement

For Group I piglets, they were placed in a light speed 64-slice CT scanner (GE Healthcare, Waukesha, WI, U.S.A), the mobile TR-NIR apparatus was brought to the CT scanner and all TR-NIR measurements were obtained while the piglets remained in a prone position on the scanner table. Each CT CBF measurement began with a scout CT

scan to choose the locations of the CT slices to coincide with the position of the NIR optodes. To measure CBF, each piglet received a 1.0-mL/kg injection of the iodinated contrast agent iohexol (300 mg I /mL; Omnipaque™, GE Healthcare, Waukesha, Wisconsin), at a rate of 1.0 mL/s into the umbilical vein. Sequential (dynamic) CT scans were acquired using 80 kVp, 190 mA with the scanner once every second, for a period of 40s. Each scan provided eight contiguous 5 mm thick coronal slices with a 12 cm field of view set to encompass the entire head and front legs of the piglet in a prone position. CBF maps were generated from the serial image sets using CT Perfusion3 software (General Electric Healthcare). This package is based on the same deconvolution routine used to calculate CBF with the NIRS data and has been validated in our laboratory against the gold standard microsphere CBF measurement.¹³ Regions of interest (ROIs) manually drawn using an in-house developed in the IDL Development Environment (ITT Visual Information Solutions, Boulder, Colorado) program on the CT perfusion images that corresponded to the brain volume interrogated by the TR-NIR probes and mean CBF within the regions were averaged before comparison with the TR-NIR CBF. The ROIs only included the top ~1.5 cm of brain to account for the depth sensitivity of NIRS.

4.1.6 Statistical Analysis

SPSS 17.0.0 (SPSS, Inc, Chicago, IL) was used for all statistical analyses. Normality of the distribution of the measurements was verified using Kolmogorov-Smirnov (KS) test. Comparisons between temperature-based measurements within groups were performed by a repeated-measures one-way ANOVA when the variables were normally distributed (Group I) or, if the normality test failed, by the Friedman test (Groups II-III). Wilcoxon test was used to determine statistical differences when the anesthetic was switched from isoflurane to propofol/N₂O (Group II) and propofol/Xe (Group III). Correlations between CT and NIRS CBF in Group I were analyzed using parametric linear regression. Statistical significance was based on p -value < 0.05. All data are presented as mean \pm SD unless otherwise noted.

4.2 Results

Experiments were conducted on fifteen newborn piglets (9 females and 6 males), with an average age of 35 ± 12 hours old and an average weight of 1.7 ± 0.2 kg. Due to difficulties to maintain normocapnia condition throughout the experiment, data from two piglets in Group I was excluded from analysis. Table 4.1 presents a summary of the averaged physiologic parameters of the piglets (MAP, HR, $p_a\text{CO}_2$, $p_a\text{O}_2$, pH, $S_a\text{O}_2$ and OEF) in the three groups, according to anesthetics used and brain temperature. In group I, there was a statistically significant decrease in HR and $P_a\text{O}_2$ ($p < 0.05$) compared to baseline (normothermia) when temperature reached below 35°C . The heart rate dropped slowly with the induction of HT from 139 ± 10 to 94 ± 13 over the whole temperature range (38 - 32°C). In group II, when the anesthetic was switched from isoflurane to Propofol/ N_2O , there was a statistically significant increase in HR and MAP ($p < 0.05$) compared to baseline (isoflurane); but HR started decreasing immediately after the initiation of cooling and return to baseline (isoflurane) level when temperature fell to 35°C and a statistically significant decrease in $p_a\text{O}_2$ when temperature fell below 35°C with the Propofol/ N_2O combination of anesthetics ($p < 0.05$). No significant $p_a\text{CO}_2$, $S_a\text{O}_2$, OEF or pH differences were found among different anesthetics and among different temperatures.

Table 4.1. Physiological parameters measured at different groups.

Variable		Baseline	Cooling		
		(38°C)	(38°C)	(35°C)	(32°C)
MAP (mmHg)	<i>Baseline / Cooling</i>				
	Group I (isoflurane / isoflurane)	42 ± 5	42 ± 5	40 ± 4	38 ± 4
	Group II (isoflurane / propofol/N ₂ O)	42 ± 4	56 ± 6*	52 ± 2*	50 ± 11*
	Group III (isoflurane / propofol/Xe)	42 ± 5	45 ± 10	36	33
HR (bpm)	Group I (isoflurane / isoflurane)	139 ± 10	139 ± 10	117 ± 11*	94 ± 13*
	Group II (isoflurane / propofol/N ₂ O)	148 ± 5	226 ± 41*	195 ± 8*	138 ± 28
	Group III (isoflurane / propofol/Xe)	148 ± 7	168 ± 26	100	84
<i>p_aCO₂</i> (mmHg)	Group I (isoflurane / isoflurane)	39 ± 1	39 ± 1	41 ± 1	38 ± 1
	Group II (isoflurane / propofol/N ₂ O)	40 ± 2	41 ± 2	41 ± 1	40 ± 2
	Group III (isoflurane / propofol/Xe)	39 ± 2	41 ± 4	40	43
<i>p_aO₂</i> (mmHg)	Group I (isoflurane / isoflurane)	122 ± 15	122 ± 15	95 ± 17*	75 ± 17*
	Group II (isoflurane / propofol/N ₂ O)	155 ± 40	210 ± 49	136 ± 4*	85 ± 16*
	Group III (isoflurane / propofol/Xe)	164 ± 49	140 ± 43	101	89
pH	Group I (isoflurane / isoflurane)	7.4 ± 0.02	7.4 ± 0.02	7.4 ± 0.03	7.4 ± 0.04
	Group II (isoflurane / propofol/N ₂ O)	7.4 ± 0.06	7.4 ± 0.06	7.3 ± 0.09	7.3 ± 0.13
	Group III (isoflurane / propofol/Xe)	7.4 ± 0.04	7.4 ± 0.03	7.46	7.42
S _a O ₂ (%)	Group II (isoflurane / propofol/N ₂ O)	100	97 ± 2	98 ± 1	97 ± 1
	Group III (isoflurane / propofol/Xe)	100	99 ± 1	99	100
[O ₂] _a	Group II (isoflurane / propofol/N ₂ O)	0.11 ± 0.01	0.11 ± 0.02	0.11 ± 0.02	0.11 ± 0.01
	Group III (isoflurane / propofol/Xe)	0.12 ± 0.01	0.11 ± 0.01	0.11	0.11

MAP=mean arterial blood pressure; HR=heart rate; [O₂]_a=arterial concentration of oxygen, *significantly ($p < 0.05$) different from baseline.

Figure 4.1(a) is a coronal CT image of a piglet showing the holder and the positions of the two TR-NIR probes (white arrows). Figure 4.1(b-e) show coronal CBF maps at different temperatures and ROIs enclosing a ellipse-shaped trajectory that light travel from the source to the detector in each case.

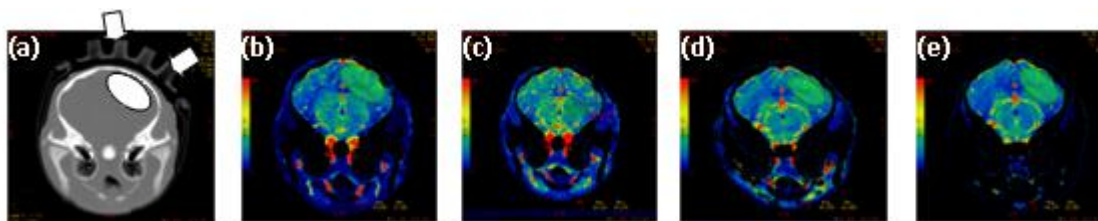


Figure 4.1. (a) Coronal CT image showing the location of the TR-NIR probes and the ROIs enclosing a ellipse-shaped trajectory that light travel from the source to the detector. (b-e) Corresponding CBF maps at 38° (normothermia), 36°, 34° and 32°C. The region of interest used to measure CBF from the CBF map in each case is also shown.

Figure 4.2 shows that decreasing the brain temperature in Group I piglets (N=7) resulted in a decrease in TR-NIR CBF from 54.3 ± 5.4 to 33.8 ± 0.9 ml.min⁻¹.100g⁻¹ and a decrease in CT CBF from 56.8 ± 2.5 to 41.9 ± 2.1 ml.min⁻¹.100g⁻¹ at 38° and 32°C, respectively.

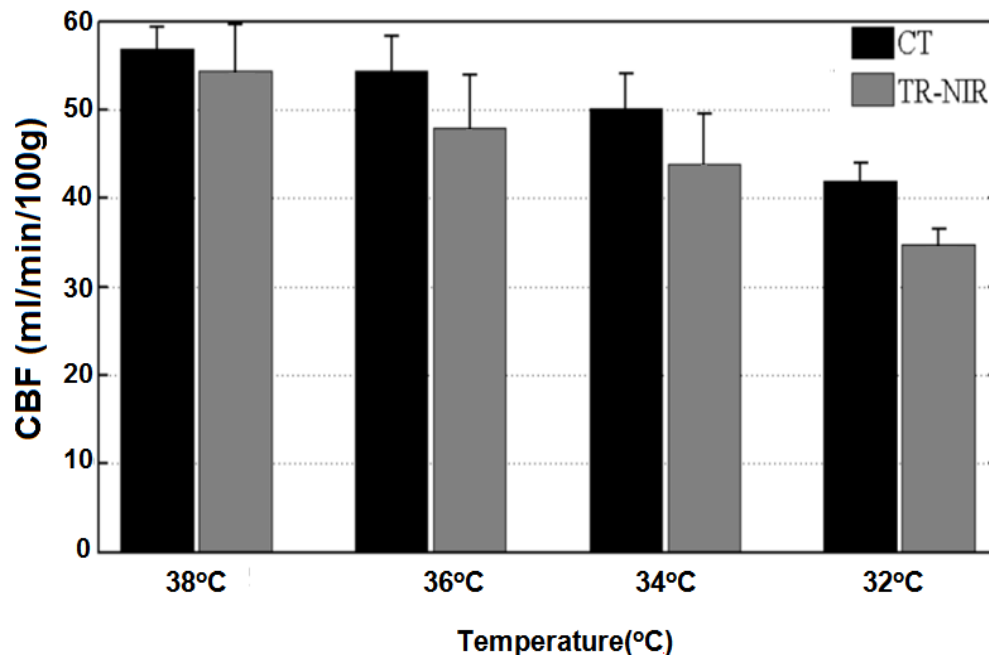


Figure 4.2. TR-NIR and CT CBF measurements in piglets (N=7) plotted as a function of brain temperature (N=7).

A correlation plot comparing CT and TR-NIR CBF and the corresponding Bland-Altman plot are shown in Figure 4.3. The average slope, intercept and R^2 value from the individual regression analyses were 1.3, $-19 \text{ ml}\cdot\text{min}^{-1}\cdot 100\text{g}^{-1}$, and 0.84 respectively. From the Bland-Altman analysis, the mean difference between the two methods was $5.84 \text{ ml}\cdot\text{min}^{-1}\cdot 100\text{g}^{-1}$. The 95% confidence limits of the difference between the two methods were from -15.3 to $27 \text{ ml}\cdot\text{min}^{-1}\cdot 100\text{g}^{-1}$.

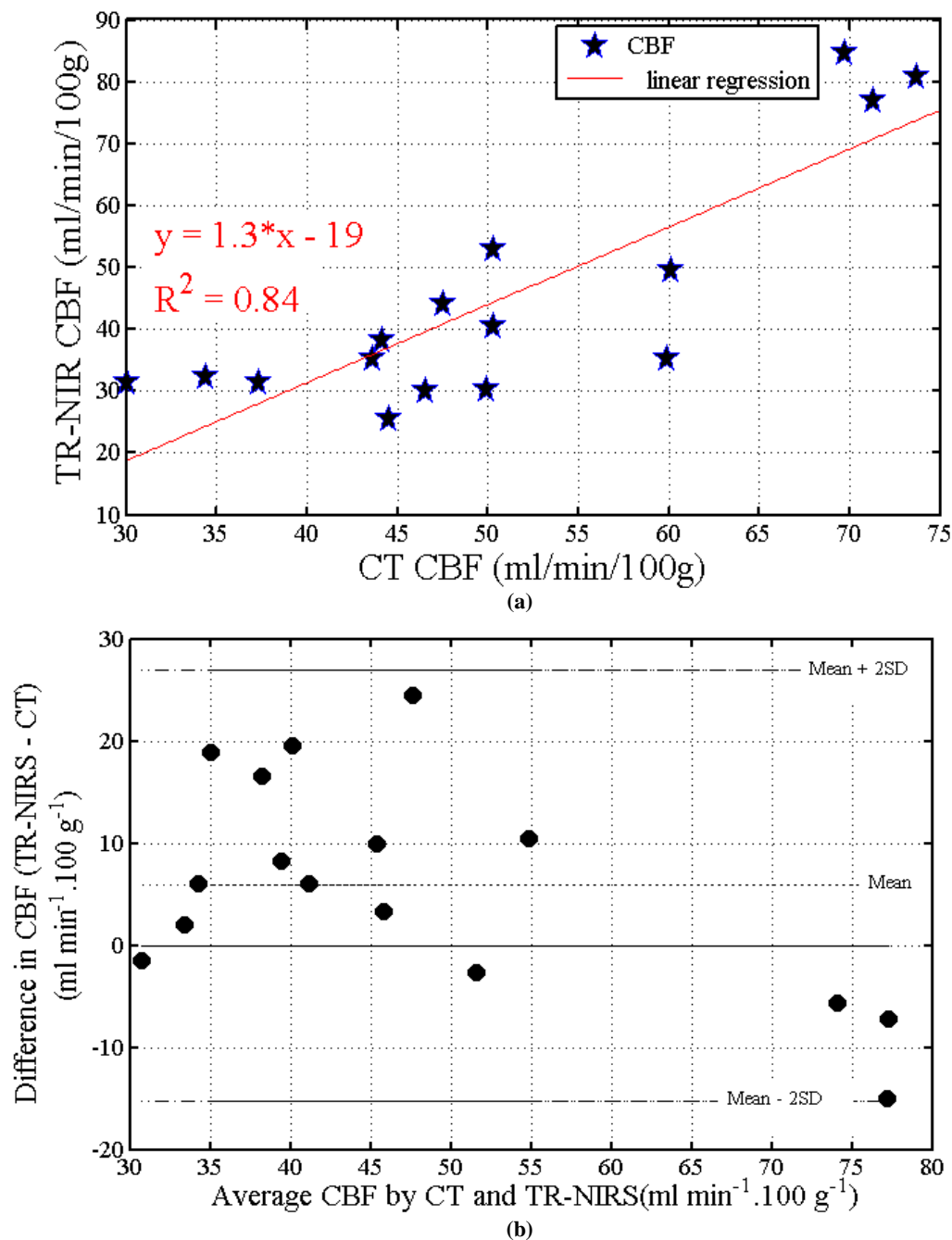
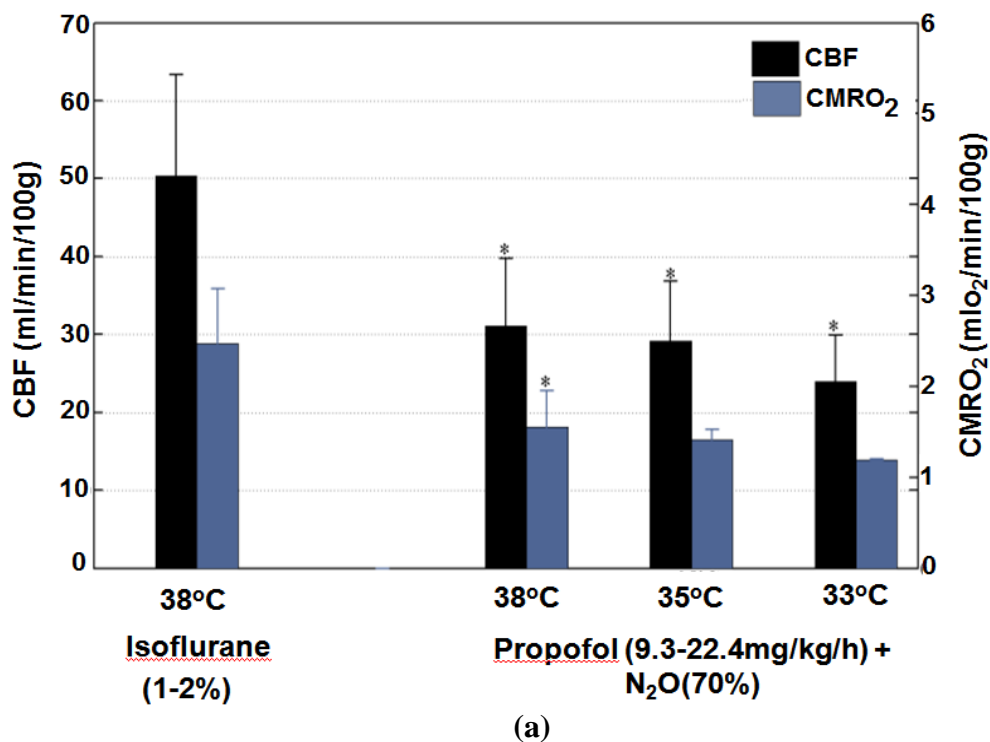


Figure 4.3. (a) Correlation plot comparing CT and the TR-NIR CBF. The solid line represents the average of all individual linear regression (slope = 1.3 and intercept = $-19 \text{ ml} \cdot \text{min}^{-1} \cdot 100 \text{ g}^{-1}$). (b) Bland-Altman plot of CT and TR-NIR CBF. The dotted line shows the mean difference and dash-dotted lines show the limits of agreement (mean \pm 2 SD).

Figure 4.4(a) displays TR-NIR CBF and CMRO_2 measurements in Group II piglets (N=4) under two different anesthetic regimes (i.e., isoflurane only and propofol/ N_2O mixture) at three different brain temperatures. Both CBF and CMRO_2 values decreased from 50.42 ± 8.7 to $31.07 \pm 8.7 \text{ ml} \cdot \text{min}^{-1} \cdot 100 \text{ g}^{-1}$ and 2.46 ± 0.6 to $1.5 \pm$

0.4 $\text{mlO}_2 \cdot \text{min}^{-1} \cdot 100\text{g}^{-1}$ at normothermia (38°C) when the anesthetic was switched from isoflurane to propofol/ N_2O and both decreased from 31.07 ± 8.7 to $23.9 \pm 5.9 \text{ ml} \cdot \text{min}^{-1} \cdot 100\text{g}^{-1}$ and 1.5 ± 0.4 to $1.1 \pm 0.01 \text{ mlO}_2 \cdot \text{min}^{-1} \cdot 100\text{g}^{-1}$ in HT when brain temperature decreased from 38° to 33°C under propofol/ N_2O anesthesia. The OEF values under the different anesthetics and brain temperatures employed in group II, was plotted in Figure 4.4(b). It shows that both HT and different anesthetics (i.e. isoflurane and propofol/ N_2O) did not deviate OEF from its basal values which expressing tight coupling of CBF to CMRO_2 ; any change in metabolic demand were met by a corresponding change in substrate delivery via CBF modulation.



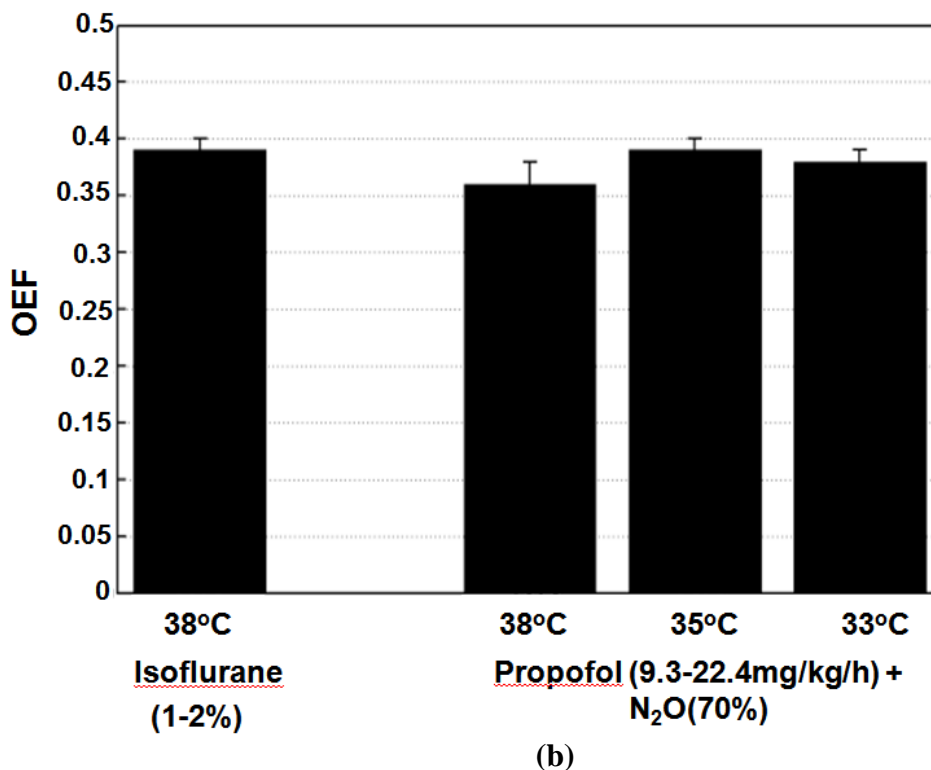


Figure 4.4. (a) Cerebral blood flow (CBF) and oxygen metabolic rate (CMRO₂); and (b) Oxygen extraction fraction (OEF) in Group II piglets (N=4) at each cerebral temperature under isoflurane or propofol/N₂O anesthetic regimens. Values are shown as mean ± SD; * $p < 0.05$ versus at 38°C with isoflurane.

Figure 4.5(a) displays TR-NIR CBF and CMRO₂ measurements in Group III piglets (N=3) under isoflurane and then propofol/Xe anesthesia at three different temperatures (only one piglet was cooled down to 33°C). Both CBF and CMRO₂ values decreased from 49.4 ± 14.2 to 34.9 ± 12.1 ml.min⁻¹.100g⁻¹ and 2.3 ± 0.7 to 1.4 ± 0.53 mlO₂.min⁻¹.100g⁻¹ at normothermia (38°C) when the anesthetic was switched from isoflurane to propofol/Xe and decreased under propofol/Xe anesthesia from 34.9 ± 12.08 to 23.6 ml.min⁻¹.100g⁻¹ and from 1.44 ± 0.53 to 1.05 mlO₂.min⁻¹.100g⁻¹ respectively when brain temperature decreased from ~38° to 33°C. Similarly, Figure 4.5(b) shows that OEF remains unchanged under isoflurane anesthesia and under propofol/Xe anesthesia at different temperatures.

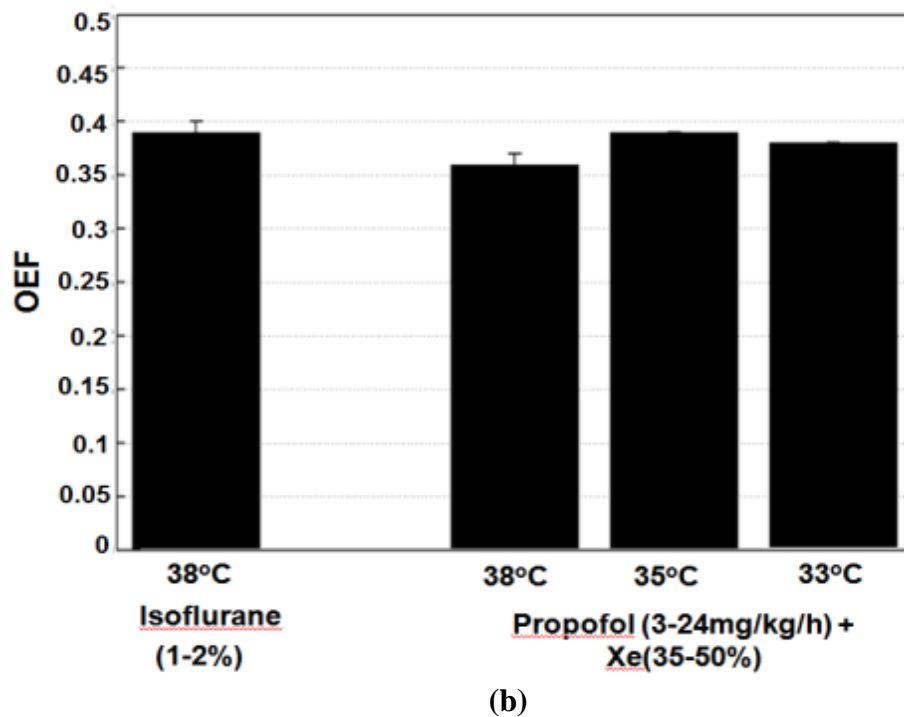
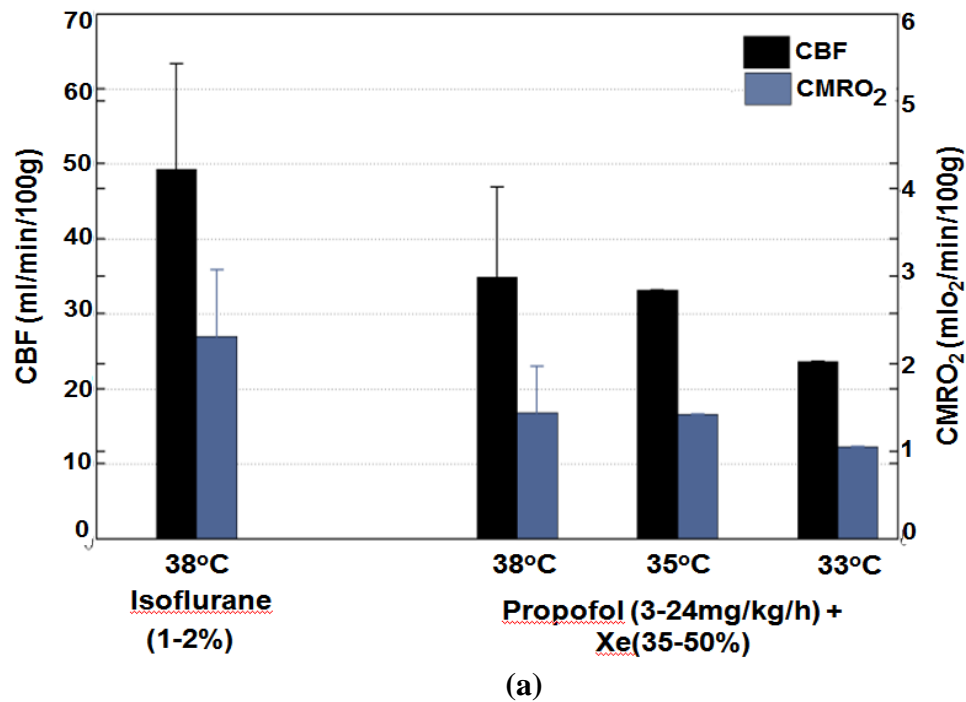


Figure 4.5. (a) Cerebral blood flow (CBF) and oxygen metabolic rate (CMRO₂), (b) Oxygen extraction fraction (OEF) in Group III piglets (N=3) at each cerebral temperature under isoflurane or propofol/Xe anesthetic regimes. Values are shown as mean \pm SD; * $p < 0.05$ versus at 38°C with isoflurane.

4.3 Discussion

In the present study TR-NIR CBF measurements were validated against CT CBF measurements in a neonatal animal model in which brain temperature was lowered from 38° to 32°C under isoflurane anesthesia. Our results revealed a linear correlation between two CBF measurement techniques, but the TR-NIR technique underestimated CBF measured with CT. There are a number of factors that can explain this discrepancy. One source of error is incorrectly characterizing the amount of dispersion caused by the TR system (i.e., variations between the measured and true instrument response function (IRF)).¹¹ Additionally, this study used CT perfusion to validate the CBF which required selecting ROIs underneath the NIRS probe that corresponded to the area interrogated by the NIR light. The error in the CBF measurements caused by variable ROI selection can also explain the differences between two techniques. Another explanation is that the method to recover optical properties is based on the diffusion approximation with the assumption that the light is propagating in a homogeneous semi-infinite geometry which is less true for the newborn model since the head size is significantly smaller than the adult.²⁶ It has been shown that the model approximation can lead to errors in the recovered optical properties by 20% at short source-detector distances (5-20mm).²⁶ In addition, the relatively thin layer of superficial tissues on the newborn head comprised of skin, muscle, and skull, could have an effect on the NIR signal and the accuracy of CBF measured with TR-NIR technique.^{26, 27} Although it becomes dominant in the adult case because of the larger thickness of the scalp and skull.^{23,28} Previous studies have reported that CBF collected using NIRS approaches can be underestimated by more than a factor of 3, due primarily to the increase in optical path length through extracerebral tissue.²⁹

Furthermore, we examined the relationship between CMRO₂ and CBF under normothermia (38°C) or mild whole-body HT (35° or 32°C) with different anesthetics, isoflurane(1-2%)/(N₂ 66%, O₂ 33%), propofol/(N₂O 70%, O₂ 30%) or propofol/(Xe 35-50%, O₂ 30-40%, N₂ 10-25%) which are representative of what may be used in clinical practice.^{14, 30} Our results showed that mild HT decreases both CBF and CMRO₂ compared to normthermia

with preserved flow-metabolism coupling and constant OEF under different anesthetics. Flow-metabolism coupling within brain is a complex physiologic process that is regulated by a combination of metabolic, glial, neural, and vascular factors.³¹⁻³³ In the normal brain, CBF is regulated by autoregulation, cerebrovascular and metabolic reactivity induced by changes in arterial carbon dioxide tension to maintain a tight coupling between CBF and CMRO₂. However, during cerebral ischemic insults, alterations of cerebral hemodynamic and metabolism are highly dynamic. As cerebral perfusion pressure (CPP) falls, CBF is maintained by vasodilatation of resistance arterioles, known as autoregulation.³⁴ When the capacity for compensatory vasodilatation has been exceeded, autoregulation fails and CBF falls as a function of pressure. When oxygen supply is diminished due to decreasing CBF, OEF increases in an effort to compensate for the reduced CBF and maintain a stable CMRO₂ to preserve neuronal function and cellular integrity.³³ If the CPP continues to fall, CBF will progressively decline until the increase in OEF is no longer sufficient to supply the oxygen to meet metabolic demand which causes to reduce CMRO₂. Energy failure will result and permanent tissue damage may develop. Therefore, deviation of OEF from its basal value may be a more specific marker to monitor for oxidative stress from whatever causes that can lead to cerebral dysfunction.

The vasodilating effects of isoflurane have limited its use as a sedative agent in the NICU because of the fear of a potential increase in intracranial pressure (ICP) caused by the increase in CBF.³⁵ However, propofol is being used more frequently in the neurosurgical intensive care unit, particularly for head-injury cases.³⁶ Propofol is known to decrease CBF while preserving brain flow-metabolism coupling and act as a global central nervous system depressant.³⁵ It has been shown that a typical anesthetic induction dose of propofol reduces blood pressure by approximately 30% resulting from a decrease in sympathetic activity, direct vasodilation, and myocardial depression.^{37, 38} When the anesthetic was switched from isoflurane to propofol, there was a statistically significant increase in HR, suggesting that decrease in peripheral vascular resistance induced by propofol was partially compensated by an increase in heart rate.³⁵ The use of a background propofol infusion with Xe and N₂O is due to the fact that both anesthetic cannot induce reliable anesthesia on their own.

Although quantitative and mobile, a limitation with the TR-NIR technique is the need to inject a bolus of ICG every time CBF is measured. However, this is a minimally invasive procedure since ICG is injected into a peripheral vein and the arterial ICG time-concentration curve can be measured noninvasively by pulse dye densitometry. Moreover, Verdecchia *et al* have shown that TR-NIR can be combined with diffuse correlation spectroscopy (DCS) to provide almost ‘continuous’ quantitative assessment of CBF and CMRO₂.³⁹ DCS is used to measure changes in CBF and CMRO₂ from their values at baseline (or calibration) which, in turn, are measured using TR-NIR with ICG injection as discussed in this report. With this approach, only infrequent injections of ICG is needed to calibrate the pseudo-continuous measurement of changes into absolute values of CBF and CMRO₂. Piglets were studied because signal contamination from extra-cerebral tissue is relatively low, which enables the measured TPSFs to be characterized by the diffusion equation for a homogeneous semi-infinite geometry.

In conclusion, we have shown the ability of TR-NIR technique to measure absolute CBF during HT and investigated the cerebral metabolic activity under different anesthetics at different temperature in a normoxia animal model. Both CBF and CMRO₂ decreased by decreasing the temperature but the OEF remained unchanged which indicates a tight coupling of flow and metabolism under different anesthetics over the mild HT temperature range (38°-33°C) which might not be the case in the ischemic brain. Furthermore, rewarming is a critical phase of therapeutic HT to monitor for oxidative stress.^{9, 40} Rapid rewarming of the injured brain commonly leads to a mismatch between cerebral metabolism and perfusion⁹ and can cause in rebound intracranial pressure elevations⁴¹, cerebral venous desaturation⁴⁰, and brain ischemia. It is suggested that controlling the rewarming rate as low as 0.1-0.4°C/hour is preferred to reduce the neurological risks.⁴² Therefore, predicting and managing possible systemic side effects of rewarming is also important for guaranteeing HT efficacy. As the next step, we will be investigating the OEF changes before, during and after HT in hypoxic-ischemic neonatal pigs.

4.4 References

1. Moore EM, Nichol AD, Bernard SA, Bellomo R. Therapeutic hypothermia: Benefits, mechanisms and potential clinical applications in neurological, cardiac and kidney injury. *Injury*. 2011;42:843-854
2. Erecinska M, Thoresen M, Silver IA. Effects of hypothermia on energy metabolism in mammalian central nervous system. *J Cereb Blood Flow Metab*. 2003;23:513-530
3. Sakoh M, Gjedde A. Neuroprotection in hypothermia linked to redistribution of oxygen in brain. *Am J Physiol Heart Circ Physiol*. 2003;285:H17-25
4. Ehrlich MP, McCullough JN, Zhang N, Weisz DJ, Juvonen T, Bodian CA, Griep RB. Effect of hypothermia on cerebral blood flow and metabolism in the pig. *Ann Thorac Surg*. 2002;73:191-197
5. Cheng GQ, Shao XM, Huang HM. [effects of selective head cooling on cerebral blood flow and cerebral metabolic rate in newborn piglets]. *Zhonghua Er Ke Za Zhi*. 2005;43:748-752
6. Powers WJ. Cerebral hemodynamics in ischemic cerebrovascular disease. *Ann Neurol*. 1991;29:231-240
7. Derdeyn CP, Videen TO, Yundt KD, Fritsch SM, Carpenter DA, Grubb RL, Powers WJ. Variability of cerebral blood volume and oxygen extraction: Stages of cerebral haemodynamic impairment revisited. *Brain*. 2002;125:595-607
8. Azzopardi D, Strohm B, Edwards AD, Halliday H, Juszczak E, Levene M, Thoresen M, Whitelaw A, Brocklehurst P, Steering G, participants TCR. Treatment of asphyxiated newborns with moderate hypothermia in routine clinical practice: How cooling is managed in the uk outside a clinical trial. *Arch Dis Child Fetal Neonatal Ed*. 2009;94:F260-264
9. Enomoto S, Hindman BJ, Dexter F, Smith T, Cutkomp J. Rapid rewarming causes an increase in the cerebral metabolic rate for oxygen that is temporarily unmatched by cerebral blood flow. A study during cardiopulmonary bypass in rabbits. *Anesthesiology*. 1996;84:1392-1400
10. Brown DW, Hadway J, Lee TY. Near-infrared spectroscopy measurement of oxygen extraction fraction and cerebral metabolic rate of oxygen in newborn piglets. *Pediatr Res*. 2003;54:861-867

11. Diop M, Tichauer KM, Elliott JT, Migueis M, Lee TY, St Lawrence K. Comparison of time-resolved and continuous-wave near-infrared techniques for measuring cerebral blood flow in piglets. *J Biomed Opt.* 2010;15:057004
12. Brown DW, Picot PA, Naeini JG, Springett R, Delpy DT, Lee TY. Quantitative near infrared spectroscopy measurement of cerebral hemodynamics in newborn piglets. *Pediatr Res.* 2002;51:564-570
13. Cenic A, Nabavi DG, Craen RA, Gelb AW, Lee TY. Dynamic ct measurement of cerebral blood flow: A validation study. *AJNR Am J Neuroradiol.* 1999;20:63-73
14. Thoresen M. The cool xenon study. (<http://www.Controlled-trials.Com/isrctn/pf/75602528>). 2011
15. Hobbs C, Thoresen M, Tucker A, Aquilina K, Chakkarapani E, Dingley J. Xenon and hypothermia combine additively, offering long-term functional and histopathologic neuroprotection after neonatal hypoxia/ischemia. *Stroke.* 2008;39:1307-1313
16. Dehaes M, Aggarwal A, Lin PY, Rosa Fortuno C, Fenoglio A, Roche-Labarbe N, Soul JS, Franceschini MA, Grant PE. Cerebral oxygen metabolism in neonatal hypoxic ischemic encephalopathy during and after therapeutic hypothermia. *J Cereb Blood Flow Metab.* 2013
17. Ossoff RH. Implementing the ansi z 136.3 laser safety standard in the medical environment. *Otolaryngol Head Neck Surg.* 1986;94:525-528
18. Zierler KL. Equations for measuring blood flow by external monitoring of radioisotopes. *Circ Res.* 1965;16:309-321
19. Roche-Labarbe N, Carp SA, Surova A, Patel M, Boas DA, Grant PE, Franceschini MA. Noninvasive optical measures of cbv, sto(2), cbf index, and rcmro(2) in human premature neonates' brains in the first six weeks of life. *Hum Brain Mapp.* 2010;31:341-352
20. Mchedlishvili G. Arterial behavior and blood circulation in the brain. *New York: Consultants Bureau.* 1986
21. Watzman HM, Kurth CD, Montenegro LM, Rome J, Steven JM, Nicolson SC. Arterial and venous contributions to near-infrared cerebral oximetry. *Anesthesiology.* 2000;93:947-953
22. White DR, Widdowson EM, Woodard HQ, Dickerson JW. The composition of body tissues (ii). Fetus to young adult. *Br J Radiol.* 1991;64:149-159

23. Nozari A, Rubertsson S, Gedeberg R, Nordgren A, Wiklund L. Maximisation of cerebral blood flow during experimental cardiopulmonary resuscitation does not ameliorate post-resuscitation hypoperfusion. *Resuscitation*. 1999;40:27-35
24. M. Diop JTE, K. M. Tichauer, M. Migueis, T. Y. Lee, and K., Lawrence S. Bedside monitoring of absolute cerebral blood flow by time-resolved nirs. *Proc. SPIE 7555*, 1–9. 2010
25. Chakkarapani E, Thoresen M, Hobbs CE, Aquilina K, Liu X, Dingley J. A closed-circuit neonatal xenon delivery system: A technical and practical neuroprotection feasibility study in newborn pigs. *Anesth Analg*. 2009;109:451-460
26. Dehaes M, Grant PE, Sliva DD, Roche-Labarbe N, Pienaar R, Boas DA, Franceschini MA, Selb J. Assessment of the frequency-domain multi-distance method to evaluate the brain optical properties: Monte carlo simulations from neonate to adult. *Biomed Opt Express*. 2011;2:552-567
27. Yoo TS. Extracerebral layers (ecl) thickness variation within a subject between subjects, http://www.Uwo.Ca/biophysics/undergrad/3970z_six_week_undergrad_projects/2011%20thickness%20variations%20in%20extracerebral%20layers%20report.Pdf, department of medical biophysics, western university, 2011.
28. Elliott JT, Diop M, Tichauer KM, Lee TY, St Lawrence K. Quantitative measurement of cerebral blood flow in a juvenile porcine model by depth-resolved near-infrared spectroscopy. *J Biomed Opt*. 2010;15:037014
29. Owen-Reece H, Elwell CE, Harkness W, Goldstone J, Delpy DT, Wyatt JS, Smith M. Use of near infrared spectroscopy to estimate cerebral blood flow in conscious and anaesthetized adult subjects. *Br J Anaesth*. 1996;76:43-48
30. Yokoe C, Hanamoto H, Boku A, Sugimura M, Morimoto Y, Kudo C, Niwa H. The effect of nitrous oxide inhalation on the hypotensive response to propofol: A randomized controlled trial. *Oral Surg Oral Med Oral Pathol Oral Radiol*. 2013
31. Attwell D, Buchan AM, Charpak S, Lauritzen M, Macvicar BA, Newman EA. Glial and neuronal control of brain blood flow. *Nature*. 2010;468:232-243
32. Peterson EC, Wang Z, Britz G. Regulation of cerebral blood flow. *Int J Vasc Med*. 2011;2011:823525
33. Powers WJ, Grubb RL, Jr., Darriet D, Raichle ME. Cerebral blood flow and cerebral metabolic rate of oxygen requirements for cerebral function and viability in humans. *J Cereb Blood Flow Metab*. 1985;5:600-608

34. MacKenzie ET, Farrar JK, Fitch W, Graham DI, Gregory PC, Harper AM. Effects of hemorrhagic hypotension on the cerebral circulation. I. Cerebral blood flow and pial arteriolar caliber. *Stroke*. 1979;10:711-718
35. Villa F, Iacca C, Molinari AF, Giussani C, Aletti G, Pesenti A, Citerio G. Inhalation versus endovenous sedation in subarachnoid hemorrhage patients: Effects on regional cerebral blood flow. *Crit Care Med*. 2012;40:2797-2804
36. Matta B, Menon D. Severe head injury in the united kingdom and ireland: A survey of practice and implications for management. *Crit Care Med*. 1996;24:1743-1748
37. Moseley H, Shankar KB, Kumar Y, Hallsworth R, Krishnan A. Propofol: A new intravenous anaesthetic. *West Indian Med J*. 1988;37:229-231
38. Kazama T, Ikeda K, Morita K, Ikeda T, Kikura M, Sato S. Relation between initial blood distribution volume and propofol induction dose requirement. *Anesthesiology*. 2001;94:205-210
39. Verdecchia K, Diop M, Lee TY, St Lawrence K. Quantifying the cerebral metabolic rate of oxygen by combining diffuse correlation spectroscopy and time-resolved near-infrared spectroscopy. *J Biomed Opt*. 2013;18:27007
40. van der Linden J, Ekroth R, Lincoln C, Pugsley W, Scallan M, Tyden H. Is cerebral blood flow/metabolic mismatch during rewarming a risk factor after profound hypothermic procedures in small children? *Eur J Cardiothorac Surg*. 1989;3:209-215
41. Shiozaki T, Sugimoto H, Taneda M, Yoshida H, Iwai A, Yoshioka T, Sugimoto T. Effect of mild hypothermia on uncontrollable intracranial hypertension after severe head injury. *J Neurosurg*. 1993;79:363-368
42. Povlishock JT, Wei EP. Posthypothermic rewarming considerations following traumatic brain injury. *J Neurotrauma*. 2009;26:333-340

Chapter 5

Conclusions and Future Work

5. Summary of Stated Objectives

The introduction chapter of this thesis discussed the importance of selective brain cooling to maximize the neuroprotective effects of mild hypothermia and avoid adverse complications from whole body cooling. The primary objective of this research, therefore, was to develop a nasopharyngeal cooling approach which targets only the brain tissue not only capable of inducing fast cooling but also can maintain the target temperature over extended period of time (Chapter 2). However, a proper evaluation of brain cooling requires accurate measurement of the brain temperature locally instead of relying on inference from core temperature. For this purpose, a non-invasive technique was developed to measure brain temperature during hypothermia as described in Chapter 3. As discussed in detail in the previous chapters, one of the important mechanisms of hypothermia-induced neuroprotection is due to suppression of brain metabolism, and it is important to determine whether the combination of anesthesia and hypothermia alters flow-metabolism coupling. In Chapter 4, we examined the effect of hypothermia on flow-metabolism coupling under different anesthetic regimes and temperatures.

The next section of this chapter will summarize each of these developments within the context of the objectives presented in Chapter 1. Following this, future directions of this research will be discussed.

5.1 Whole-Body and Selective Brain Cooling Approach

(i) Selective Brain Cooling Using Nasopharyngeal Method

Cooling the nasopharynx may offer the capability to cool the brain selectively by cooling inflowing blood in both internal carotid arteries (ICAs) via counter-current heat exchange mechanism with the neighboring cavernous sinuses which collect cold venous blood from the mucosal linings of the nasal cavities. Furthermore, cerebrospinal fluid chilled at the basal cistern cools the whole brain through the cerebrospinal fluid (CSF) circulation. We have demonstrated an effective, safe and simple method of nasopharyngeal cooling by continuously blowing room temperature or humidified cold air at different flow rates into the nostrils of normal new-born piglets with developed thermal regulation (Chapter 2). Effective brain cooling in new-born piglets was achieved with a median cooling rate of $1.7 \pm 0.9^{\circ}\text{C}/\text{h}$ by setting the flow rate of room temperature air to 3-4 $\text{L}\cdot\text{min}^{-1}$. Results of comparing different temperatures and flow rates in the nasopharyngeal cooling approach reveal that the brain temperature could be reduced rapidly at a rate of $5.6 \pm 1.1^{\circ}\text{C}/\text{h}$ by increasing air flow rate to 14-15 $\text{L}\cdot\text{min}^{-1}$ while keeping air at a cold temperature ($\approx -8^{\circ}\text{C}$). It was also possible to maintain brain temperature within $\pm 0.45^{\circ}\text{C}$ for an hour once it reached the target temperature of 33-34 $^{\circ}\text{C}$ by decreasing the flow rate to 0.5-1.5 $\text{L}\cdot\text{min}^{-1}$.

In new-born piglets, when the brain was kept at the target temperature, rectal temperature continued to drop until it reached the brain temperature. This decline in rectal temperature despite a constant brain temperature could be due to the imbalance between heat production in the rest of the body and the heat lost through cold air-flow in nasal cavities. It was possible to maintain the brain-body temperature gradient ($\approx -3^{\circ}\text{C}$) during nasopharyngeal cooling by using colder air temperature and higher flow rate in older heavier than new-born pigs, i.e. 16 kg versus 2-3 kg and by using heating blanket/sheets to cover the whole body (Appendix B). The nasopharyngeal air cooling method can be easily implemented in hospitals and even on ambulances to selectively cool down the brain to ameliorate brain damage from hypoxia-ischemia in newborns and traumatic brain injuries in children and adults and in resuscitated cardiac arrest patients and in stroke

patients. This study was the first step in developing a reliable, safe and efficient cooling device for future clinical trials on the neuroprotective effects of mild hypothermia and will be of benefit to different patient populations.

(ii) Whole-Body Cooling with Mechanical Ventilation of Cold Air via the Respiratory Tract

Based on considerations of their anatomical architecture and intimate contact with the entire cardiac output, lungs and the pulmonary circulation may act as *in-vivo* exchanger by transferring heat from the pulmonary blood to cold air introduced by ventilation into alveolar spaces in the lungs and then to the environment. Experimental results described in Appendix A, show that the brain temperature fell from $38.3 \pm 0.3^{\circ}\text{C}$ to $36.5 \pm 0.6^{\circ}\text{C}$ during three hours of ‘pulmonary’ cooling which corresponded to a mean cooling rate of $0.6 \pm 0.1^{\circ}\text{C/h}$. The relatively small cooling rate observed in this study could be explained by a combination of reasons. Using a single endotracheal tube for both inspiration and expiration allows rapid warming of the incoming cold air by countercurrent heat exchange between inspired and expired gas in the endotracheal tube and upper airways before reaching the alveoli. The heat exchange between inspiratory and expiratory gas is a powerful mechanism for thermal isolation of alveolar gas and normally prevents penetration of cold environmental gas beyond 10-15 cm in the upper airway.¹ Another drawback of pulmonary cooling is adverse side effects associated with whole body cooling as discussed in “Introduction”.

5.2 Monitoring of Brain Temperature by TR-NIRS Technique

Wide clinical adaptation of mild hypothermia has been hampered by the lack of a reliable noninvasive method for monitoring local brain temperature to adjust cooling and rewarming rate. The commonly used core (rectal) temperature is a poor substitute as it has been shown to not always reflect brain temperature. Since the brain is composed of

80-90% water and its absorption of near infrared (NIR) light depends on temperature, the goal of this work was to develop an optical technique for measuring brain temperature by exploiting the temperature-dependency of water absorption of NIR light.

Specifically, we developed a method based on TR-NIRS to measure temperature continuously and noninvasively in tissue-mimicking phantoms (*in-vitro*) and deep brain tissue (*in-vivo*) during heating and cooling. For deep brain tissue temperature monitoring, experiments were conducted on newborn piglets wherein hypothermia was induced by packing the whole body in ice packs. Brain temperature was concomitantly measured by TR-NIRS and by an invasive thermometer. Our proposed TR-NIRS method was able to measure the temperature of tissue-mimicking phantoms and brain tissues with a correlation of 0.82 and 0.66 to temperature measured with a thermometer, respectively. The mean difference between the TR-NIRS and thermometer measurements was $0.15 \pm 1.1^\circ\text{C}$ for the *in-vitro* experiments and $0.5 \pm 1.6^\circ\text{C}$ for the *in-vivo* measurements.

5.3 Coupling of Cerebral Blood Flow and Oxygen Consumption During HT Under Different Anaesthetics Measured with a TR-NIRS Technique

As discussed in detail in the introduction chapter of this thesis, neuroprotective effects of HT is partly due to suppression of cerebral metabolism to match the demand of oxygen with supply so as to maintain the tissue oxygenation status. In the brain, tissue oxidation status is reflected by the OEF, which is the ratio of CMRO_2 to CBF, as this is tightly controlled to be around 33% under normal conditions. Imbalance in supply and demand of oxygen, or oxidative stress, whatever the cause will lead to an increase in OEF. The focus of our work in this project was, therefore, two-fold: first, to evaluate the ability of the TR-NIR technique to measure CMRO_2 and CBF in piglet brain and second, to investigate the effects of hypothermia and different anesthetic regimes on OEF in normal piglets.

A bolus-tracking method, using ICG as a flow tracer with TR-NIR technique, was used to measure CBF and CMRO₂ in newborn piglets in which brain temperature was lowered from $\approx 38^{\circ}\text{C}$ to $\sim 33^{\circ}\text{C}$ under three anesthetic regimes, i.e., Isoflurane, Propofol/Nitrous-Oxide (N₂O) and Propofol/Xenon (Xe)_{40-50%}. Results demonstrate that TR-NIR can measure CBF with reasonable accuracy as compared to the reference CT Perfusion method² and is sensitive to flow changes induced by either hypothermia or anesthetic drugs. There was a good agreement between CBF obtained with the two methods ($R^2=0.84$, $\Delta(\text{mean difference between CT Perfusion and TR-NIR})=5.84 \text{ ml. min}^{-1} \cdot 100 \text{ g}^{-1}$), demonstrating the ability of the TR-NIR technique to non-invasively measure absolute CBF *in-vivo* during HT. The TR-NIR technique reveals that CBF decreases from $54.3 \pm 5.4 \text{ ml. min}^{-1} \cdot 100 \text{ g}^{-1}$, at normothermia (brain temperature $\sim 38^{\circ}\text{C}$), to $33.8 \pm 0.9 \text{ ml. min}^{-1} \cdot 100 \text{ g}^{-1}$ at a brain temperature of $\sim 32^{\circ}\text{C}$ during HT treatment under isoflurane anesthesia. Both CBF and CMRO₂ were affected by changing the anesthetic regime. However, the ratio of CMRO₂ to CBF (or OEF) remained unchanged at around 33% which indicates, as expected, different anesthetics over the mild hypothermia temperature range does not cause oxidative stress in the brain such that the tight coupling of flow and metabolism is maintained in the resulting normoxia condition.

5.4 Future Work

(i) Advances in the Selective Brain Cooling Approach

Our *in-vivo* experimental studies have demonstrated the feasibility of selective brain cooling using the nasopharyngeal air cooling approach. One important aspect which was not tested in our experiments is controlling the rewarming rate. As discussed in detail in the introduction chapter, rewarming is a critical phase of therapeutic hypothermia in that too fast a rewarming rate will lead to oxidative stress and subsequent brain damage. Thus, understanding, predicting, and managing possible adverse effects of rewarming is important for guaranteeing hypothermia efficacy. To better control cooling and rewarming rates, further development required include developing and testing a prototype device with a computer-controlled feedback system to automatically adjust settings of

cold air temperature and flow rate to arrive at desired brain temperature or cooling or rewarming rates.

Before the nasopharyngeal air cooling method can be used in clinical trials, more experimental studies are necessary to evaluate the efficiency of the device and reproducibility of the results in large animal models of normal and injured brain. In addition, patient safety is a critical aspect of the evaluation. Although it is unlikely that air at subzero temperature and high flow rate will induce freezing damage to the mucosa and embedded blood vessels and nerves of the nasal cavity, histological analyses of the excised tissue from the nasal cavities of animals studied should be performed to assess for tissue damages.

(ii) Improvement in Temperature Prediction

Compared to discrete-wavelength approaches, access to a continuous NIR absorption spectrum offers two important advantages i.e., better chromophore identification and improved concentration quantification. These features are particularly useful when chromophore spectra are used to predict deep tissue temperature. To obtain chromophore spectra, broadband optical spectroscopy will be made available within the existing TR system through the incorporation of a broadband spectrometer. The intensity spectra from broad band spectroscopy will be calibrated by the scattering and absorption coefficients measured by time-resolved (TR) method at a number of wavelengths to provide an absolute scattering and an absolute absorption spectrum of the tissue from 600-1050nm. From the absorption spectrum, the absolute chromophore concentrations along with water spectral information within the tissue can be determined. Furthermore, as a water molecule hydrogen bonds to other molecules its absorption changes by red-shifting and broadening. As a result, a bound water correction should be used to account for the shifting and broadening of the water spectra to improve temperature prediction^{3,4}.

The major challenge in adapting this technique to adult patients is the significant signal contamination from superficial tissues. This is not a concern in neonatal

applications, where the scalp and skull is negligible and it is reasonable to assume that all the collected light has traveled through brain tissue. However, in the adult subjects, the scalp, skull, and cerebral spinal fluid surrounding the brain can contribute significantly to absorption. In this case, it becomes very difficult to measure absolute concentrations of cerebral chromophores. It has previously been demonstrated that the depth sensitivity of the NIR signal is proportional to the distance separating emitter and detector.⁵ This multi-distance, or depth-resolved approach allows the separation of information into superficial and deep components on the basis that light penetration increases with source-detector distance. Consequently, by collecting information at multiple distances simultaneously, it is possible to separate out information in terms of tissue layers, using an optical reconstruction approach.⁶

(iii) Investigate the Effects of HT/Xe Administration on Flow-Metabolism Coupling in a Hypoxic-Ischemic Model Using TR-NIR

We have already shown that under normoxic conditions, mild hypothermia with different anesthetics preserved flow-metabolism coupling resulting in constant oxygen extraction fraction at ~33%. As the next step, it is necessary to investigate using piglet hypoxia-ischemia models whether under oxidative stress, the neuroprotective effect of mild hypothermia will preserve tight coupling of flow and metabolism as observed in normoxia. Since TR-NIR is safe and measurements can be obtained at the bedside in only a few minutes, it is believed that this technique could assist in monitoring of neuroprotection in the neonatal intensive care unit during combination therapies of hypothermia and Xe administration.

5.5 Conclusion

In summary, the significant findings in this thesis include:

- 1) Nasopharyngeal air cooling by spraying humidified and cold air into nasal cavities is an effective, safe and simple method to selectively reduce and maintain brain temperature, with no major disturbances in physiological variables or adverse effects.
- 2) The developed TR-NIRS temperature measurement technique is able to measure brain temperature non-invasively in neonatal pig to an accuracy of $0.5 \pm 1.6^{\circ}\text{C}$.
- 3) Both cerebral metabolic activity (CMRO_2) and CBF can be measured by TR-NIRS. Moreover, mild hypothermia under different anesthetics preserves the coupling between CBF and CMRO_2 in normoxia.

5.6 References

1. Webb P, Bennett P, Elliot DM. *The physiology and medicine of diving*. London: Bellaire Tindall; 1974.
2. Cenic A, Nabavi DG, Craen RA, Gelb AW, Lee TY. Dynamic ct measurement of cerebral blood flow: A validation study. *AJNR Am J Neuroradiol*. 1999;20:63-73
3. Chung SH, Mehta R, Tromberg BJ, Yodh AG. Non-invasive measurement of deep tissue temperature changes caused by apoptosis during breast cancer neoadjuvant chemotherapy: A case study. *J Innov Opt Health Sci*. 2011;4:361-372
4. Chung SH, Cerussi AE, Merritt SI, Ruth J, Tromberg BJ. Non-invasive tissue temperature measurements based on quantitative diffuse optical spectroscopy (dos) of water. *Phys Med Biol*. 2010;55:3753-3765
5. Bonner RF, Nossal R, Havlin S, Weiss GH. Model for photon migration in turbid biological media. *J Opt Soc Am A*. 1987;4:423-432
6. Elliott J. On the development of a dynamic contrast-enhanced near-infrared technique to measure cerebral blood flow in the neurocritical care unit. *PhD thesis, Department of Medical Biophysics, Western University: London*. 2013

Appendix A

Brain Cooling With Ventilation of Cold Air Over Respiratory Tract: Experimental and Numerical study

Appendix A is adapted from the work entitled “Brain Cooling With Ventilation of Cold Air Over Respiratory Tract: an Experimental and Numerical study”, by M Fazel Bakhsheshi, EE Stewart, H Vafadar, L Keenliside and TY Lee, submitted to the *Journal of International Communications in Heat and Mass Transfer*. The focus of this paper is to investigate the effects of cold gas (O₂-Air) introduced through an endotracheal tube on brain temperature.

A. Introduction

From the neonatal asphyxia studies, only one in six children benefit from this treatment¹, and the rate of death and disabilities remains high in these cooled infants.¹ Xenon (Xe) is a rare noble gas with anesthetic properties, also showing a great promise as a neuroprotectant.²⁻⁵ Recent investigation showed that inhalation of Xe had an additive neuroprotective effect with HT; shown to increase neuroprotection from ~35% (hypothermia only) to ~70% when hypothermia was combined with 50% inhaled Xe gas.⁶

Based on anatomical features and effectiveness of pulmonary architecture and its intimate contact with the entire cardiac output, lung and pulmonary circulation may act as *in vivo* heat exchanger, such that heat can move from the blood to alveolar space and then to the environment.⁷⁻¹⁰ In the present study, we evaluate the efficiency of pulmonary and brain cooling with and without xenon administration over respiratory tract. These data are difficult to acquire in clinical setting, as the cost and scarcity of Xe, as well as accuracy of invasive measurements of brain tissue temperature cannot be easily justified. Therefore, we took advantage of advances in the numerical modeling of heat and water vapor transport in tissues and used computational approach to predict temperature distribution

in the brain during pulmonary cooling using two different gas mixtures, i.e., O₂-Air (1:2) and O₂-Xe (1:2). In addition, we have investigated the effect of some physiological parameters across respiratory tract through numerical simulation. Following numerical simulations, we examined the theoretical predictions in anesthetized piglets to investigate the effects of cold gas (O₂-Air) introduced through an endotracheal tube on brain temperature, and we concurrently measured physiological parameters during whole experiments.

A.1 Materials and Methods

A.1.1 Theoretical Model

Analysis of heat and water transport process in the respiratory tract is a difficult task because the flow patterns inside this area are rather complex. For simplicity, the airway can be idealized as a long, right circular cylinder structure¹¹, which simplifies the theoretical analysis (Figure A.1). Based on the well-known Pennes bioheat transfer equation¹², balance of the energy in the tissue between heat conduction through cellular tissue portion, heat convection by flow of blood and the heat production due to cellular metabolism results as follows:

$$\rho C \frac{\partial T}{\partial t} = \nabla(k \nabla T) + \omega_b c_b (T_b - T) + Q \quad (\text{A.1})$$

where ρ (kg.m⁻³), C (J.kg⁻¹.°C⁻¹), and k (w.m⁻¹.°C⁻¹) are the density, specific heat, and thermal conductivity of tissue, T (°C) is the local tissue temperature, and t (s) is the time, ω_b (kg.m⁻³.s⁻¹) is the volumetric blood perfusion rate, C_b (J.kg⁻¹.°C⁻¹) is the specific heat of blood, T_b (°C) is the supplying arterial blood temperature and Q (W.m⁻³) is the metabolic heat generation rate.

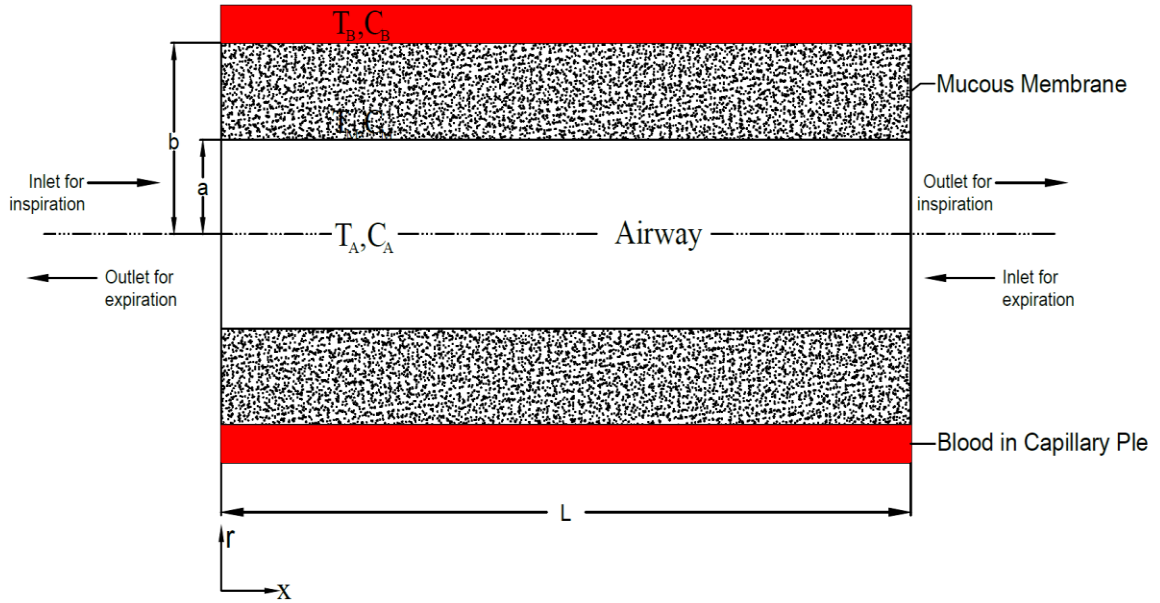


Figure A.1. Schematic diagram of the airway model.

At the mucous-air interface ($r = a$), the boundary condition for the heat transfer is generally composed of two parts, i.e., convection and evaporation. At the entrance of the nasal cavity ($x = 0$), the continuity of heat flux is imposed as a convective boundary condition and also at both deep tissue ($r = b$) and the end of human respiratory tract ($x = L$) heat flux is assumed to approach zero. The boundary conditions can be written as follows¹¹:

$$k \frac{\partial T}{\partial r} = h(T - T_A) + 0.001HM_m (P_m^* - \varphi P_f^*) \quad r = a \quad (\text{A.2})$$

$$\frac{\partial T}{\partial r} = 0 \quad r = b \quad (\text{A.3})$$

$$k \frac{\partial T}{\partial x} = h'(T - T_m) \quad x = 0 \quad (\text{A.4})$$

$$\frac{\partial T}{\partial x} = 0 \quad x = L \quad (\text{A.5})$$

where $T_{in}(^{\circ}\text{C})$ is the breathing air temperature, h' is the apparent heat convection coefficient between the tissue and the breathing air, $h(\text{W}\cdot\text{m}^{-2}\cdot^{\circ}\text{C}^{-1})$ is the heat convection coefficient between the mucosal surface and the flowing airstream for each air stream, i.e., $\text{O}_2\text{-Air}$ and $\text{O}_2\text{-Xe}$ ^{13, 14}. φ is the relative humidity of flowing air from ventilator;

$H(\text{J.kg}^{-1})$ is the latent heat of water vapor; $M_m (\text{kg.s}^{-1}.\text{m}^{-2}.\text{Pa}^{-1})$ is water penetrative coefficient in mucosal surface; $P_f^*(\text{Pa})$ is the saturated vapor pressure at breathing air temperature and $p_m^*(\text{Pa})$ is the saturated vapor pressure at tissue temperature which can be calculated as following¹⁵:

$$\ln(P^*) = \frac{c_1}{T} + c_2 + c_3T + c_4T^2 + c_5T^3 + c_6\ln(T) \quad (\text{A.6})$$

where \ln is the natural logarithm. In the respiratory tract, the energy balance equation for the air can be defined as¹¹:

$$\rho_A C_A \left(\frac{\partial T_A}{\partial t} + u \frac{\partial T_A}{\partial x} \right) = \frac{S}{A} \left(h(T - T_A) + \frac{HM_m (P_t^* - \phi P_a^*)}{1000} \right) \quad (\text{A.7})$$

where $C_A(\text{J.kg}^{-1}.\text{C}^{-1})$ and $\rho_A(\text{kg.m}^{-3})$ are the specific heat and density of the air at each condition; $S(\text{m}^2)$ and $A(\text{m}^2)$ are the local airway cross-section and perimeter; $u(\text{m/s})$ is the mean longitudinal air velocity. The air temperature gradients in the axial direction are usually much smaller than that in the radial direction. Correspondingly, the axial conduction is neglected here for simplicity. During the inspiration and expiratory phases of the breathing cycle, the axial inlet ($x = 0$) boundary condition is considered as the ventilator air temperature ($T_A = T_{in}$) and the heat flux is assumed to approach zero ($\partial T_A / \partial x = 0$) at the end of the human respiratory tract ($x = L$). The energy balance for the blood and tissue is defined by conduction in the tissue and convection in the blood as follows:

$$k \frac{T_m(x, a, t) - T_m(x, b, t)}{(b - a)} = h_{bt} [T_m(x, b, t) - T_b(x, t)] \quad (\text{A.8})$$

Where h_{bt} is heat convection coefficient between blood and tissue, $a(\text{m})$ is the radius of respiratory tract, $b(\text{m})$ is the external radius of calculation domain and $k(\text{W.m}^{-1}.\text{C}^{-1})$ is the thermal conductivity of tissue. Numerical simulation was applied to solve above equations and calculate the thermal impact of inhaled cold air to the mucous membrane and blood temperature which therefore used to predict the brain tissue temperature using

the mathematical model of temperature distribution in Equation (A.1) for the brain tissue parameters. For the thermal boundary condition, the heat flux is assumed to approach zero at the outer boundaries of the brain tissue.¹⁶ The initial condition is a steady-state temperature uniform distribution at thermoneutral conditions ($T = 38.5^{\circ}\text{C}$). The typical values for tissue and air properties for following numerical calculation are presented in Table A.1.^{12, 15, 17, 18}

Table A.1: Base set of parameters used in heat sink thermal model.^{12, 15, 17, 18}

<i>Symbol</i>	<i>Unit</i>	<i>Value</i>
$\rho_{B,m}$	($\text{kg}\cdot\text{m}^{-3}$)	1030
C_b	($\text{J}\cdot\text{kg}^{-1}\cdot^{\circ}\text{C}^{-1}$)	3643
Q_m	($\text{W}\cdot\text{m}^{-3}$)	420
Q_B	($\text{W}\cdot\text{m}^{-3}$)	5370
M_m	($\text{kg}\cdot\text{s}^{-1}\cdot\text{m}^{-2}\cdot\text{pa}^{-1}$)	1.3 e-6
h_{bt}	($\text{W}\cdot\text{m}^{-2}\cdot^{\circ}\text{C}^{-1}$)	10000
h	($\text{W}\cdot\text{m}^{-2}\cdot^{\circ}\text{C}^{-1}$)	50
H	($\text{J}\cdot\text{kg}^{-1}$)	2431
a	(m)	0.005
b	(m)	0.025
L	(m)	0.3
u	($\text{m}\cdot\text{s}^{-1}$)	0.68
T_{in}	($^{\circ}\text{C}$)	5
k	($\text{W}\cdot\text{m}^{-1}\cdot^{\circ}\text{C}^{-1}$)	0.5
A	(m^2)	7.85 e-5
S	(m)	0.032
ω_b	($\text{kg}\cdot\text{m}^{-3}\cdot\text{s}^{-1}$), ($\text{ml}\cdot 100\text{g}^{-1}\cdot\text{min}^{-1}$)	3-11, (15-66)
$c_1, c_2, c_3,$ c_4, c_5, c_6		-5800, 1.4, -0.05, 4.2 e-5, 7.8 e-5, 6.5
ϕ		0.3

A.1.2 Animals Preparation and Experimental Procedure

Experiments were conducted on nine piglets. All animal experiments were approved by the Animal Use Subcommittee of the Canadian Council on Animal Care at the University of Western Ontario. Newborn Duroc cross piglets were obtained from a local supplier on the morning of the experiment. Piglets were anesthetized with 1-2% isoflurane (3-4% during preparatory surgery). A tracheotomy was performed and the piglet was ventilated with a volume-controlled mechanical ventilator to deliver O_2 and medical air mixture with the following variable values: tidal volume 10 mL/kg, frequency 35-45/min and fractional concentration of inspired O_2 (F_{IO_2}) 1.0. A femoral artery was

catheterized to monitor HR and MAP and to intermittently collect arterial blood samples for gas ($p_a\text{CO}_2$, $p_a\text{O}_2$), pH and glucose analysis. Arterial CO_2 tension ($p_a\text{CO}_2$) was monitored throughout the experiment, either directly by blood gas measurements or by the end-tidal CO_2 tension, and maintained at normocapnia between 37-42 mmHg by adjusting the breathing rate and volume. Arterial oxygen tension ($p_a\text{O}_2$) was maintained at a level between 90-130 mmHg by adjusting the ratio of O_2 to medical air. Blood glucose was monitored intermittently and if it fell below 4.5 mmol/L, a 1-2 ml infusion of 25% glucose solution was administered intravenously. After surgery, piglets were maintained on 1-2% isoflurane at normothermia using heated water blanket to maintain rectal temperature between 37.5-38.5°C. Piglets were randomized in two groups, control group in which piglets were just covered with blankets to maintain their body temperature (Group I, $n = 4$); and pulmonary cooling group in which heat loss through respiratory airways occur by cooling of inhalation gases ($T_{\text{in}} \approx -3 \pm 3^\circ\text{C}$) right before going to trachea via shortened endotracheal tube while their body were covered with blankets during whole experiments (Group II, $n = 5$). Rectal temperature was recorded from a rectal probe inserted to 3-4 cm from the anal margin. Deep brain temperature was also measured continuously with a thermocouple probe. A hole was made in the skull with a Dremel tool. The needle thermocouple probe was inserted laterally through the skull into the brain to a depth of 2 cm vertical from the brain surface and 0.5 cm posterior to the bregma. Each experiment was completed within 5 hours. After the last measurement, the animals were sacrificed using potassium chloride IV (1-2 ml/kg) while on 5% inhaled isoflurane. The ambient temperature of the animal laboratory was maintained relatively constant at $22 \pm 0.5^\circ\text{C}$.

A.1.3 Pulmonary Cooling Approach

Cold inspired air was generated by circulating inhalation air, delivered from ventilator, through coiled heat exchanger immersed completely in water bath before delivering to piglet, as shown in Figure A.2. Before starting the cooling process, the cooling unit which control the temperature of water bath was set to -20°C with a

temperature stability of $\pm 0.05^{\circ}\text{C}$ over 30-45 min; settings were kept the same during the entire experiment. The inhaled temperature ($-3 \pm 3^{\circ}\text{C}$) was monitored between the air cooling system and endotracheal tube. During expiration, air leaving the lungs at body temperature is cooled as it passes along the respiratory tract by mixing with cold inspired air.

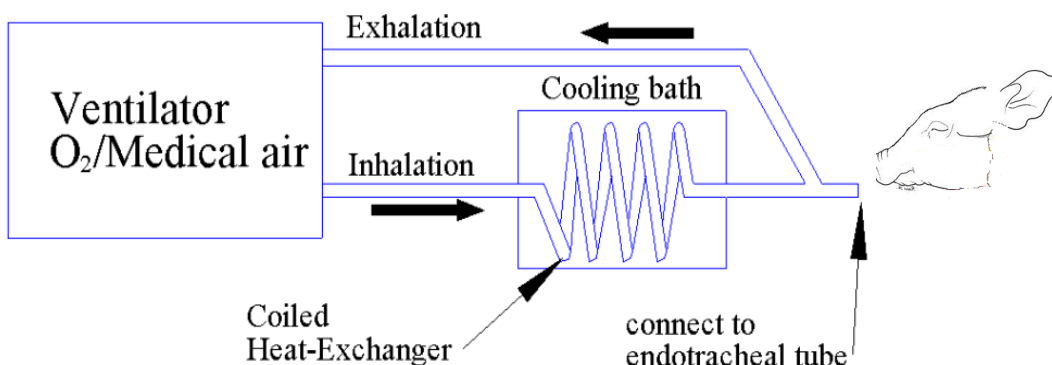


Figure A.2. Schematic representation of the cooling circuit used for pulmonary cooling.

A.1.4 Statistical Analysis

SPSS 17.0.0 (SPSS, Inc, Chicago, IL) was used for all statistical analyses. Normality of the distribution of the measurements was verified using Kolmogorov-Smirnov (KS) test. Comparisons between time-based measurements within groups were performed by Friedman test. Man Whitney U test was used to determine statistical differences of cooling rates as a function of treatment group. Statistical significance was based on p -value < 0.05 . All data are presented as mean \pm SD unless otherwise noted.

A.2 Results

Animal experiments were conducted on nine piglets (five females and four males), with an average age of 4.5 ± 1.5 days old and an average weight of 3.7 ± 1.2 kg. Table A.2 present a summary for the averaged physiologic parameters of the piglets (MAP, HR and

$p_a\text{CO}_2$) in each group. The results presented in Table A.2 demonstrate that HR and MAP dropped slowly through nasopharyngeal cooling approach. The results of arterial blood gas analysis were corrected for temperature. No significant changes were found between two groups with respect to HR, MAP, $p_a\text{O}_2$, $p_a\text{CO}_2$, $t\text{Hb}$, or $p\text{H}$.

Table A.2: Physiological parameters measured at different groups.

Variable		Baseline	Cooling		
		1-60min	0.5hr	1.5hr	3hr
MAP (mmHg)	Group I	55 ± 7	52 ± 6	54 ± 7	53 ± 5
	Group II	55 ± 10	56 ± 10	52 ± 7	47 ± 7
HR (bpm)	Group I	162 ± 16	163 ± 15	162 ± 16	157 ± 18
	Group II	152 ± 38	156 ± 51	155 ± 40	141 ± 31
$p_a\text{CO}_2$ (mmHg)	Group I	39 ± 3	40 ± 3	39 ± 3	39 ± 2
	Group II	42 ± 3	41 ± 2	37 ± 2	41 ± 2
$p_a\text{O}_2$ (mmHg)	Group I	131 ± 44	133 ± 32	125 ± 30	142 ± 24
	Group II	127 ± 40	132 ± 35	128 ± 30	127 ± 34

Figure A.3 (a) displays the maximum absolute cooling rates as monitored in the brain obtained from groups I and II as well as theoretical models for O_2 -air (1:2) and O_2 -Xe(1:2) conditions. In animal experiments, mean brain cooling rate was significantly greater ($p < 0.05$) in pulmonary group i.e., (Group II) as compared with control group (Group I). In the control group, both rectal and brain temperatures did not drop more than $0.3 \pm 0.1^\circ\text{C}$. Figure A.3-b displays the measurements of the brain temperature as a function of time during ventilation of cold O_2 -air (1:2) in both experimental and theoretical models. In animal experiments, following the baseline ($38.3 \pm 0.3^\circ\text{C}$), the brain temperature reached to $36.5 \pm 0.6^\circ\text{C}$ which corresponded to a mean cooling rate of $0.6 \pm 0.1^\circ\text{C}/\text{h}$, respectively. Average temperature difference between rectal and brain was $0.5 \pm 0.1^\circ\text{C}$ during whole animal experiments. Numerical simulations for two different air conditions (i.e., O_2 -Air and O_2 -Xe) during pulmonary cooling show that brain temperature drop to $35.1 \pm 0.4^\circ\text{C}$ and $35.7 \pm 0.5^\circ\text{C}$ which corresponded to a mean cooling rate of $0.98 \pm 0.35^\circ\text{C}/\text{h}$ and $0.8 \pm 0.3^\circ\text{C}/\text{h}$, respectively (Figure A.3-a). Average temperature difference between two air streams was $0.2 \pm 0.1^\circ\text{C}$ over three hour's simulation. Numerical simulations show no significant differences between two different inhaled conditions with respect of cooling rate.

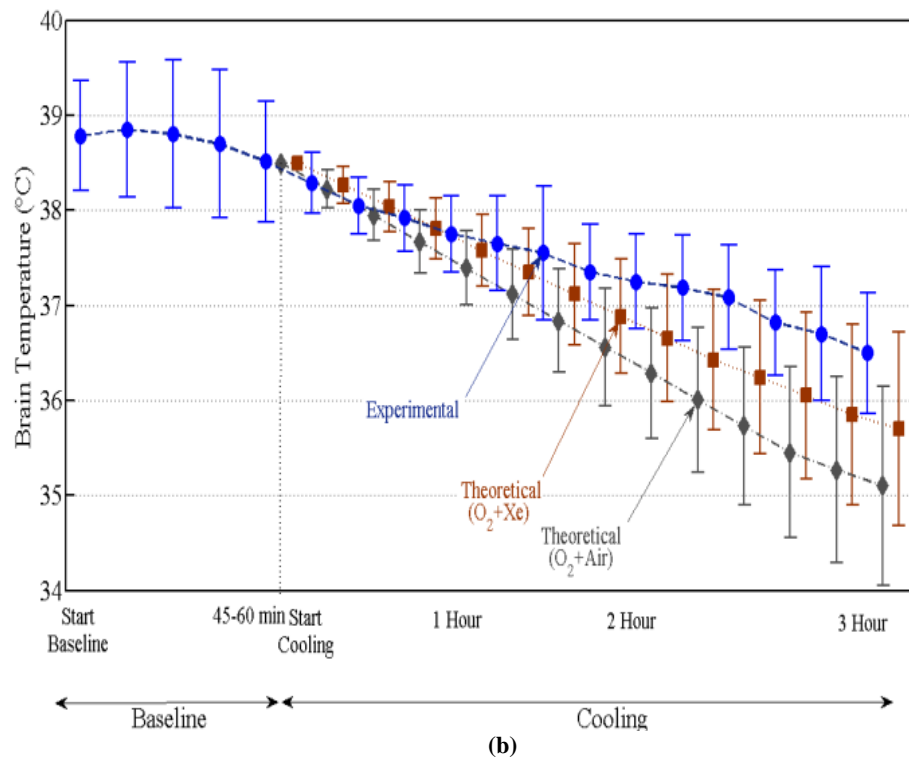
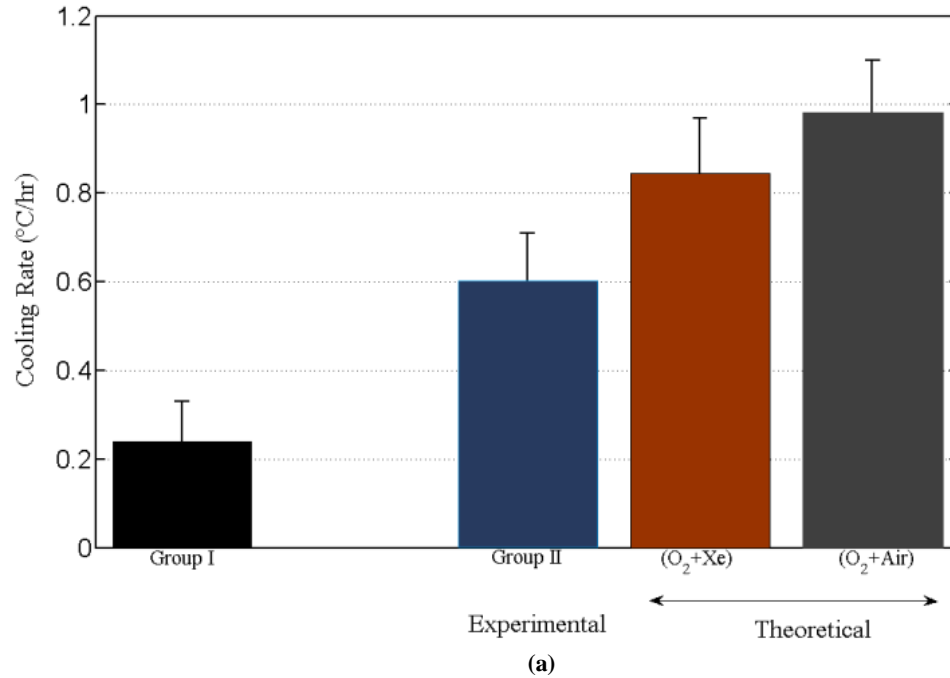
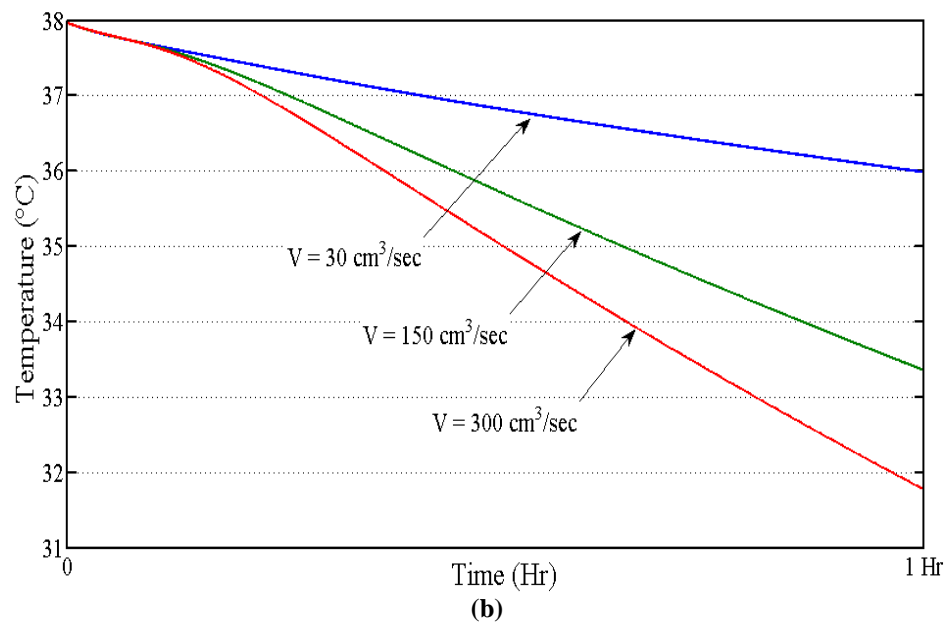
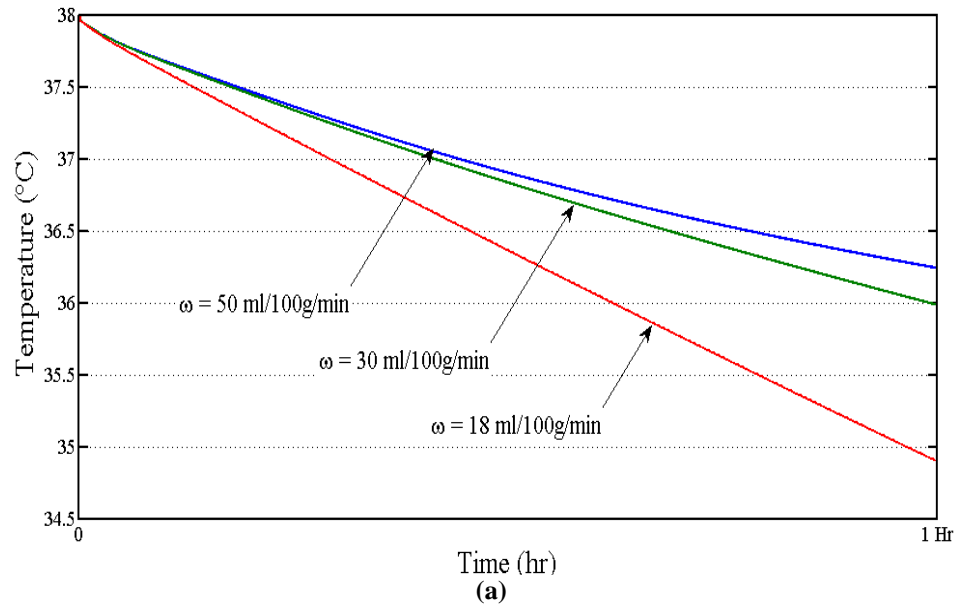


Figure A.3. (a) Maximum cooling rate for brain as a function of groups and theoretical predictions; (b) Brain temperature measurements over time for experimental and theoretical model.

In addition, numerical calculations were performed to investigate the effect of some physiological parameters such as blood perfusion, thermal conductivity, metabolic

rate and air velocity across respiratory tract as displayed in Figure A.5 (a-d), respectively. According to the numerical results, decreasing the perfusion, metabolic rate and increasing the thermal conductivity and flowing air velocity is accelerated cooling in respiratory tract and brain tissue accordingly. For simplicity, all tests for respiratory tract in order to investigate the effect of different parameters on temperature profiles have been carried out for only an hour.



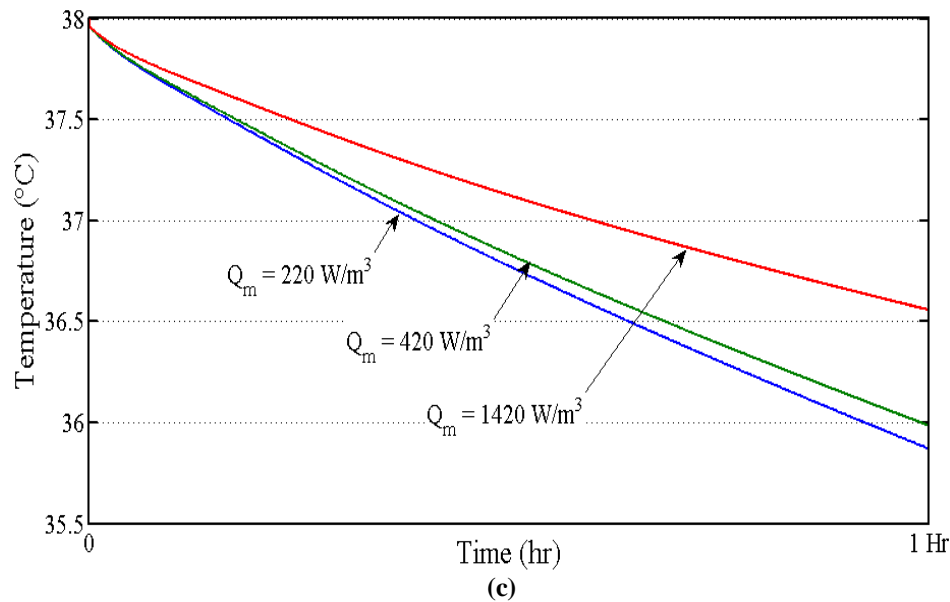


Figure A.4. Effects of (a) blood perfusion level; (b) air velocity, and (c) metabolic rate across respiratory tract response on blood temperature. Calculation were carried out with thermal conductivity $k = 0.5 \text{ w.m}^{-1}.\text{°C}^{-1}$, flowing air temperature $T_{in} = 5\text{°C}$, metabolic rate $Q_m = 420 \text{ w.m}^{-3}$, local mean longitudinal air velocity $V = 30 \text{ cm}^3.\text{s}^{-1}$ and blood perfusion rate $\omega_b = 50 \text{ ml. min}^{-1}.\text{100 g}^{-1}$ as a default values for each simulations.

A.3 Discussions

There are different methods of cooling which utilize different physiological mechanisms of convective and conductive heat loss. Since the entire cardiac output passes through the pulmonary capillary network and the heat of the body can be transferred to the environment via the vast alveolar surface, the lung can serve as a core heat exchanger. As a consequence of conduction, convection, and water evaporation, heat is lost from the trachea and respiratory tract, and the temperature of these surfaces falls below body temperature and this eventually cooled down the whole body.⁷⁻¹⁰ Forman *et al.* and Shaffer *et al.* have demonstrated the feasibility of liquid ventilation to induce hypothermia.^{8,9} In their methods, liquid ventilation was used to induce hypothermia with the cooling rate of 4.8-8.4°C/h, in which perfluorocarbon (PFC) liquids of 20-30°C were tidally exchanged from the lung by an extracorporeal circuit. The problem with their method is associated with the safety profile of its coolant. PFCs are powerful greenhouse gases and deplete the ozone layer and are listed as toxic substances under the Canadian Environmental Protection Act (CEPA).¹⁹ Another safety concern is the risk of coolant

aspiration which might cause lung damage over prolonged periods since neural protection therapy may involve mild hypothermia being maintained for period of 72 hours.²⁰ Insufflations of cold gas have also been studied; however, sufficient cooling rates can only be achieved with very cold inhalation.^{7, 10}

Our study shows that the brain temperature of those animals breathing cold O₂-Air fell to $36.5 \pm 0.6^\circ\text{C}$ in three hours without significant hemodynamic deterioration which corresponded to a mean cooling rate of $0.6 \pm 0.1^\circ\text{C/h}$. Relatively small cooling rate in this study could be explained by combination of different reasons. Employing single endotracheal tube for both of inspiratory and expiratory gas increases the efficiency of the heating as cold air warmed rapidly by countercurrent heat exchange between inspired and expired gas in the endotracheal tube and upper airways before reaching to the alveoli. The heat exchange in the upper airway is a powerful mechanism for thermal insulation of alveolar gas and normally prevents penetration of cold environmental gas beyond 10-15 cm.²¹ The potential for increasing evaporative heat loss from the respiratory tract is also limited by the detrimental effects of prolonged ventilation with dry gas and should not be used clinically used to lower temperature.²²

In the present study, a computational program was written with MATLAB to calculate and analyze the transient temperature distribution across the respiratory tract and within the brain using control-volume finite-difference method.²³ We also show how changes of different parameters can affect the temperature profiles in the respiratory tract. The heat exchange across the respiratory tract depends on the airflow rate, the temperature of expiratory and the inspiratory gas, and its thermal properties. Figure A.5 (a) shows the temperature change for three different blood perfusion rates. It can be seen that larger blood perfusion tends to prevent the biological tissues from cooling. This result can explain the fact that newborns, whose blood perfusion is generally lower, are easier to be cooled than adults. As Figure A.5 (b) displays, higher air velocity yields greater cooling effects. Figure A.5(c) also shows the temperature responses with different metabolic rates. Clearly, the cooling rate can be increased with lower metabolic rate.

They are several limitations in our numerical study that should be pointed out. For example, more complex geometrical and physiological parameters of the respiratory system may be incorporated for a more comprehensive estimation of brain tissue temperature during pulmonary cooling. In this study, some brain and respiratory thermal parameters, including air velocity and the metabolic rate are assumed to be constant in the tissue due to relatively small change in temperature. However, It has been shown that reducing brain tissue temperature from 37 to 34°C reduces the metabolic rate by about 25%. Piglets were studied because they are commonly used animal model of newborn human neurology.

The effect of different thermal properties of respiratory gas on brain cooling was examined using two different air streams with theoretical model. Although the thermal conductivity and specific heat capacity of air are 5-6 times more than Xe, but the heat exchange via the respiratory tract and brain cooling rate was still very smile by substituting Air with Xe. The thermal properties of O₂-Air and O₂-Xe are compared in Table A.3.²⁴ Numerical simulations show no significant differences between two different inhaled conditions with respect of cooling rate with average temperature difference of 0.2 ± 0.1°C over three hours simulation. Neuroprotective effect of hypothermia has been linked to how rapidly cooling is initiated, how quickly the brain is cooled, the etiology of injury and the extent of tissue that reaches the therapeutic hypothermic zone.^{25, 26} Therefore, the results of this work suggest that simultaneous administration of HT and Xe with pulmonary cooling technique is inefficient to induced rapid cooling.

Table A.3: Comparison of some physical properties of O₂-Air and O₂-Xe at normal atmospheric pressure.²⁴

		<i>O₂-Air(1:2)</i>	<i>O₂-Xe(1:2)</i>
<i>Density</i>	(kg.m ⁻³)	1.5	4.014
<i>Specific Heat</i>	(J.kg ⁻¹ .°C ⁻¹)	900	246
<i>Thermal Conductivity</i>	(W.m ⁻¹ .°C ⁻¹)	0.021	0.010

A.4 References

1. Gluckman PD, Wyatt JS, Azzopardi D, Ballard R, Edwards AD, Ferriero DM, Polin RA, Robertson CM, Thoresen M, Whitelaw A, Gunn AJ. Selective head cooling with mild systemic hypothermia after neonatal encephalopathy: Multicentre randomised trial. *Lancet*. 2005;365:663-670
2. Ma D, Wilhelm S, Maze M, Franks NP. Neuroprotective and neurotoxic properties of the 'inert' gas, xenon. *Br J Anaesth*. 2002;89:739-746
3. Ma D, Hossain M, Chow A, Arshad M, Battson RM, Sanders RD, Mehmet H, Edwards AD, Franks NP, Maze M. Xenon and hypothermia combine to provide neuroprotection from neonatal asphyxia. *Ann Neurol*. 2005;58:182-193
4. Dingley J, Hobbs C, Ferguson J, Stone J, Thoresen M. Xenon/hypothermia neuroprotection regimes in spontaneously breathing neonatal rats after hypoxic-ischemic insult: The respiratory and sedative effects. *Anesth Analg*. 2008;106:916-923, table of contents
5. Martin JL, Ma D, Hossain M, Xu J, Sanders RD, Franks NP, Maze M. Asynchronous administration of xenon and hypothermia significantly reduces brain infarction in the neonatal rat. *Br J Anaesth*. 2007;98:236-240
6. Thoresen M, Hobbs CE, Wood T, Chakkarapani E, Dingley J. Cooling combined with immediate or delayed xenon inhalation provides equivalent long-term neuroprotection after neonatal hypoxia-ischemia. *J Cereb Blood Flow Metab*. 2009;29:707-714
7. Zikria BA, Ferrer JM, Malm JR. Pulmonary hypothermia in dogs. *J Appl Physiol*. 1968;24:707-710
8. Shaffer TH, Forman DL, Wolfson MR. Physiological effects of ventilation with liquid fluorocarbon at controlled temperatures. *Undersea Biomed Res*. 1984;11:287-298
9. Forman DL, Bhutani VK, Tran N, Shaffer TH. A new approach to induced hypothermia. *J Surg Res*. 1986;40:36-42
10. Harrison MR, Hysing ES, Bo G. Control of body temperature: Use of the respiratory tract as a heat exchanger. *J Pediatr Surg*. 1977;12:821-828
11. Hanna LM, Scherer PW. A theoretical model of localized heat and water vapor transport in the human respiratory tract. *J Biomech Eng*. 1986;108:19-27

12. Duck FA. *Physiological properties of tissues: A comprehensive reference book*. San Diego Academic; 1990.
13. Hanna LM, Scherer PW. Measurement of local mass transfer coefficients in a cast model of the human upper respiratory tract. *J Biomech Eng*. 1986;108:12-18
14. Nuckols ML. Heat and water transfer in the human respiratory system at hyperbaric conditions. 1981;Ph. D. Dissertation
15. American Society of Heating Refrigerating and Air-Conditioning Engineers. *Ashrae handbook – fundamentals*. 2009.
16. Xu X, Tikuisis P, Giesbrecht G. A mathematical model for human brain cooling during cold-water near-drowning. *J Appl Physiol*. 1999;86:265-272
17. Liu J. *Bioheat transfer*. Beijing: Science Press; 1997.
18. Holmes KR. Thermal properties
"http://users.Ece.Utexas.Edu/~valvano/research/thermal.Pdf".2013
19. Chemicals Management Division of Environment Canada. List of toxic substances managed under cepa (schedule 1), available at: [Http://www.Ec.Gc.Ca/toxiques-toxics/default.Asp?Lang=en&n=98e80cc6-1&xml=aa329670-c3c7-4ad5-a7ab-5fd8a05439f1](http://www.Ec.Gc.Ca/toxiques-toxics/default.Asp?Lang=en&n=98e80cc6-1&xml=aa329670-c3c7-4ad5-a7ab-5fd8a05439f1). 2005;2013
20. Azzopardi D, Strohm B, Edwards AD, Halliday H, Juszczak E, Levene M, Thoresen M, Whitelaw A, Brocklehurst P, Steering G, participants TCR. Treatment of asphyxiated newborns with moderate hypothermia in routine clinical practice: How cooling is managed in the uk outside a clinical trial. *Arch Dis Child Fetal Neonatal Ed*. 2009;94:F260-264
21. Webb P, Bennett P, Elliot DM. *The physiology and medicine of diving*. London: Bellaire Tindall; 1974.
22. Marfatia S, Donahoe PK, Hendren WH. Effect of dry and humidified gases on the respiratory epithelium in rabbits. *J Pediatr Surg*. 1975;10:583-592
23. Recktenwald G. The control-volume finite-difference approximation to the diffusion equation. 2003
24. Katz I, Caillibotte G, Martin AR, Arpentinier P. Property value estimation for inhaled therapeutic binary gas mixtures: He, xe, n2o, and n2 with o2. *Med Gas Res*. 2011;1:28
25. Behringer W, Prueckner S, Safar P, Radovsky A, Kentner R, Stezoski SW, Henchir J, Tisherman SA. Rapid induction of mild cerebral hypothermia by cold

aortic flush achieves normal recovery in a dog outcome model with 20-minute exsanguination cardiac arrest. *Acad Emerg Med.* 2000;7:1341-1348

26. Kuboyama K, Safar P, Radovsky A, Tisherman SA, Stezoski SW, Alexander H. Delay in cooling negates the beneficial effect of mild resuscitative cerebral hypothermia after cardiac arrest in dogs: A prospective, randomized study. *Crit Care Med.* 1993;21:1348-1358

Appendix B

Comparison of Selective Brain Cooling in Juvenile and Newborn Piglets Using a Nasopharyngeal Method

B.1 Materials and Methods

Animals were anesthetized with 1-2% isoflurane. A tracheotomy was performed and the animal was ventilated with a volume-controlled mechanical ventilator to deliver Oxygen (O₂) and medical air mixture. A femoral artery was catheterized to monitor HR and MAP and to intermittently collect arterial blood samples for gas ($p_a\text{CO}_2$, $p_a\text{O}_2$), pH and glucose analysis. Animals were randomized into the different groups:

I. control group in which whole body of piglet was covered with blankets, (n=3);

II. nasopharyngeal cooling group in which hypothermia was induced by directing humidified and cooled medical air ($\approx -8^\circ\text{C}$) at the flow rate of 14-15 Liter.min⁻¹ into the nasal cavities via catheters while core body temperature was maintained within 35.5-36.5°C using heating blanket and hot water gloves by iteratively turning heating blanket "on" and "off" at;

II-a. New-born piglets with an average age 1-2 days old and an average weight of ≈ 1 -2kg, (n=3) and;

II-b. Juvenile pigs with an average age of 3 weeks old and an average weight of ≈ 16 kg, (n=2);

Rectal temperature was recorded from a rectal probe inserted to 3-4 cm from the anal margin. Brain temperature measured far away from nasal cavities (7-8cm) to make sure to achieve whole brain cooling at depth of 2 cm vertical from the brain surface and 1.5 cm posterior to the bregma.

B.2 Results

Table B.1 presents a summary for the averaged physiologic parameters for each group related to Figure B.1. Both the heart rate (HR) and mean arterial blood pressure (MAP) dropped slowly through nasopharyngeal cooling approach in the new-born piglets, i.e. group II-a. No significant changes were found in the juvenile pig, i.e. group II-b, with respect to HR or MAP.

Table B.1. Physiological parameters measured at each group.

		<i>Baseline</i>	<i>Cooling</i>			
		<i>1-60min</i>	<i>30 min</i>	<i>1 hr</i>	<i>2 hr</i>	<i>3 hr</i>
<i>MAP</i> (mmHg)	<i>Control</i>	36 ± 7	34 ± 6	36 ± 7	36 ± 7	36 ± 7
	<i>Nasal Cooling</i> <i>New-born piglet</i>	46 ± 2	44 ± 2	44 ± 5	37 ± 3	36 ± 5
	<i>Nasal Cooling</i> <i>Juvenile pig</i>	52 ± 3	53 ± 5	55 ± 4	50 ± 5	52 ± 4
<i>HR</i> (bpm)	<i>Control</i>	162 ± 16	163 ± 15	162 ± 16	162 ± 16	162 ± 16
	<i>Nasal Cooling</i> <i>New-born piglet</i>	164 ± 15	145 ± 16	133 ± 19	133 ± 19	133 ± 19
	<i>Nasal Cooling</i> <i>Juvenile pig</i>	181 ± 9	176 ± 13	165 ± 19	168 ± 14	170 ± 17

Figure B.1 displays the maximum absolute cooling rates achieved at each group as monitored in the brain and core rectal compartment. Results of comparing both groups in the nasopharyngeal cooling approach using cold and high air-flow rate reveals that it was possible to increase the brain-rectal temperature gradient in the heavier pigs compared to new-born piglets, i.e. 16 kg versus 2-3 kg. The rectal cooling rate was approximately one-third of the corresponding brain cooling rate. Effective selective brain cooling was achieved with a median cooling rate of $2.3 \pm 0.3^\circ\text{C/h}$ in the juvenile pigs.

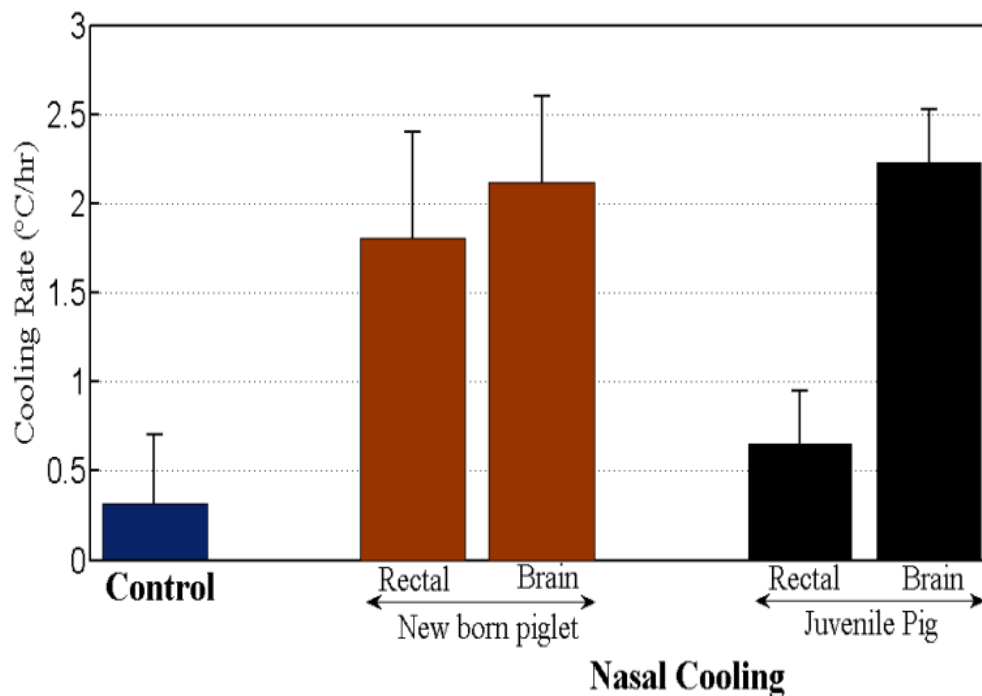


Figure B.1. Maximum cooling rate for brain as a function of different conditions in Nasal cooling.

Figure B.2(a,b) demonstrate the mean brain and rectal temperature profile as a function of time in both groups. Results shown in Figure B.2(b) demonstrated that maximum brain-rectal temperature gradient of -2.5°C reached about 20-30 min after the initiation of cooling and remained unchanged during the rest of nasopharyngeal cooling.

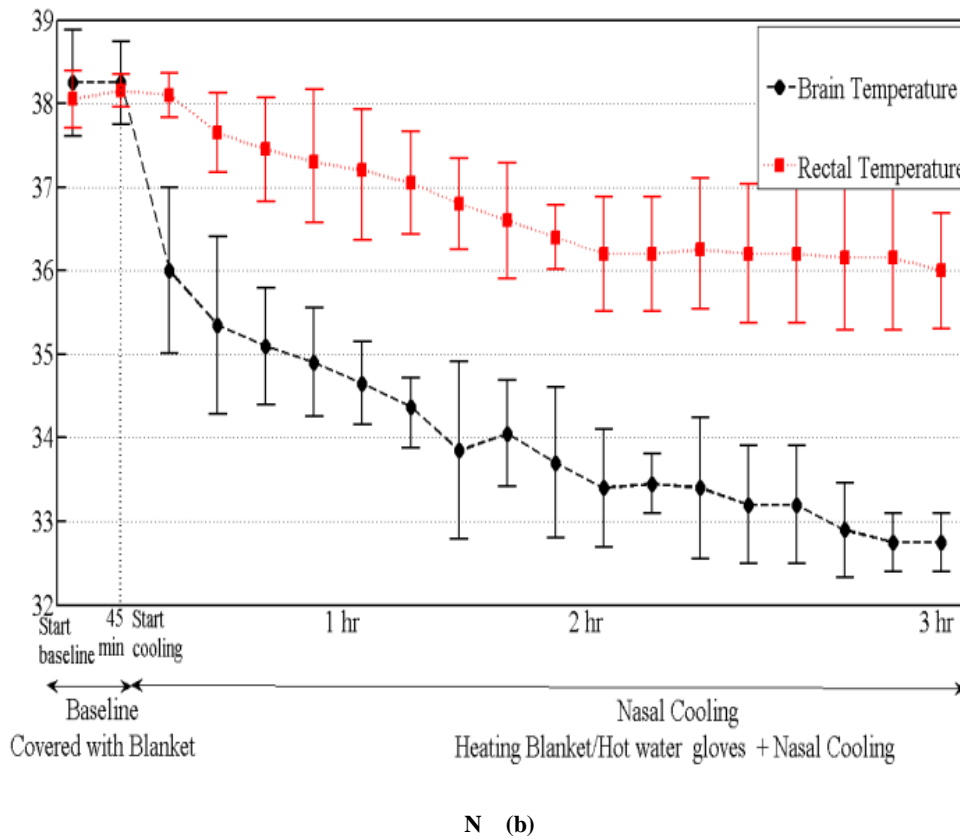
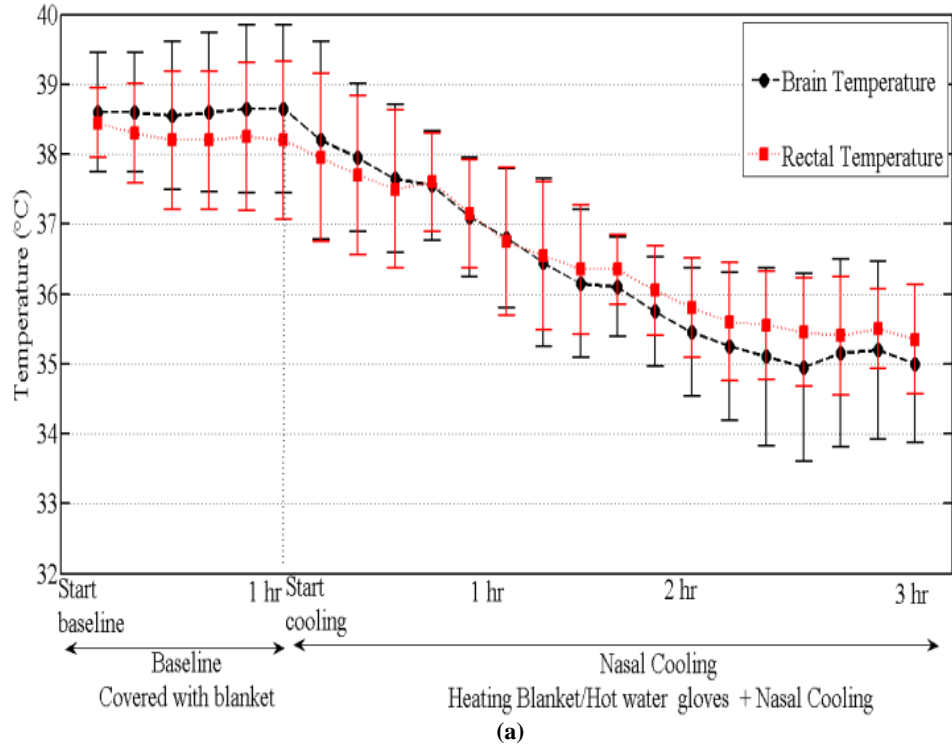


Figure B.2. Changes in the brain-rectal temperature over time for intra-nasal cooling method with setting the air flow rate to 14-15 L.min⁻¹ for (a) piglets with average weight of ≈2-3kg; and (b)

juvenile pig with average weight of $\approx 16\text{kg}$.

B.3 Conclusions

We demonstrated that nasopharyngeal cooling by spraying humidified and cooled air into nasal cavities is an effective, safe and simple method to selectively reduce and maintain the brain-body temperature gradient in the heavier pig compare to new-born ones using heating blanket/sheets.

FROM:
SENT: Monday, January 28, 2013 10:07 AM
TO:
CC:
SUBJECT: eSirius Notification - Annual Protocol Renewal APPROVED by the
AUS 2007-081-09::5

2007-081-09::5:

AUP NUMBER: 2007-081-09
AUP TITLE: Impaired Cerebral Oxygen Consumption Is An Early Predictor of
Brain Damage Following Hypoxia-Ischemia

YEARLY RENEWAL DATE: 01/01/2013

THE YEARLY RENEWAL TO ANIMAL USE PROTOCOL (AUP) 2007-081-09 HAS BEEN
APPROVED, AND WILL BE APPROVED FOR ONE YEAR FOLLOWING THE ABOVE REVIEW
DATE.

* THIS AUP NUMBER MUST BE INDICATED WHEN ORDERING ANIMALS FOR THIS
PROJECT.

* ANIMALS FOR OTHER PROJECTS MAY NOT BE ORDERED UNDER THIS AUP NUMBER.

* Purchases of animals other than through this system must be cleared
through the ACVS office.
Health certificates will be required.

REQUIREMENTS/COMMENTS

Please ensure that individual(s) performing procedures on live animals,
as described in this protocol, are familiar with the contents of this
document.

THE HOLDER OF THIS ANIMAL USE PROTOCOL IS RESPONSIBLE TO ENSURE THAT ALL
ASSOCIATED SAFETY COMPONENTS (BIOSAFETY, RADIATION SAFETY, GENERAL
LABORATORY SAFETY) COMPLY WITH INSTITUTIONAL SAFETY STANDARDS AND HAVE
RECEIVED ALL NECESSARY APPROVALS. PLEASE CONSULT DIRECTLY WITH YOUR
INSTITUTIONAL SAFETY OFFICERS.

Submitted by: Kinchlea, Will D
on behalf of the Animal Use Subcommittee

From:

Sent: Friday, December 23, 2011 12:21 PM

To:

Cc:

Subject: eSirius Notification - New Animal Use Protocol is APPROVED2007-081-09::5



AUP Number: 2007-081-09

PI Name: St. Lawrence, Keith

AUP Title: Impaired Cerebral Oxygen Consumption Is An Early Predictor Of Brain Damage Following Hypoxia-ischemia

Official Notice of Animal Use Subcommittee (AUS) Approval: Your new Animal Use Protocol (AUP) entitled "Impaired Cerebral Oxygen Consumption Is An Early Predictor Of Brain Damage Following Hypoxia-ischemia

" has been APPROVED by the Animal Use Subcommittee of the University Council on Animal Care. This approval, although valid for four years, and is subject to annual Protocol Renewal.2007-081-09::5

1. This AUP number must be indicated when ordering animals for this project.
2. Animals for other projects may not be ordered under this AUP number.
3. Purchases of animals other than through this system must be cleared through the ACVS office. Health certificates will be required.

The holder of this Animal Use Protocol is responsible to ensure that all associated safety components (biosafety, radiation safety, general laboratory safety) comply with institutional safety standards and have received all necessary approvals. Please consult directly with your institutional safety officers.

Submitted by: Copeman, Laura
on behalf of the Animal Use Subcommittee
University Council on Animal Care

The University of Western Ontario
Animal Use Subcommittee / University Council on Animal Care
Health Sciences Centre, • London, Ontario • CANADA - N6A 5C1
PH: 519-661-2111 ext. 86768 • FL 519-661-2028
Email: auspc@uwo.ca • <http://www.uwo.ca/animal/website/>

Curriculum Vitae

Name: Mohammad Fazel Bakhsheshi

Post-secondary Education and Degrees: Tehran University
Tehran, Iran
2001-2005, Bachelor of Science (B.Sc), Mechanical Engineering (Major Field: Fluid and Heat Transfer)

Western University
London, Ontario, Canada
2007-2009, Master of Science (M.Sc), Mechanical Engineering (Major Field: Fluid and Heat Transfer)

Western University
London, Ontario, Canada
2009-2014, (P.hD), Medical Biophysics
(Major Field: Therapeutic Hypothermia and Optical Imaging)

Publications:

Manuscripts

1. **M Fazel Bakhsheshi**, JM Floryan, PN Kalon, Spectrally-Accurate Method For Analyzing Motions Of Ellis Fluid Over Corrugated Boundaries, *J Fluids Eng*, 133(2), 021401 (Feb 04, 2011)
2. **M Fazel Bakhsheshi**, M Diop, KSt Lawrence, TY Lee, Non-Invasive A Time-Resolved Near Infrared Technique For Bedside Monitoring Of Brain Tissue Temperature *Journal of Bio-Medical Optics*, 19(5), 057005 (May 2014)
3. **M Fazel Bakhsheshi**, L Keenlside, EE Stewart, TY Lee, Feasibility of Selective Brain Cooling Using a Nasopharyngeal Method in Piglets, *Submitted to Journal of Critical Care Medicine*
4. **M Fazel**, L Keenlside, TY Lee, A New Approach To Selective Brain Cooling, *Journal of Critical Care Medicine*, *In progress*
5. **M Fazel**, H Vafadar, TY Lee, Numerical Modeling Of Temperature Distributions Within Human Respiratory Tract And Neonatal Brain During Hypothermia Treatment, *Submitted to Journal of International Heat and Mass Transfer*
6. **M Fazel Bakhsheshi**, J Hadway, M Diop, KSt Lawrence, TY Lee, Coupling of Cerebral Blood Flow and Oxygen Consumption During Hypothermia Under Different Anesthetics in

Conference Papers And Abstracts

1. **M Fazel Bakhsheshi**, Stewart, L Morrison, TY Lee, Rapid Selective Brain Cooling Using a Nasopharyngeal Method, *12th Imaging Network Ontario Symposium*, Toronto, Ontario, Canada, 2014.
2. **M Fazel Bakhsheshi**, M Diop, KSt Lawrence, TY Lee, Identification Of Optimal Wavelengths To Improve Broadband Optical Thermometry, SPIE Photonics West, Optical Tomography And Spectroscopy Of Tissue, San Francisco USA, 2014.
3. **M Fazel Bakhsheshi**, EE. Stewart, L Morrison, TY Lee, Comparison Of Selective Brain Cooling In Juvenile And Newborn Piglets Using A Nasopharyngeal Method, *The 8th International Of Brain Monitoring And Neuroprotection In Neonates Conference*, Clearwater beach, FL USA, 2014.
4. **M Fazel Bakhsheshi**, EE Stewart, L Morrison, TY Lee, Feasibility Of Selective Brain Cooling Using A Nasopharyngeal And Pulmonary Circulation Methods In Piglets, London Imaging Discovery, London Canada, June 2013.
5. **M Fazel Bakhsheshi**, M Diop, KSt Lawrence, TY Lee, Quantitative Measurement Of Cerebral Blood Flow During Hypothermia With A Time-Resolved Near-Infrared Technique, SPIE Photonics West, Optical Tomography And Spectroscopy Of Tissue, San Francisco USA, Jan 2012.
6. **M Fazel Bakhsheshi**, M Diop, KSt Lawrence, TY Lee, Quantitative Measurement Of Cerebral Blood Flow During Hypothermia With A Time-Resolved Near-Infrared Technique, SPIE Photonics West, Optical Tomography And Spectroscopy Of Tissue, San Francisco USA, Jan 2012.
7. **M Fazel Bakhsheshi**, M Diop, KSt Lawrence, TY Lee, Quantitative Measurement Of Cerebral Blood Flow During Hypothermia With TR Near Infrared Technique, London Imaging Discovery, London Canada, June 2012
8. **M Fazel Bakhsheshi**, KM Tichauer, M Diop, M Migueis, TY Lee, Time-Resolved Near-Infrared Technique For Bedside Monitoring Of Brain Tissue Temperature. 5th Annual London Imaging Discovery Forum, London Canada, June 2010
9. **M Fazel Bakhsheshi**, KM Tichauer, TY Lee, Non-Invasive Monitoring Of Brain Temperature By Near-Infrared Spectroscopy, Radiological Society Of North America Conference, Chicago USA, Nov 2010.
10. **M Fazel Bakhsheshi**, KM Tichauer, TY Lee, Non-Invasive Monitoring Of Brain Temperature By Near-Infrared Spectroscopy, Lawson Research Day, London Canada, March 2010
11. **M Fazel Bakhsheshi**, JM Floryan, PN Kaloni, Spectrally-Accurate Method For Analysis Of Ellis Fluid In A Channel With Arbitrary Roughness, Computational Fluid Dynamics Society Of Canada (CFDSC), London Canada, May 2010

12. **M Fazel Bakhsheshi**, JM Floryan, PN Kaloni, Immersed Boundary Conditions Method For Analyzing Flow Of Ellis Fluid Over Corrugated Boundaries, Computational Fluid Dynamics Society Of Canada (CFDSC), Ottawa Canada, May 2009
13. **M Fazel Bakhsheshi**, JM Floryan, PN Kaloni, IBC Method For Analyzing Motion Of Ellis Model Fluid Over Corrugated Boundaries, Canadian Applied And Industrial Mathematics Society (CAIMS), London Canada, May 2009